Structural Controls on Zn-Pb-Ag Mineralisation Determined by Scale Integrated Analysis at Mount Isa, Queensland, Australia

Thesis submitted by

Toby Patrick Davis BSc (Hons) *University of New South Wales*

June 2004

for the degree of Doctor of Philosophy

in the School of Earth Sciences

James Cook University

STATEMENT OF ACCESS

I, the undersigned, author of this work, understand that James Cook University will make this thesis available for use within the University Library and, via the Australian Digital Theses network, for use elsewhere.

I understand that, as an unpublished work, a thesis has significant protection under the Copyright Act and I wish the following restrictions to be placed on this work; all users consulting this thesis will have to sign the following statement:

"In consulting this thesis I agree not to copy or closely paraphrase it in whole or in part without the written consent of the Author; and to make proper written acknowledgement for any assistance obtained from it."

_____ _____

Toby Patrick Davis
June 2004

STATEMENT OF SOURCES

DECLARATION

I declare that this thesis is my own work and has not been submitted in any form for another degree or diploma at any university or other institution of tertiary education. Information derived from the published or unpublished work of others has been acknowledged in the text and a list of references is given.

Signature

Date

Acknowledgements

Firstly I'd thank my supervisor Tim Bell for his enthusiastic supervision of this project and for introducing me to the exciting side of structural geology. I especially appreciate Tim allowing me to take this project in the directions that I wanted. It was a great to have the opportunity to work with you. The SAMRI den was the site of numerous lively and stimulating discussions on many subjects that sometimes included structural and metamorphic geology and I thank the other members of SAMRI for their company and ideas, most notably during the SAMRI "discussions", especially Chris Bell, Nikki Adshead-Bell, Mustafa Cihan, Andrew Ham, Ken Hickey, Cameron H_2, Nick Timms, Muhammad Sayab, Mike Rubenach and Peter Welch. I'd also like to thank the other staff and students in the School for their willing assistance at all times. Thanks in particular to Andrew Allibone and Lucy Chapman who were willing sparring partners on the controversial topic of the genesis of the Mount Isa orebody.

This project was supported and funded, including stipend, by MIM Ltd, Mount Isa Business Unit. It was initially proposed by Steve Law and Alice Clarke and they are thanked for creating this opportunity and for showing me the ropes around the mine when I first arrived, including a stern warning about having preconceived ideas on the genesis of this deposit, which I had no idea about. On site I was given abundant logistical assistance by many staff in the geology department at the mine, who also took the time the discuss aspects of the deposit that they thought would be of use. I greatly appreciated your suggestions, insights and help. I hope the geologists among you find this work useful in understanding the formation this deposit or at least it gives you something to discuss or argue about for a while. Thanks to the many people, especially at the beginning of this project who offered their ideas on which was the best way forward.

Thanks to Chris Bell for stimulating discussions on all aspects of geology and other deep and meaningful aspects of life such as climbing. Thanks for introducing me to rock climbing, I will especially remember the morning and afternoon climbs and bouldering sessions at Kissing Point as these were some of my favourite moments in Townsville, besides microstructure sessions with Tim, of course. During this project I was reintroduced to piscatorial pleasures and introduced to the excitement of barramundi fishing in the Houghton River by Roger Mustard and Adam Webb. Thanks for your excellent company on numerous fishing trips and although these were not always successful in terms of catching big fish, they were in terms of rest and relaxation as well as being the highlight of living in Townsville.

Thank you Mum and Dad for your support during this PhD and for teaching me the value of persistence not to mention your many other gifts over the years. Thanks to my brothers and sisters for putting up with my PhD ramblings. I have always been appreciative for your support. Advice and encouragement from Richard Crookes and Denis Clarke gave me the nudge needed to leave my job as a mine geologist and do this PhD, and it is greatly appreciated.

Finally I'd like to thank Cathy. Above all she experienced this more than anyone else and going through another PhD so soon after your own can't have been a thrilling prospect. Thank you for convincing that it was a good thing to do in the first place, and for all your encouragement and companionship, which kept me sane along the way. It's out of my system now.

Preface

Preface

This study analyses the structural geology of the Mount Isa Zn-Pb-Ag orebody to determine the role of structure in its evolution. A comparison with the nearby copper orebodies is included because the two ore types are potentially related. The Mount Isa Zn-Pb-Cu-Ag deposit is one of the largest and most enigmatic base metal accumulations on Earth. It is located on the western margin of the Leichhardt River Fault Trough in the Western Fold Belt of the Mount Isa Inlier, northwestern Queensland, Australia. The deposit lies east of and adjacent to the Mount Isa and Paroo faults and is traversed by folds that formed during the Isan Orogeny (1610-1500 Ma). It is hosted by the Urquhart Shale, a dolomitic sedimentary sequence in the Upper Mount Isa Group. Prior to mining the base metal deposit contained in excess of 405 million tonnes of ore including 150 Mt at 7 % Zn, 6% Pb and 150 g/t Ag and 255 Mt at 3.3 % Cu (Forrestal 1990, McGoldrick and Large 1998, Waring et al. 1998) in spatially separate copper and Zn-Pb-Ag orebodies that show contrasting features when examined at similar scales. The Zn-Pb-Ag orebody contains a series of conformable lenses that consist of centimetre scale bedding parallel sulphide bands and breccias and belongs to the stratiform sediment hosted Zn-Pb-Ag class of deposits (Large et al., 2002). Other deposits in this class include Red Dog (Alaska), Sullivan (Canada), HYC (Northern Territory), Century (Queensland), and George Fisher-Hilton (Queensland). In contrast to the Zn-Pb-Ag orebody the copper orebodies at Mount Isa are discordant at the mine scale and consist of cross-cutting breccias.

The genesis of the Mount Isa base metal deposit is controversial because of apparently conflicting features between and within the copper and Zn-Pb-Ag orebodies. Blanchard and Hall (1937) and Grondijs and Schouten (1937) considered the deposits to be epigenetic because of the proximity of ores to folds and high strain zones. However, this early deposit model was replaced by ones involving predeformation mineralisation, including exhalative and diagenetic depositional styles, in order to explain the conformable nature of sulphide bands within the Zn-Pb-Ag ores (Murray, 1961; Neudert, 1986; McGoldrick and Large, 1998; Large et al, 1998). In these models, various discordant features documented by the earliest workers were attributed to remobilisation (McDonald, 1970; McClay, 1979). The copper ores were initially considered to be related to the Zn-Pb-Ag ores and were likewise regarded as having a predeformation origin, but establishment of a tectono-metamorphic origin for copper (Perkins, 1984; Swager, 1985; Bell et al, 1988) led to the notion that the different ore styles are spatially coincidental but not temporally related. Evidence of syntectonic sulphide deposition presented by Perkins (1997) has largely been dismissed as an effect of remobilisation because of the ambiguous representivity of

these features (Betts and Lister, 2002; Large et al., 2002). However, remobilisation has never been documented at Mount Isa.

Tectonic structures can be involved in either syn-tectonic mineralisation or modification of orebodies, or a combination of these processes. The ambiguity surrounding the genesis of the Mount Isa Zn-Pb-Ag orebody arises because it is not known which of these scenarios is the case. The focus of this study is to determine the relationship between the structural geology and the metal distribution throughout the Zn-Pb-Ag orebody at a range of scales. The scale integrated approach taken has made it possible to establish the representivity of features and to determine the role of tectonic structures in the evolution of the ores.

The thesis contains four papers (Parts A-D) that were written to be submitted for publication in international journals. Part A deals with the mine scale metal distribution and structural geology. It was published in 2004 in Economic Geology, volume 99. The results of this study have significant implications for the timing of mineralisation. Part B examines the formation of folds that were shown in Part A to have controlled the distribution of metal in the deposit. The results may have implications for other types of ore deposits that are associated with folding and lie proximal to high strain zones. This paper will also be submitted to Economic Geology. Part C is an examination of two potential and topical kinematic indicators that are present in the deposit. These are flanking structures and asymmetric boudins. This paper will be submitted the Journal of Structural Geology. Part D is an in depth analysis of the ore textures in the Zn-Pb-Ag orebody. It defines their large scale distribution, and the kinematics involved in their formation based on microstructural analysis. This paper will be submitted to either Economic Geology or Ore Geology Reviews.

The four sections are summarised below:

Part A

This section examines the mine scale distribution of metals within in the Zn-Pb-Ag orebody and its relationship to the structural framework and the nearby copper orebodies. The metal distribution was defined by modelling grade control data and the structural framework was determined by mapping the underground workings and from historical mapping. There is a ubiquitous relationship between folds and the metal distribution with disharmonic NNW-plunging asymmetric folds hosting ore shoots as well as controlling the low grade distribution. Comparison of the geometries of the Zn-Pb-Ag and copper orebodies show that they are virtually the same. Several remobilisation and syntectonic mineralisation scenarios are presented to explain the large scale features defined in this study.

Part B

Folds identified in Part A as controlling the distribution of metals in the Zn-Pb-Ag orebody are examined to determine how they formed and why they were centres of mineralisation. The formation of these folds was determined using large scale and microstructural features. Folds controlling the metal distribution formed over several deformations. Spatial partitioning of deformation within and along competency domains in the rock was important during folding and was also responsible for the size, continuity and location of the folds. The fold model presented accounts for the switch of shear sense along axial planar foliations either side of the fold hinge and the preservation of older generations of folds, which are important to the localisation of the ores.

Part C

Flanking structures and asymmetric boudins have been the subject of recent publications because of their potential as kinematic indicators. Flanking structures are located around both veins that formed early during mineralisation as well as asymmetric boudins. They are common components of the ores. This section examines flanking structures and asymmetric boudins in the Mount Isa Zn-Pb-Ag orebody and presents new mechanisms for their formation based on meso and microstructural analysis. The formation of various components of structures is linked to separate deformations. Consequently, recently devised classification schemes were found to be overly simple and cannot be applied in this case. The use of these structures as simple kinematic indicators can be misleading. However, detailed examination of such structures reveals important information about the deformation history.

Part D

This study examined the range of ore textural styles in the Zn-Pb-Ag orebody. The petrographical, textural and microstructural features of each ore textural style were examined to determine the kinematic processes involved in mineralisation. The range and distribution of ore textural styles was determined by detailed logging of diamond drill core across the orebody. The microstructural study utilised oriented samples collected from underground workings. By showing the distribution of ore textures of a large area this study was able to clearly demonstrate the extent of structurally controlled mineralisation.

Terminology

- The Mount Isa deposit refers to the entire Mount Isa base metal accumulation.
- There are two sources of Zn-Pb-Ag ore in the Mount Isa deposit. The first is the Lead mine. The second is the Rio Grande orebody which is a minor source of ore to the south

of the Lead mine. Zn-Pb-Ag deposits are actually present around all margins of the silica-dolomite body above the Paroo fault. The deposits in the Lead mine are the main subject of this study, though the Rio Grande orebody and Zn-Pb-Ag deposits at the south end of the Mount Isa deposits were examined. The latter were studied in drill core only. Both contain the same features as the Zn-Pb-Ag deposits in the Lead mine. Several samples (4078 and 4079) from the aforementioned drilling are presented in the study.

- Orebody refers to either the copper or Zn-Pb-Ag part of the base metal accumulation. The copper orebody contains several large copper bodies that are referred to with individual orebody names in mining operation, such as the 650 or 3000 copper orebodies. Because these are large and easily separable in nature this convention is also used here.
- The Zn-Pb-Ag orebody contains ten broadly conformable bodies of peak grade termed Zn-Pb-Ag lenses. These lenses are the smallest recognisable ore units in the plans of modelled metal distribution that cover the entire orebody.
- Zn-Pb-Ag packages are collections of individual centimetre scale conformable sulphide bands or breccias. These packages are usually separated by more than a metre of barren siltstones or mudstones and correspond to ‘lead orebodies’ defined at the mine. A single Zn-Pb-Ag lens may contain numerous Zn-Pb-Ag packages.
- The orientation of photomicrographs and photographs is shown in the top right corner. A single barbed arrow over a numeral denotes a vertical section with the number indicating the strike. Horizontal sections contain north arrows. Sample numbers or locations of exposures are given in the lower left corner and a list of samples and their locations is presented in Appendix C. Where possible all images are presented looking to the north. In some cases this means mirror images of photographs of exposures taken looking south were used.
- A complete collection of longitudinal sections showing the metal distribution for the Zn-Pb-Ag orebody are provided in a compact disc in Appendix A in Portable Document Format (PDF).

Contents

Table of Contents

List of Tables

List of Figures

Part A

List of Figures continued

Part B

List of Figures continued

Part C

List of Figures continued

Part D

Part A

Mine-scale structural controls on the Mount Isa Zn-Pb-Ag and Cu orebodies

(Published in Economic Geology, volume 99, number 3)

T. P. Davis, PhD 2004

Mine-scale structural controls on the Mount Isa Zn-Pb-Ag and Cu orebodies

Abstract

The Mount Isa Zn-Pb-Cu-Ag deposit contained almost 30 million tonnes of base metals, prior to mining, in spatially separate copper and Zn-Pb-Ag orebodies. The origin of the Zn-Pb-Ag ores is debated due to apparently conflicting features at intermediate to microscales. Ambiguity is associated with small scale features, which can be interpreted either in terms of syndeformation mineralisation or in terms of remobilisation of a predeformation orebody when considered in isolation of larger scale characteristics of the orebody. Understanding the relationship between metal distribution and the structural framework at the mine-scale helps to determine whether the orebody is deformed and leads to a better understanding of its formation.

The deposit contains ten stratabound Zn-Pb-Ag lenses in an en echelon array. The extremities of the orebodies correlate with F_4 folds, and high grade shoots are centred on F_4 hinges and short limbs that contain older F_2 folds. Contours of Pb/Zn ratios throughout the lenses are parallel to F_4 hinges and silica-dolomite alteration fronts. Restoring the large scale effects of folding by rotating bedding and the lenses to horizontal indicates that a sedimentary exhalative style of mineralisation cannot account for the present geometries of the Zn-Pb-Ag lenses. This reconstruction places the depositional basin in a compressional setting, or places the ores on topographic highs. These scenarios are considered to be incompatible with synsedimentary processes.

There are a number of important similarities between the geometries of the Zn-Pb-Ag lenses and the copper orebodies, which are interpreted to have a syntectonic origin. The Zn-Pb-Ag lenses display the same structural controls as the syntectonic copper ores and appear to have been emplaced at the same time in D_4. Older F_2 folds are preserved on the hinges and short limb areas of F_4 folds and are interpreted to have behaved as structural heterogeneities during D_4, which caused the dilation that led to metal deposition. F_4 folds closest to the copper orebodies contain the highest grade Zn-Pb-Ag ore shoots, possibly indicating decreasing metal deposition away from the copper ores as fluids became progressively depleted in metals and/or concentration of fluid flow near the copper orebodies. In some areas, Zn-Pb-Ag ores wrap around silica-dolomite alteration associated with syntectonic copper mineralisation, suggesting a similarly late timing. The continuity of metal grades and Pb/Zn ratios throughout the Zn-Pb-Ag lenses indicates that the ores are not the result of local remobilisation. Instead, large-scale processes whereby the metals were introduced from an external source in D_4 must have been involved in the formation of the Zn-Pb-Ag orebody.

Introduction

Mount Isa is a globally significant base metal deposit which, prior to mining, contained 405 million tonnes of ore including 150 Mt at 7 % Zn, 6% Pb, and 150 g/t Ag and 255 Mt at 3.3 % Cu (Forrestal, 1990; McGoldrick and Large, 1998; Waring et al., 1998). Zn-Pb-Ag and copper orebodies are spatially separate and, when examined at the same scales, in most cases display significant differences in geometry and structure. At the mine-scale the Zn-Pb-Ag orebody contains a series of stratabound lenses, whereas copper orebodies occur in large nonconformable breccias hosted in a silica-dolomite alteration envelope.

Debate over the timing of Zn-Pb-Ag mineralisation continues because of conflicting interpretation of several features of the deposit (cf. Valenta, 1994; Perkins, 1997; McGoldrick and Large, 1998; Perkins and Bell, 1998; Chapman, 1999). The strongly stratabound nature of the Zn-Pb-Ag ores and the lack of identifiable channelways, structure, and alteration at exposure-scale appear to indicate a predeformation origin, whereas microstructures such as sulphide -cleavage overprinting relationships and replacive sulphide textures, as well as tectonic veins, suggest that regional deformation had a strong influence on mineralisation. The difference in style between the copper and the adjacent Zn-Pb-Ag ores has generally been attributed to different mineralising events and has added to the genesis debate by requiring spatially coincident mineralising events separated by over 100 Ma. The debate is further complicated by some field observations that can be interpreted to support either predeformation mineralisation with remobilisation, or syntectonic mineralisation, as shown by Perkins (1997, 1998).

Most studies of the structure of the ores have been at microscopic to exposure-scales (Grondijs and Schouten, 1937; Blanchard and Hall, 1942; McDonald, 1970; McClay 1979; Perkins, 1997). At these scales some observations are ambiguous and of uncertain representivity relative to the size of the deposit. The aim of this study is to determine the influence of regional-scale deformation on the deposit to define the large-scale relationship between the Zn-Pb-Ag ores and the structural framework in the mine. The influence of deformation on the metal distributions is discussed in the context of remobilisation of pre-existing deposits versus syndeformation mineralisation as examined by Marshall and Gilligan (1987, 1993) and Marshall et al. (2000). The geometries of the Zn-Pb-Ag ores are compared to those of the copper orebodies, which have been interpreted to be tectono-metamorphic in origin (Perkins, 1984; Swager, 1985; Bell et al., 1988; Waring et al., 1998), and the possible genetic links between the two ore types are discussed.

Geological Background

Deposit description

Mount Isa is located on the western margin of the Leichhardt River Fault Trough in the Mount Isa Inlier (Fig. 1), a Palaeo- to Mesoproterozoic terrane in NW Queensland. The inlier is subdivided into the Western, the Kalkadoon-Leichhardt, and the Eastern Fold Belts (Carter et al., 1961; Blake and Stewart,1992). It comprises basement metamorphic rocks unconformably overlain by rift-fill sedimentary and volcanic rock sequences and intrusive rocks of various ages. The rift-fill package is divided into four cover sequences, summarised in Table 1. The Mount Isa deposit is hosted by the Urquhart Shale member of the Upper Mount Isa Group in Cover Sequence 4. The Urquhart Shale comprises a sequence of interbedded dolomitic, shales, siltstones and mudstones with an average bed thickness of 11.6 mm (Neudert, 1986), which imparts a strong structural anisotropy.

The deposit is located on the western limb of a regional D_2 anticline (Bell et al., 1988), east of the Mount Isa Fault (Fig. 1). This reverse fault dips steeply west and juxtaposes amphibolite facies rocks to the west against greenschist facies rocks to the east, and truncates a D_2 anticline south of the mine (Bell, 1991). The host rocks have been affected by three macroscopic folding events; D_1 resulted from N-S shortening and included north to south thrusting (Bell, 1991), whereas D_2 and D_4 produced N-S trending upright folds in response to east-west compression (Bell, 1983). Locally at Mount Isa, D_4 produced NNW-SSE-striking folds. Bell and Hickey (1998) recognised a localised deformation, D_3, between D_2 and D_4. The effects of this deformation are generally subtle and recognised by rotation of F_2 fold axes into flat orientations and a shallow-dipping crenulation cleavage. According to Rubenach (1992), prograde Isan metamorphism was synchronous with, and peaked around, the end of D_2.

Genetic models

Central to the debate about the genesis of Mount Isa is the timing of mineralisation with respect to deposition of the host rocks and regional deformation, and the relationship between the copper and Zn-Pb-Ag orebodies. The following section reviews the genetic models that have been proposed for the Mount Isa deposits.

Zn-Pb-Ag orebody: A syndeformation model for Zn-Pb-Ag ores was initially proposed by Blanchard and Hall (1937, 1942) and more recently by Perkins (1997, 1998) and Perkins and Bell (1998). It is based on replacement textures (Grondijs and Schouten, 1937; O'Malley and McGhie, 1939; Perkins, 1997), mesoscopic relationships of ore to folds and high strain zones

(Blanchard and Hall, 1937, 1942), and the transgressive nature of Zn-Pb-Ag lenses (Perkins, 1997). The Syn-D_4 timing of mineralisation proposed by Perkins (1997) is based on sulphide - cleavage overprinting relationships. Perkins (1997) further proposed that Zn-Pb-Ag ores formed contemporaneously with the copper orebodies in a zoned system with synchronous deformation and alteration.

Synsedimentary models have been proposed for Mount Isa by Murray (1961), Stanton (1962), Russell et al. (1981), Sawkins (1984), Large et al. (1998) and McGoldrick and Large (1998) based on the lack of evidence for fluid channelways and wallrock alteration and the stratiform nature of the ores at the deposit to exposure-scale. It is argued that primary sedimentary features that are typical of exhalative deposits were destroyed by deformation and metamorphism (McDonald, 1970; McClay, 1979; Betts and Lister, 2002). Cooke et al. (2000) explain the general lack of an identifiable feeder system in the Zn-Pb-Ag deposits in northern Australia, including the Mount Isa, Hilton, and McArthur River deposits, as the result of mineralisation from oxidized fluids that would have required exceptional circumstances to deposit sulphides in a feeder system.

A diagenetic origin was proposed by Neudert and Russell (1981) and Neudert (1984, 1986), who interpreted water depths during sedimentation as being too shallow for exhalative processes to form these deposits. However, Large et al. (1998) used sedimentological data to argue that the host rocks at HYC (McArthur River), located in the Batten Trough north of Mount Isa, accumulated when water depths were sufficient for exhalative style mineralisation to occur. A diagenetic timing is also proposed by Chapman (1999) based on stable isotope signatures of carbonates in the host rocks.

Various authors (e.g., McDonald, 1970; McClay, 1979; Neudert, 1986; Betts and Lister, 2002) have invoked remobilisation of the ores to account for the observed syntectonic features. Valenta (1994) proposed similar remobilisation at Hilton, 20 km north. McDonald (1970) and McClay (1979), who examined features at the scale of centimetres to several tens of meters, found that fold hinges were generally enriched in galena relative to sphalerite, but unmetamorphosed samples could not be identified in these studies.

Copper orebody: Perkins (1984) and Swager (1985) showed that copper mineralisation, dolomitisation and silicification (referred to locally as silica-dolomite alteration) at Mount Isa were coincident with D_4. Bell et al. (1988) proposed that mineralising fluids entered the depositional environment across the Basement Fault which they described as the primary structural control on copper mineralisation. Fluid flow was facilitated by brecciation caused by differential shearing (opposing shear sense) on opposite sides of the Basement Fault during D_4.

Myers et al. (1996) and Perkins (1997) proposed that copper and Zn-Pb-Ag mineralisation were cogenetic and syntectonic. Perkins (1997) argued for a zoned Cu-Pb-Zn system, whereas Myers et al. (1996) preferred synchronous copper and Zn-Pb-Ag mineralisation from separate fluids.

Methodology

The geometry and grade distribution of Zn-Pb-Ag and copper orebodies in the northern part of the Mount Isa deposit were analysed at the mine-scale and in individual exposures. The copper orebodies examined include the 650, 500 and 200 orebodies in the Lead Mine and the 3000 and 3500 orebodies in the Enterprise Mine, situated below the Lead Mine (Fig. 2). The geometries of the orebodies are illustrated in series of plans and sections constructed using grade control data, including drill core and wall sampling and underground mapping. Maps of five levels of the Lead Mine were compiled from historical mapping by company geologists and mapping by the author to establish the mine-scale structural framework (Appendix A). The grade database contains over 514,000 assays of samples collected from 1927 to 2000. Drilling data came mainly from underground diamond drill holes, horizontally and vertically spaced at approximately 25 m, and intersecting the orebody at high angles. Assay data from wall-rock chip samples and drill core were compared on a log-log plot (Fig. 3). The plot for this data set is close to a straight line so both sample types were used in modelling grade distribution, although a slight bias towards higher Pb+Zn in drill core samples was found.

Metal distribution was modelled for the mapped levels, which are spaced at approximately 200 m. Only data from 100 m above and below each level was used. A block model was created with individual block dimensions of 4 m north-south, 2 m east-west, and 4 m vertically. These dimensions were chosen to reflect the shape of the orebodies and the sample spacing. The grade of individual blocks was calculated by interpreting between samples using the inverse distance method which weights each sample inversely according to its distance from the block being estimated (Isaaks and Srivastava, 1989). This method was used because of its simplicity, the concentration of metals and the scale of the study.

The Zn-Pb-Ag lenses defined in this study are different to the ‘orebodies’ of earlier studies (e.g., Perkins, 1997). Previous workers used a system of 31 orebodies that are not reflected in the modelled metal distributions of this study. Individual ‘orebodies’ of earlier workers in some cases represent only a portion of a Zn-Pb-Ag lens defined here and thereby give an incomplete picture of the Zn-Pb-Ag distribution. Table 2 lists the correlation between orebody names used in previous studies and the Zn-Pb-Ag lenses used here. The deposit was

found to be dominated by ten Zn-Pb-Ag lenses with Pb+Zn >7.75 %, which are shown in Figure 4.

Grade distribution in longitudinal sections was determined using inverse distance weighted contouring of the product of the average grade and the width of intersections through each Zn-Pb-Ag lens. The metal distribution was compared to the geological structure over the modelled areas. Plans and sections of modelled metal distribution in addition to those presented in the figures are located in Appendix A.

Structural Framework

The Paroo fault

The Paroo Fault is the largest discrete structure associated with the deposit. It truncates the mine sequence at depth where it forms the faulted contact between the steeply west-dipping Urquhart Shale above, and the shallowly dipping Eastern Creek Volcanics (or greenstone basement; Fig. 2) below. The Paroo Fault has a complex but well constrained geometry determined by drilling. Below the mine it dips at a low angle to the east, where it is termed the Basement Fault, but progressively steepens to the west (Fig. 2b). This geometry was explained by Bell (1983, 1991) as the result of overturning of the Eastern Creek Volcanics in the roof sheet on the western lateral ramp of the Kokkalukkanurker Duplex. There is a change in the depth of the Basement Fault portion of the Paroo Fault in longitudinal section from south to north. Drill hole intersections show that between 3200 mN to 5970 mN (all grid references are in mine grid coordinates) the Basement Fault is consistently located around 2500 mRL. However, north of 5970 mN the Basement Fault dips steeply to the north so that at 6600 mN it is at 1990 mRL, a change of over 500 m (Fig. 2c). The Lead Mine is situated above the deeper parts of the Basement Fault in the north.

Folding

The mine-scale fabric is dominated by NNE-SSW-striking bedding in the south that progressively rotates to N-S in the north of the mine (Fig. 5). This fabric is traversed by numerous narrow NNW-SSE-striking linear fold zones that are the short limbs of asymmetric, ENE-verging folds formed in D_4. The relative timing of folding was determined by microstructural studies (Bell and Hickey, 1998; Part B). Folds are correlatable throughout the mine despite their discontinuous nature. The interlimb angle of the folds generally decreases as the width of the NNW-SSE-striking fold zones decreases. The fold zones have arcuate boundaries within which bedding orientations vary relative to the dominant fabric outside these

zones. The fold zones pinch out along strike and may narrow, bifurcate and/or pinch out with depth. An approximately 100 m-wide, N-S-striking corridor of unfolded, N-S-striking bedding exists in the middle of the mine.

The short limb areas of the major F_4 fold zones have been named and are shown in Figure 5. Folds along the margins of the fold zones are referred to as either the anticline or the syncline of the couplet. For example, the fold on the WSW margin of the Black Star fold zone is termed the Black Star anticline. The 650 fold zone is the largest and most southerly in the Lead Mine and hosts the 650 copper orebody. The Mount Isa fold zone at the north end of the mine is a large, east-verging, asymmetric fold that can be traced through all levels of the mine and is persistent across the mine. Close examination of the fold zones shows that they contain folds with N-S and NE-SW-trending axes (Fig. 6), but consistent orientations are not clearly distinguishable on an equal area projection. This is most likely the result of reactivation and rotation of D_2 structures during D_4 because of the similar orientations of σ_1 during the two deformations (cf. Adshead-Bell and Bell, 1999; Timms, 2002).

Geometric Analysis of the Ores

The spatially separate copper and Zn-Pb-Ag orebodies are exploited through three main mine workings (Fig. 2). The Copper Mine, located in the south, is dominated by the 1100 and 1900 copper orebodies, where the Basement Fault attains its highest structural level at 2500 mRL, with only minor Zn-Pb-Ag ore (Fig. 2c). Conversely, in the Lead Mine, Zn-Pb-Ag ores dominate and the Basement Fault is up to 500 m deeper (at 1990 mRL). Several small copper orebodies are located at the south end of the Zn-Pb-Ag lenses in the Lead Mine. Approximately 100 m vertically below the base of the Zn-Pb-Ag lenses in the Lead Mine is the top of the Enterprise Mine which contains the 3000 and 3500 copper orebodies adjacent to the Basement Fault.

Geometry of Zn-Pb-Ag lenses

The Zn-Pb-Ag lenses are separated into two groups based on their arrangement, termed the Black Star and Racecourse domains (Fig. 4). These names are not directly related to those of the fold zones already defined. The Black Star domain contains two Zn-Pb-Ag lenses (B and C) and the Racecourse domain contains eight (D to K). South of 7000 mN the domains are separated by barren host rocks and the 200 copper orebody. This barren zone is not present between the domains in the north where the deposits occur continuously over a stratigraphic thickness greater than 500 m.

The Racecourse domain comprises NNE-SSW to N-S-striking, Zn-Pb-Ag lenses, each typically 30 m across strike (ranging from 10 to 50 m) and 600 m along strike, arranged in an en echelon array with NNW-SSE-striking enveloping surfaces (Figs. 4 and 7). The ENE enveloping surface coincides with the hinge of the Mount Isa anticline. The WSW enveloping surface coincides with either the hinge of the 650 anticline or the ENE boundary of the silica-dolomite halo around the 200 copper orebody (Fig. 4). The highest Pb+Zn grades of individual orebodies are situated adjacent to the WSW enveloping surface and gradually decrease towards the north (Fig. 7).

The Black Star domain strikes N-S, has a maximum across-strike width of 200 m, and extends for more than 1.2 km along strike. High grade mineralisation terminates near the Mount Isa anticline to the north and in the short limb of the 650 fold in the south. The Black Star domain is adjacent to the footwall of the 650-500 copper orebody.

Individual Zn-Pb-Ag lenses are sheetlike bodies with a long axis up to 1.2 km long and plunging in the range of 23-60^{o} towards 323-348^{o} (Figs. 8 and 9). In drill core and underground exposures the ores comprise semi-massive to massive, sheetlike, nearly conformable sulphide bands and breccias typically up to 40 cm thick and interlayered with unmineralised siltstones. Bedding in mineralised packages may be straight or exhibit intensive folding (Fig.10). The intermediate axes of the Zn-Pb-Ag lenses are between 250 and 700 m. This dimension decreases from west to east across the deposit. An abrupt decrease in the grade of the Zn-Pb-Ag lenses occurs at the hinge of the Mount Isa anticline in the north and the 650 fold in the south. Low grade ores are present on the north side of the Mount Isa fold couplet, where drilling has been sporadic.

The geometries of the Zn-Pb-Ag lenses are clearly illustrated in contoured longitudinal sections (Fig. 9). All lenses are composed of narrow high grade shoots. These may have simple shapes, such as the NNW-plunging shoots in lenses B, C, H, I, J, and K, or complex shapes where more than one shoot can be identified. Zn-Pb-Ag lenses that abut the 200 copper orebody (E, F, and G) have complexly-shaped high grade shoots, the southern margins of which are concave where they terminate against the 200 silica-dolomite body (Fig. 9e). Here, two NNW-plunging shoots occur along the upper and lower margins of the Zn-Pb-Ag lens, with a third plunging down the dip of bedding between them and immediately north of the 200 silica-dolomite front (Fig. 9e).

When considered separately in individual Zn-Pb-Ag lenses, zinc and lead display the same grade distribution with contours having the same shape as those for the total metal. However, the zinc is situated further from the copper ores than the lead (Fig. 11). Silver correlates with lead ($r = 0.87$) so it was not considered individually here.

Geometry of copper orebodies

The copper orebodies are dominantly NNW-plunging. The largest copper orebodies are situated adjacent to the Basement Fault (e.g., 3000 and 3500 orebodies), whereas those distal to the fault, such as the 650, 500 and 200 orebodies, are much smaller. Copper orebodies are enveloped by silica-dolomite alteration that extends to the fault (Fig. 2).

The 650 and 500 copper orebodies are situated in the western part of the Lead Mine in the structural hanging wall of the Zn-Pb-Ag deposits. It is evident from the plans that these orebodies are bifurcated fingers of a single body with NNW-SSE-striking and N-S-striking portions represented by the 650 and 500 orebodies, respectively (Fig. 12). The 500 copper orebody is a vertically-dipping, flattened cigar-shaped body that plunges 25°N (Fig. 12b). The 650 orebody plunges 40° towards 340° and extends for 500 m down plunge (Fig. 12c). Copper grades are highest and the combined body has its largest down dip and across strike extents where the 500 and 650 orebodies intersect. The 200 copper orebody has lower grade and is situated in the centre of the Lead Mine along the WSW enveloping surface of the Racecourse Zn-Pb-Ag domain (Fig. 4). These orebodies and the Zn-Pb-Ag ores have similar geometries.

The 3000 orebody consists of an en echelon series of N-S-striking, high grade shoots with a NNW-SSE-striking enveloping surface (Fig. 12). Individual shoots are up to 80 m wide and extend 220 m up dip of bedding from the Paroo Fault. They dip shallowly to the west near the fault and become progressively steeper up dip. The overall plunge of the 3000 orebody is 32° towards 324°. The 3500 orebody is a 500 m long N-S-striking, steeply west-dipping body located east of the 3000 orebody (Figs. 12d and e), and extends up dip of bedding for 320 m. Overall the 3500 orebody plunges 35° towards 339°. Together, the 3000 and 3500 copper orebodies have the same shape as the combined Racecourse and Black Star Zn-Pb-Ag domains (cf. Figs. 4 and 12d).

Comparison with structure

Copper orebodies: The copper orebodies are located in the short limbs and hinges of asymmetric folds. Figure 2 shows that the 1100 orebody is located on the synclinal hinge and short limb of a large fold at the contact between the Mount Isa Group units and the Eastern Creek Volcanics, as first noted by Perkins (1984). The 650 and 500 orebodies in Figure 4 are centred on the short limb of the 650 fold bounded by the associated antiform and synform. The 200 orebody is located in the short limb region of the Black Star Fold (Figs. 4, and 9g). Here, silica-dolomite alteration and copper mineralisation were constrained by intrafolial folding of the rocks in the orebody between surrounding unfolded and unmineralised rocks.

The 3000 and 3500 copper orebodies are located on the limbs of mine-scale folds in a

manner similar to the Zn-Pb-Ag orebodies (Figs. 4 and 12d). The external geometry of the 3000 orebody is constrained by the Basement Fault and the Mount Isa anticline. The 3000 orebody is located on the southern long limb of the Mount Isa fold whereas the 3500 orebody is located on the northern long limb. High grade shoots within the orebody are parallel to the plunge of F_4 hinges, but it is difficult to precisely map fold structures within the orebodies as the fabrics were destroyed during mineralisation.

Zn-Pb-Ag lenses: At all scales there is a close correlation between folds and the Zn-Pb-Ag ores (cf. Figs. 4 and 9). At the mine-scale, the Zn-Pb-Ag lenses are located between the anticlinal hinges of the 650 and Mount Isa folds. Overlapping grade distribution and structural maps show that folds are also located centrally to NNW-plunging high grade shoots that host the bulk of the ore, as illustrated in Figure 9. However, the west-plunging shoots in orebodies abutting the 200 copper orebody are more complicated and bedding is not folded in them at the mapped scale (Fig. 9g).

East of the 200 copper deposit the H-K lenses consist of a single broad NNW-plunging shoot hosted in a large short limb zone in which bedding strikes NNE-SSW, whereas in the long limbs bedding strikes N-S (Figs. 9 h and i). The highest total metal grades are concentrated along the lower margins of the lenses and there is a rapid decrease in grade where the strike of bedding changes to N-S, indicating a clear relationship between bedding orientation and ore grade.

Contours of decreasing metal grade away from the high grade shoots are parallel to F_4 hinges (Figs. 9 a, c, e and h). Low grade ores extend onto the long limbs of folds that host the high grade shoots. Lens B demonstrates this where the northern boundary of high grade mineralisation coincides with the hinge of the Black Star anticline (Figs. 9 a and b). Here the locus of high grade ore (>7.75 % Zn + Pb) is centred on a parasitic fold on the southern long limb of the Black Star fold and has an across-strike width of 70 m. The grade gradually decreases towards the 650 fold in the south. On the northern long limb of the Black Star fold, high grade ore occurs in three narrow bedding parallel shoots, each approximately 10 m across strike so the overall grade is much lower. On longitudinal sections there is a clear boundary to the high grade ore which is coincidental with the folds. Ore in the vicinity of the Mount Isa anticline has a similar grade distribution but the pattern is less obvious because the grades are lower.

Zoning patterns

In both cross section and plan, zones of high grade Pb+Zn have a tabular, stratiform appearance (Fig. 7a-c). Zn-Pb-Ag lenses are grouped around the copper orebodies with the highest Pb+Zn grades proximal to them as illustrated by cross sections through the Lead Mine (Fig. 7). Grade contours are parallel to F_4 hinges and silica-dolomite boundaries. Contours of Pb/Zn ratios cut stratigraphy and are also parallel to silica-dolomite boundaries and F_4 trends throughout the Lead Mine. The Pb/Zn contours are centred around, and highest Pb/Zn values are proximal to the copper orebodies at either the same structural level or at deeper levels in the Enterprise Mine (Figs. 7d-f).

Distribution of low grade populations

Cumulative frequency plots of the grades were examined to determine if multiple populations existed in the data that were not evident in the grade maps of the deposit. Where a possible second population was identified the samples were plotted on indicator maps to determine their spatial distribution. A single population will plot as a sigmoidal curve when the data is normally distributed (Fig. 13a). Deviations from this may indicate the presence of multiple populations, which may reflect remobilisation, multiple episodes of mineralisation, or other variations in structural or chemical characteristics of the deposit.

Most of the Zn-Pb-Ag lenses have grade distributions that indicate the presence of a separate low grade population in the samples but they are small and overlap with the main distribution, which makes them difficult to separate (e.g., Fig. 13a). In lens B there is a discernable separation between low grade samples (<1.2% Pb and <1.2% Zn) and higher grade samples. Zinc-poor samples group together in a north-plunging cluster in the lower part of lens B (Fig. 13b) and are dispersed above this cluster. Lead-poor samples cluster in the north with a north-plunging upper surface (Fig. 13c).

Discussion and Conclusions

The observations presented here strongly support a syn-D_4 timing for the development of the present geometries of the Zn-Pb-Ag orebody. This is indicated by the close spatial correlation between the ores and F_4 folds at all scales, both along the margins of the Zn-Pb-Ag lenses and within them. High grade shoots are centred on the hinges and short limbs of NNW-plunging D_4 folds, and contours defining metal zonation are parallel to F_4 hinges and silica-dolomite fronts throughout the mine (Figs. 9 and 10).

Similarities between the geometries of the Zn-Pb-Ag lenses and the copper ores, which

are interpreted to have formed during D_4 (Perkins, 1984; Swager, 1985; Bell et al., 1988; Waring et al., 1998), suggests that both ore types had the same structural history. Folds control the overall geometries of the 1100, 650, 500 and 200 copper orebodies as well as the high grade shoots in Zn-Pb-Ag lenses. This is illustrated in Figure 9g, where silica-dolomite alteration associated with the 200 copper orebody is restricted to an area where bedding is folded, similar to the Zn-Pb-Ag shoots (Figs. 9d and f). The 3000 copper orebody and the collective Racecourse Zn-Pb-Ag lenses exhibit the same geometries in high and low grade areas, notably N-S-striking high grade orebodies with NNW-striking enveloping surfaces (in plan) indicating a strong influence from the structural anisotropy imparted by bedding. These deposits are located in the same structural domain (i.e., on the western long limb of the Mount Isa anticline) with the 3000 copper orebody situated vertically below the Racecourse Zn-Pb-Ag lenses. This relationship is evident at a larger scale than the folds hosting the high grade Zn-Pb-Ag shoots described above.

Some aspects of the Zn-Pb-Ag lenses indicate that their geometry was established after silica-dolomite alteration. Zn-Pb-Ag lenses abutting the 200 copper orebody, as shown in Figure 9e, enfold the silica-dolomite body that contains the copper orebody. This pattern suggests that the silica-dolomite alteration, which Perkins (1984) and Swager (1985) interpreted as syntectonic, predates the Zn-Pb-Ag shoots, and the geometries of the Zn-Pb-Ag lenses were locally controlled by the presence of copper ores, or more precisely their enveloping silica-dolomite alteration. This feature is not the result of localised remobilisation around the silica-dolomite body because the grade distribution that defines it is continuous through the entire Zn-Pb-Ag orebody. Rather, it may reflect more widespread fluid-assisted remobilisation and/or syntectonic mineralisation. The proximity of the Zn-Pb-Ag ores to copper orebodies, the lack of overprinting between them, their common geometries and association with structures, and metal zonation patterns in the Zn-Pb-Ag orebodies that are centred about the copper orebodies may be interpreted as evidence of syntectonic mineralisation or in terms of remobilisation. On one hand, McDonald (1970) reported enrichment of galena in the hinge of a fold exposed in the underground workings and attributed this to remobilisation. However the patchy distribution of the highest grade contour of Pb+Zn (%) is not reflected in lower orebodies and the lead distribution, which should be the most sensitive to the enrichment of galena during folding, shows no indication of being deformed. Perkins (1997) argued the features described by McDonald (1970) could equally be interpreted as evidence for D_4 mineralisation because there was no corresponding depletion on the limbs of the fold.

The results of this study support the observations of Myers et al. (1996) and Perkins (1997) who showed that Zn-Pb-Ag orebody boundaries are parallel and coincident with large D_4

folds. Marshall and Spry (2000) and McClay (1979) alternatively suggest that the D_4 trends in the orebody reflect the structural controls on pre-existing syndiagenetic mineralisation, i.e. D_4 controlled by syndiagenetic structures.

A synsedimentary origin for the present geometries of the lenses can be excluded because reconstructions of the predeformation orientations are not consistent with this mode of formation. The enveloping surface to the initial stack of lenses in a synsedimentary setting was determined by rotating bedding to horizontal using a 59º clockwise rotation along the rotational axis to 006º and applying the same rotation to the present enveloping surface of the en echelon array of lenses (Fig. 14a). It was found that this surface would have dipped 46º to 222º. In this case, the orientation of the enveloping surface would reflect the structural controls on basin development in a synsedimentary environment or the structures controlling emplacement of the ores during diagenesis. The location of the highest total metal grades along the WSW enveloping surface indicates that sulphides would have accumulated on the NE block of a SW-dipping fault that was the conduit for metal bearing fluids. If the orebody formed in a basin then the controlling structures must have had reverse movement, as shown in Figure 14b, which is inconsistent with the interpreted synsedimentary rift setting (e.g., Smith, 1969; 2000; Large et al. 1998; Cooke et al., 2000). Alternatively, if the basin margin faults had normal displacement then sulphides would have had to accumulate and be preserved on highs, which is unlikely (Fig. 14c).

The preservation of older F_2 folds in nearly their original orientations in F_4 short limbs areas (Fig. 6) indicates that these NNW-SSE-striking F_4 folds formed by rotation of bedding on the long limbs. This would require localised progressive shearing on the long limb and around the high grade shoots if the orebodies were present in their current positions prior to D_4. This is inconsistent with the expected localisation of deformation in the massive sulphide bodies rather than around them (Marshall and Gilligan, 1987, 1993).

Orebody formation during deformation can involve either syndeformation mineralisation or remobilisation of pre-existing massive, semi-massive, or disseminated sulphides or a combination of these processes (Marshall et al., 2000). It is arguable as to whether remobilisation can ever be entirely ruled out in orebody formation (Marshall and Spry, 2000; Marshall et al. 2000). However, without evidence of a pre-deformation deposit remobilisation is difficult to substantiate. In any case, the results of this study suggest that the Zn-Pb-Ag mineralisation was broadly synchronous with the late stage copper orebodies.

There is no indication of a source deposit overlapping with the Zn-Pb-Ag lenses in the large scale metal distribution patterns. However, this does not discount the possibility that a source deposit in the vicinity was of a grade too low to be recognised in these patterns. A small

low grade population, as indicated in Figure 13 may be an indication of an earlier low grade and possibly disseminated Zn-Pb-Ag deposit overlapping with the present orebody. However, this low grade mineralisation follows an F_4 trend (Fig. 13b and c), and is only obvious in one of the ten Zn-Pb-Ag lenses. It is therefore more likely that the low grade population reflects the same structural controls on metal deposition exhibited by the main orebody.

If remobilisation processes played a role in the formation of the Mount Isa Zn-Pb-Ag lenses, based on the observations of this study the source would have been distal to the present orebody. The termination of the Urquhart Shale against the Paroo Fault below the copper orebodies (cf. Figs. 2b and c) and the lack of zinc or lead anomaly in these orebodies indicate that a source deposit for the present Zn-Pb-Ag orebody was not located between the current Zn-Pb-Ag ores and the Paroo Fault. The other possible location for an external Zn-Pb-Ag protore is north of the Mount Isa fold and present Zn-Pb-Ag deposit, which requires fluid flow in the opposite direction of the copper mineralising fluids (cf. Waring, 1990) to form the present Zn-Pb-Ag orebody.

F_4 short limbs containing older folds at the centre of high grade shoots were important in the localisation of metals in the Zn-Pb-Ag orebody. These are interpreted to have behaved as structural heterogeneities that were centres of strain incompatibility during D_4 and resulted in dilation which facilitated fluid movement into these areas where metals were then deposited. These folds occur throughout the Zn-Pb-Ag orebody but those closest to the copper orebodies have the highest grade, indicating decreasing metal deposition away from the copper orebodies as fluids became progressively depleted in ore metals and/or concentration of fluid flow near the copper orebodies. Strain localisation in less competent units played an important role in the formation of this deposit in two ways, it permitted the fluids access to only specific parts of the rock producing the stratiform ores at low grades and secondly, structural heterogeneities formed by unevenly distributed deformation within those units concentrated metals into high grade shoots. Where early F_2 folds are located on the short limbs of the F_4 folds, the structural heterogeneity likely enhanced fluid flow and promoted the formation of high grade shoots. Where the older F_2 folds were absent, such as in the Mount Isa fold, there was no heterogeneity and high grade shoots were not developed.

Acknowledgements

The author gratefully acknowledges his supervisor, Prof. Tim Bell, and associate supervisor, Dr Andrew Allibone, in this study. Drs. Tom Blenkinsop and Tim Baker provided valuable comments on the manuscript. Funding and data were provided by MIM Limited; Alice Clarke, Steve Law, Ron Eggins and the Lead Mine Geologists are especially thanked. Micromine Pty Ltd and Surpac Software International Pty Ltd contributed software used in the study. This paper benefited significantly from the reviews and suggestions of Drs. Cees van Staal (Geological Survey of Canada) and Mike Solomon (University of Tasmania, CODES) and the additional comments of the Editor and a member of the Editorial Board, for these the author is greatly appreciative.

Table 1. Summary of Cover Sequences

Sequence	Description	Age (Ma)	References
Cover Sequence 4	Basal Surprise Creek Formation; conglomerate, sandstone and siltstone. Thought to be deposited in an alluvial fan or shallow marine environment. Overlain by the shallow marine Mount Isa Group (which comprises siltstones and carbonates.	>1652	O'Dea et al. (1997)
Cover Sequence 3	Basal conglomerate and sandstone of the Bigie Formation overlain by the bimodal Fiery Creek Volcanics	1710-1709	O'Dea et al. (1997)
Cover Sequence 2	Basal Bottletree Formation comprising bimodal volcanic and clastic sedimentary rocks overlain by the Mount Guide Quartzite then the extensive basaltic Eastern Creek Volcanics (up to 6 km thick) and clastic sediments and carbonates of the Myally Subgroup and Quilalar Formation.	1790-1760 or 1720	Blake and Stewart (1992) O'Dea et al. (1997).
Cover Sequence 1	Felsic Leichhardt Volcanics that are coeval with the Ewen and Kalkadoon Batholiths. Related to the Barramundi Orogeny rather than rifting.	1870-1850	Blake and Stewart (1992)
Basement	Yaringa Metamorphics in the Western Fold Belt, Kunbayia Migmatite in the Kalkadoon-Leichhardt Belt.	1890-1870	Blake et al., (1990)

Table 2. Correlations between the Zn-Pb-Ag Lenses Used in This Study and The System of 'Orebodies' Used at the Mine.

Orebody[1]	Previously Defined Included Orebodies	Value of 80th percentile	
		Pb (%)	Zn (%)
B	0001, 0002	5.30	5.60
C	0005	5.80	6.80
D	0560, 5110	3.60	4.05
E	5200, 0006	4.60	6.30
F	0007, 0720	5.10	5.20
G	0008, 0009, 0010	6.10	3.80
H	0011, 1130	4.30	5.20
I	0012, 0013	4.00	5.80
J	1320, 1380	3.30	4.50
K	1312, 1314, 0014, 1410, 1430	5.30	5.95

[1] Zn-Pb-Ag Lenses are based on ten Pb+Zn peaks in the modelled grade distribution of level 12. (see Figs.4 and 7)

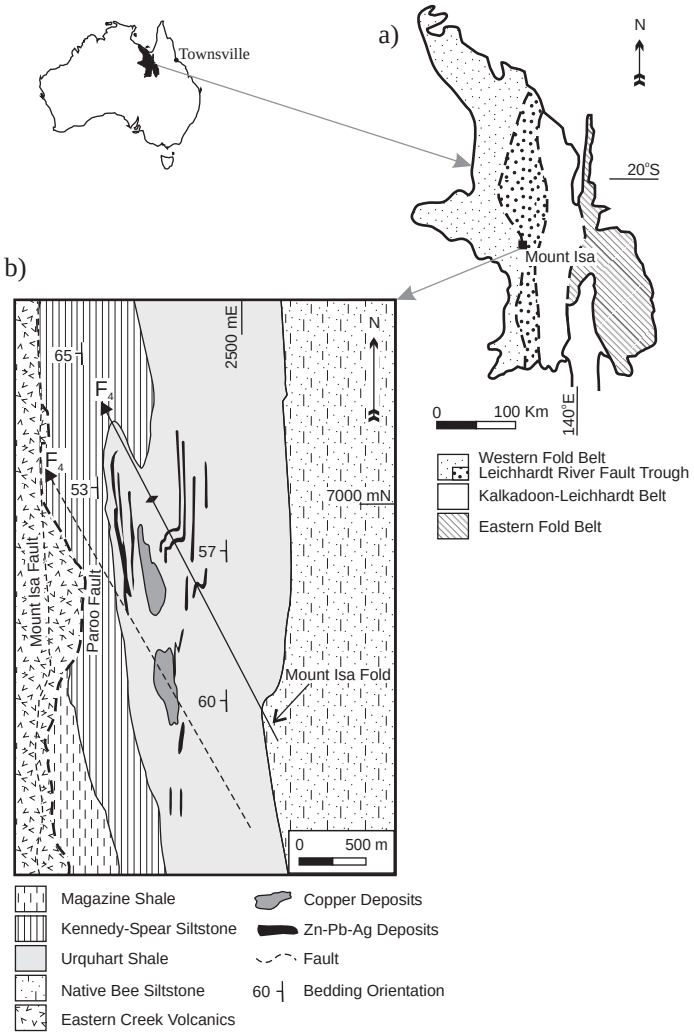

Figure 1. Locality map of the a) Mount Isa Inlier and b) Mount Isa deposit. Modified after a) Blake and Stewart (1992) and b) Perkins (1997).

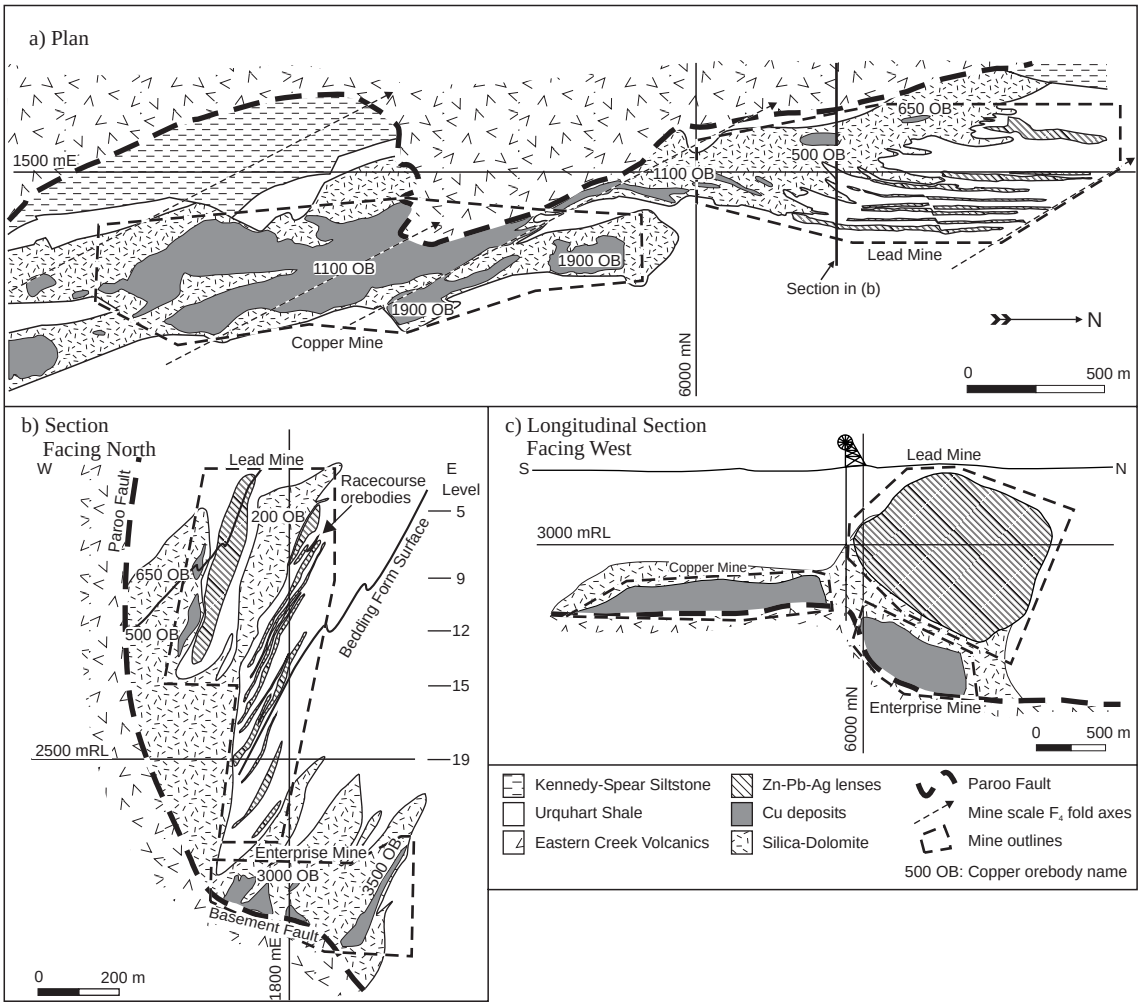

Figure 2. Mine layout and mine scale distribution of copper and Zn-Pb-Ag orebodies at Mount Isa. a) Level 17 plan showing deposit-scale separation between copper and Zn-Pb-Ag. b) Section looking north through 6510 mN intersecting the Lead and Enterprise mines and showing the geometry of the Paroo Fault (Basement Fault portion) below the deposits and the relationships between the fault, the orebodies and their associated alteration halos. Note that the Racecourse Zn-Pb-Ag lenses are vertically above the 3000 copper orebody. Both are located on the same limb of the Mount Isa fold and have the same geometries indicating a common deformation history. c) Longitudinal section looking west.

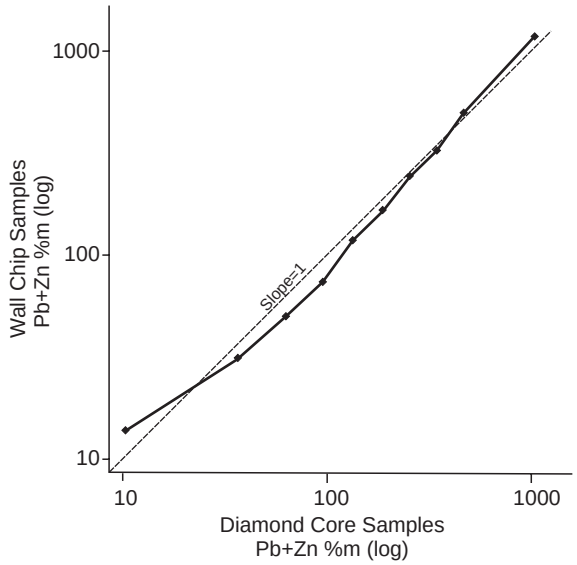

Figure 3. Log-log plot of wall chip and core samples in percent meters (%m), obtained by calculating the product of the average grade of individual intersections by the perpendicular width of the orebody. This plot compares deciles from each data source to determine biases based on the sample type (Isaaks and Srivastava, 1989). A data set with no biases between the variables being compared will plot as a straight line with a slope of 1. The deviation from the straight line demonstrates there is bias for higher grades in drill core compared to wall chip samples. There are over 514,000 samples in the data set.

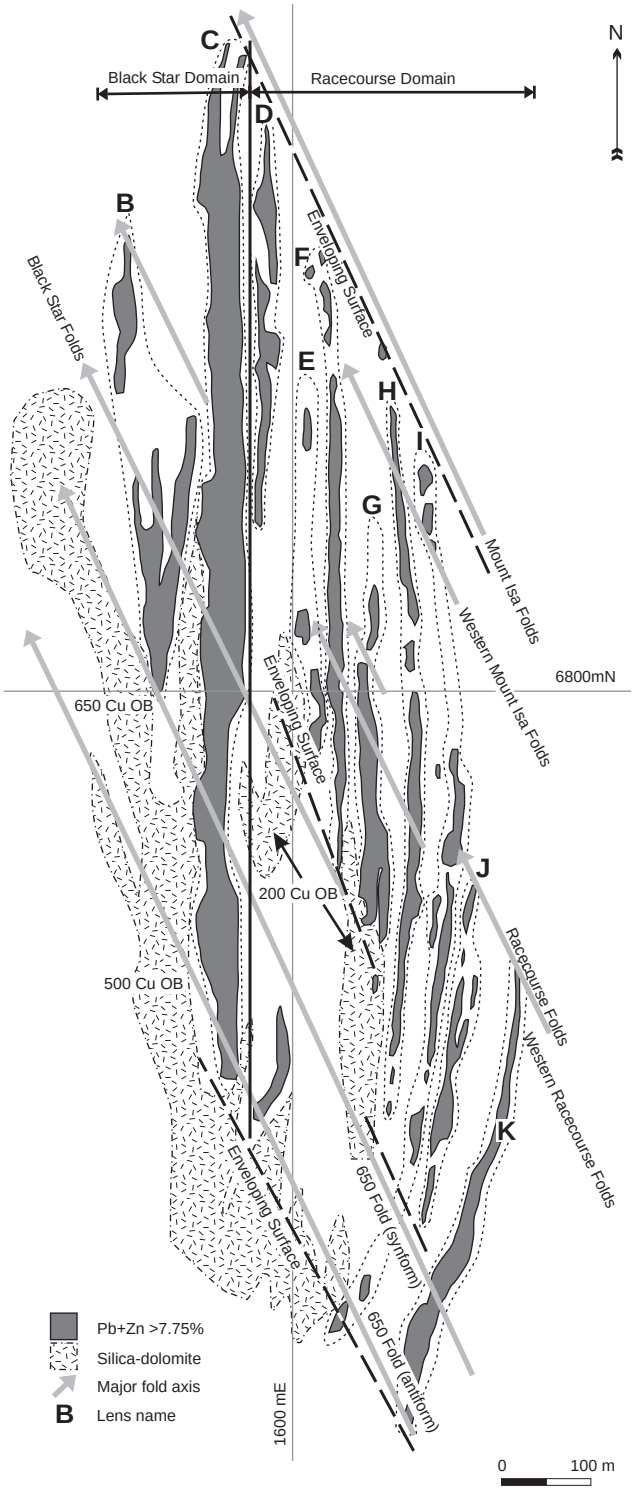

Figure 4. Level 12 (2910 mRL) plan of Pb+Zn > 7.75 % and silica-dolomite alteration in the Mount Isa Lead mine. Zn-Pb-Ag lenses are labeled B-K. Lenses B and C comprise the Black Star domain and lenses D-K the Racecourse domain. The silica-dolomite alteration halos to the main copper orebodies in the Lead mine occur on the WSW side of the Zn-Pb-Ag deposits. Major folds are labeled. See Figure 5 for structural measurements.

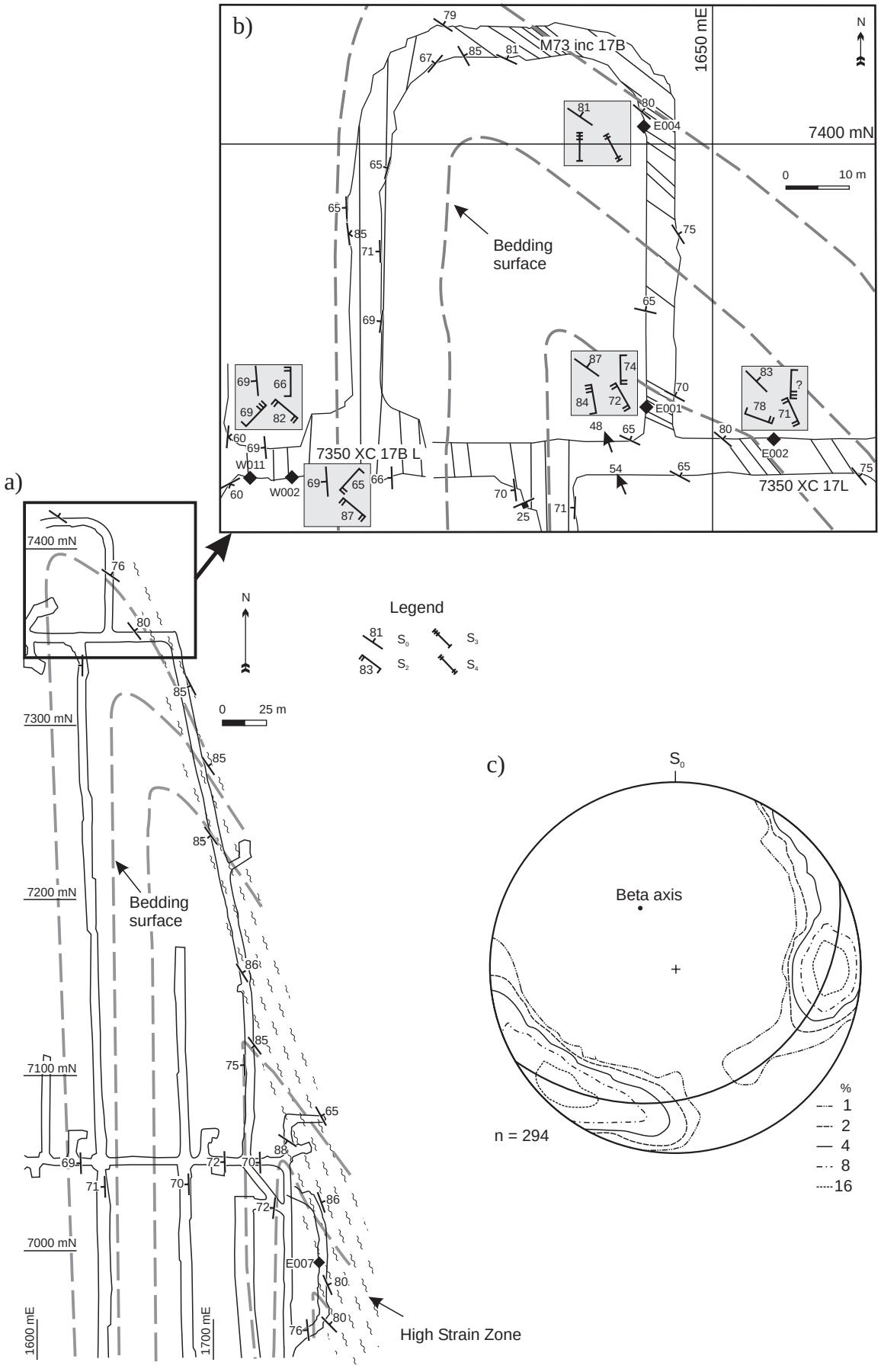
a)
b)
c)
7400 mN
7300 mN
7200 mN
7100 mN
7000 mN
1600 mE
1700 mE
1650 mE
M73 inc 17B
Bedding surface
7350 XC 17B L
7350 XC 17L
E004
E001
E002
E007
W011
W002
0 25 m
0 10 m
N
Legend
S_0
S_2
S_3
S_4
High Strain Zone
Beta axis
n = 294
%
1
2
4
8
16

Figure 5. a) Bedding plan in the Lead Mine at Level 9 (3080 mRL). NNW-SSE-striking fold zones are defined by bedding orientations that deviate from the dominant N-S to NNE-SSW-striking fabric. Fold zones are labelled and can be correlated throughout the mine. The inset lower hemisphere equal area projection shows poles to bedding and illustrates a spread of bedding orientation from N-S to NE-SW-striking. The girdle and axis are plotted. A modified Schmidt contouring method was used. b) Section oriented normal to the fold zones, along A-A'. From left to right the fold zones are, 650, Western Black Star (WBS), Black Star (BS), Western Racecourse (WR), Racecourse (R), Western Mount Isa (WMI), and Mount Isa (MI). Silica-dolomite alteration overlaps with the short limb areas, and high grade shoots are vertically above or below, or overlapping the folds.

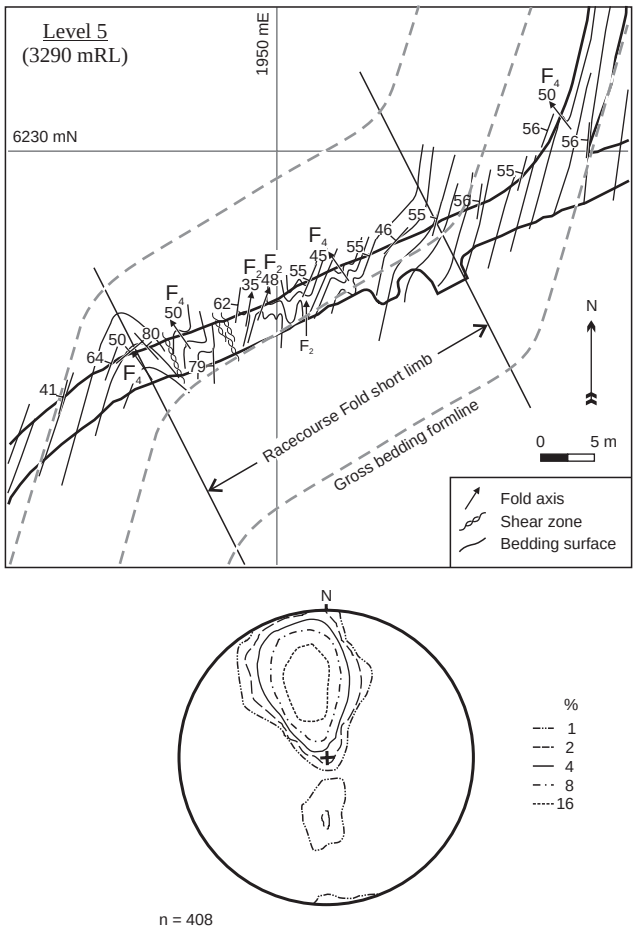

Figure 6. Cross cut (S61 NE XC) map of the Racecourse Fold Zone on the 5 Level. The fold zone is bounded by NNW striking F_4 folds. Within the short limb of the large asymmetric fold, folds of various orientations are preserved. Outside of the fold zone straight bedding persists. At this locality high grade Zn-Pb-Ag ore is confined to the short limb. An equal area projection of fold axes from short limb zones of mine scale NNW-SSE striking asymmetric folds shows a spread of orientations between NW-SE to NNE-SSW that reflect the different generations of folds in the area.

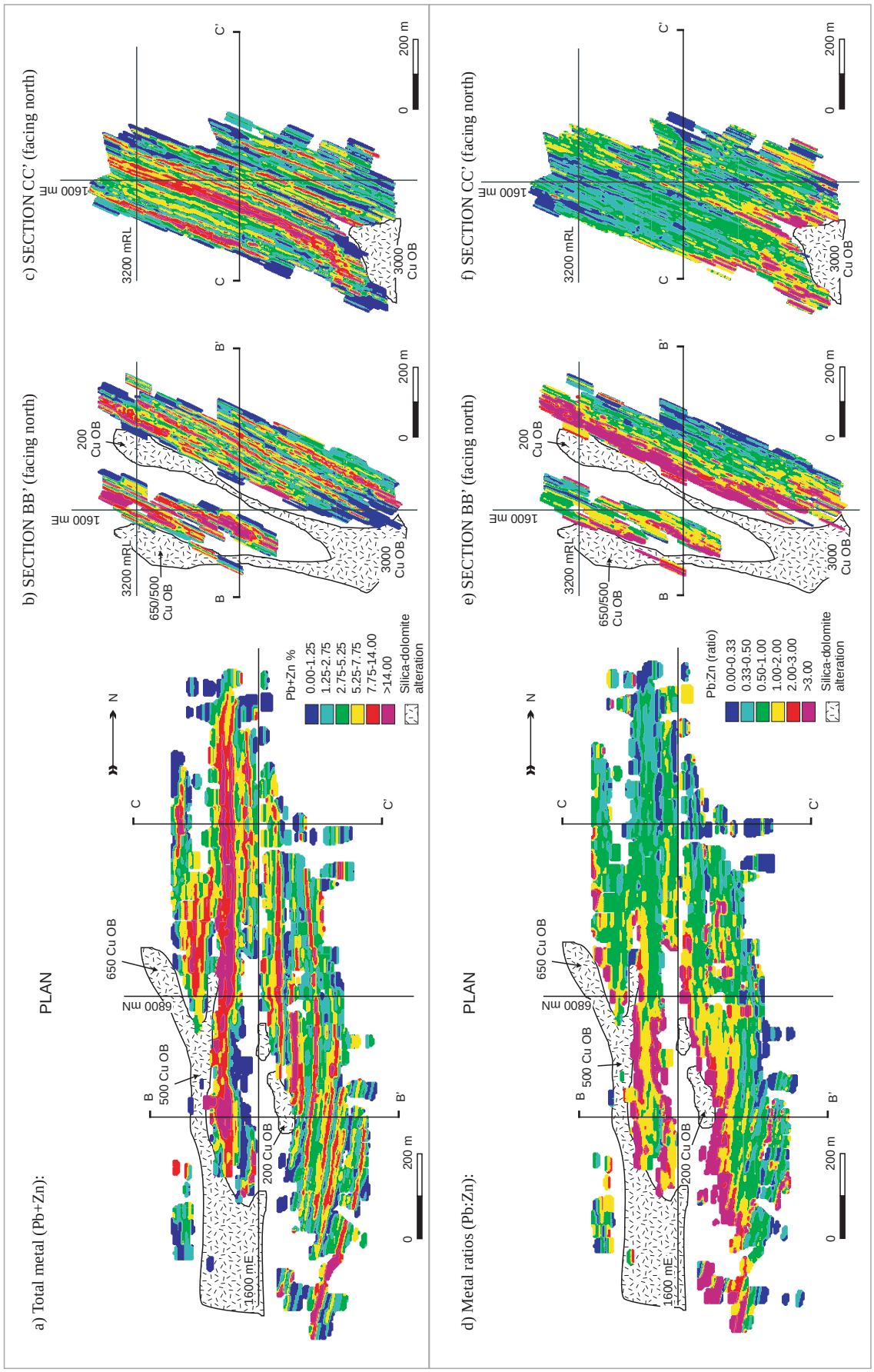
a) Total metal (Pb+Zn):
PLAN
N
650 Cu OB
6800 mN
B
500 Cu OB
200 Cu OB
1600 mE
C
C'
B'
0
200 m
Pb+Zn %
0.00-1.25
1.25-2.75
2.75-5.25
5.25-7.75
7.75-14.00
>14.00
Silica-dolomite alteration
b) SECTION BB' (facing north)
200 Cu OB
3200 mRL
650/500 Cu OB
3000 Cu OB
1600 mE
B
B'
c) SECTION CC' (facing north)
3200 mRL
3000 Cu OB
1600 mE
C
C'
d) Metal ratios (Pb:Zn):
PLAN
Pb:Zn (ratio)
0.00-0.33
0.33-0.50
0.50-1.00
1.00-2.00
2.00-3.00
>3.00
Silica-dolomite alteration
e) SECTION BB' (facing north)
f) SECTION CC' (facing north)

Figure 7. Modelled grade distribution plans (Level 12, see Fig. 4) and sections that display total metal content (a, b, and c) and the ratio of Pb to Zn (d, e, and f). Total metal (Pb+Zn) plots demonstrate the stratabound appearance of the Zn-Pb-Ag ores in these projections, whereas the metal ratio (Pb/Zn) highlights the transgressive nature of the metal distribution as well as the change in metal ratios in the Zn-Pb-Ag deposit with proximity to silica-dolomite which envelopes the copper orebodies. a) Total metal plan of Level 12. b) Section through the Lead Mine that includes the 650, 500 and 200 copper deposits (see Fig. 2b). c) Section that does not include a copper deposit within the Zn-Pb-Ag environment, however copper deposits are located below the base of the section in the Enterprise Mine (see Fig. 2b). d) Level 12 plan of metal zonation. The highest Pb/Zn values are clustered around copper/silica-dolomite bodies. e and f) Sections through Zn-Pb-Ag. Highest Pb/Zn values are adjacent to silica-dolomite bodies.

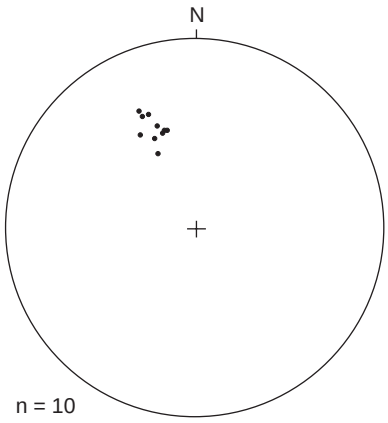

Figure 8. Lower hemisphere equal area projection of long axes of Zn-Pb-Ag lenses

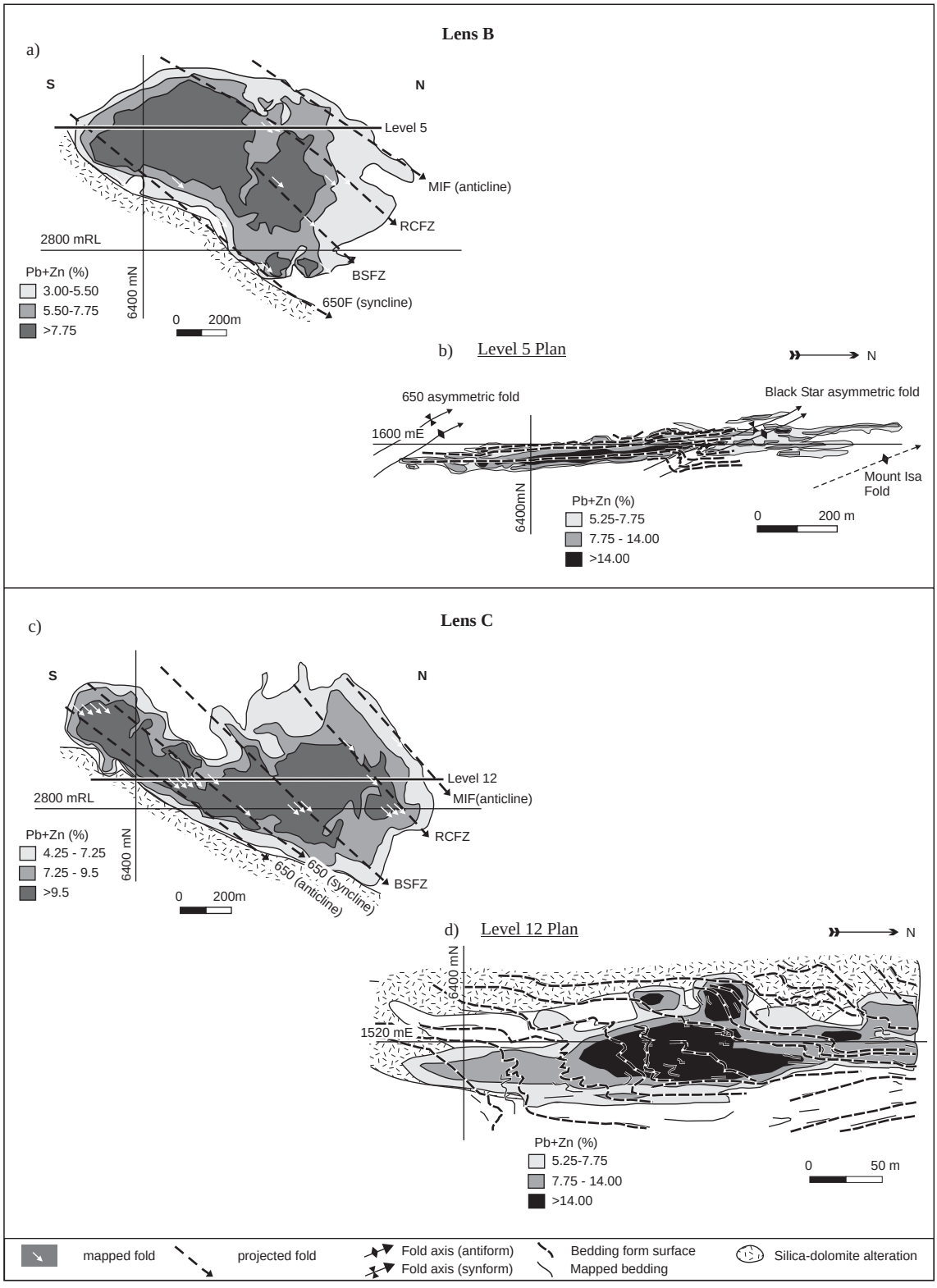
Lens B
a)
S
N
Level 5
MIF (anticline)
RCFZ
2800 mRL
BSFZ
650F (syncline)
Pb+Zn (%)
3.00-5.50
5.50-7.75
>7.75
6400 mN
0 200m
b) Level 5 Plan
N
650 asymmetric fold
Black Star asymmetric fold
1600 mE
Mount Isa Fold
6400mN
Pb+Zn (%)
5.25-7.75
7.75 - 14.00
>14.00
0 200 m
Lens C
c)
S
N
Level 12
MIF(anticline)
2800 mRL
RCFZ
Pb+Zn (%)
4.25 - 7.25
7.25 - 9.5
>9.5
6400 mN
650 (anticline)
650 (syncline)
BSFZ
0 200m
d) Level 12 Plan
N
6400 mN
1520 mE
Pb+Zn (%)
5.25-7.75
7.75 - 14.00
>14.00
0 50 m
mapped fold
projected fold
Fold axis (antiform)
Fold axis (synform)
Bedding form surface
Mapped bedding
Silica-dolomite alteration

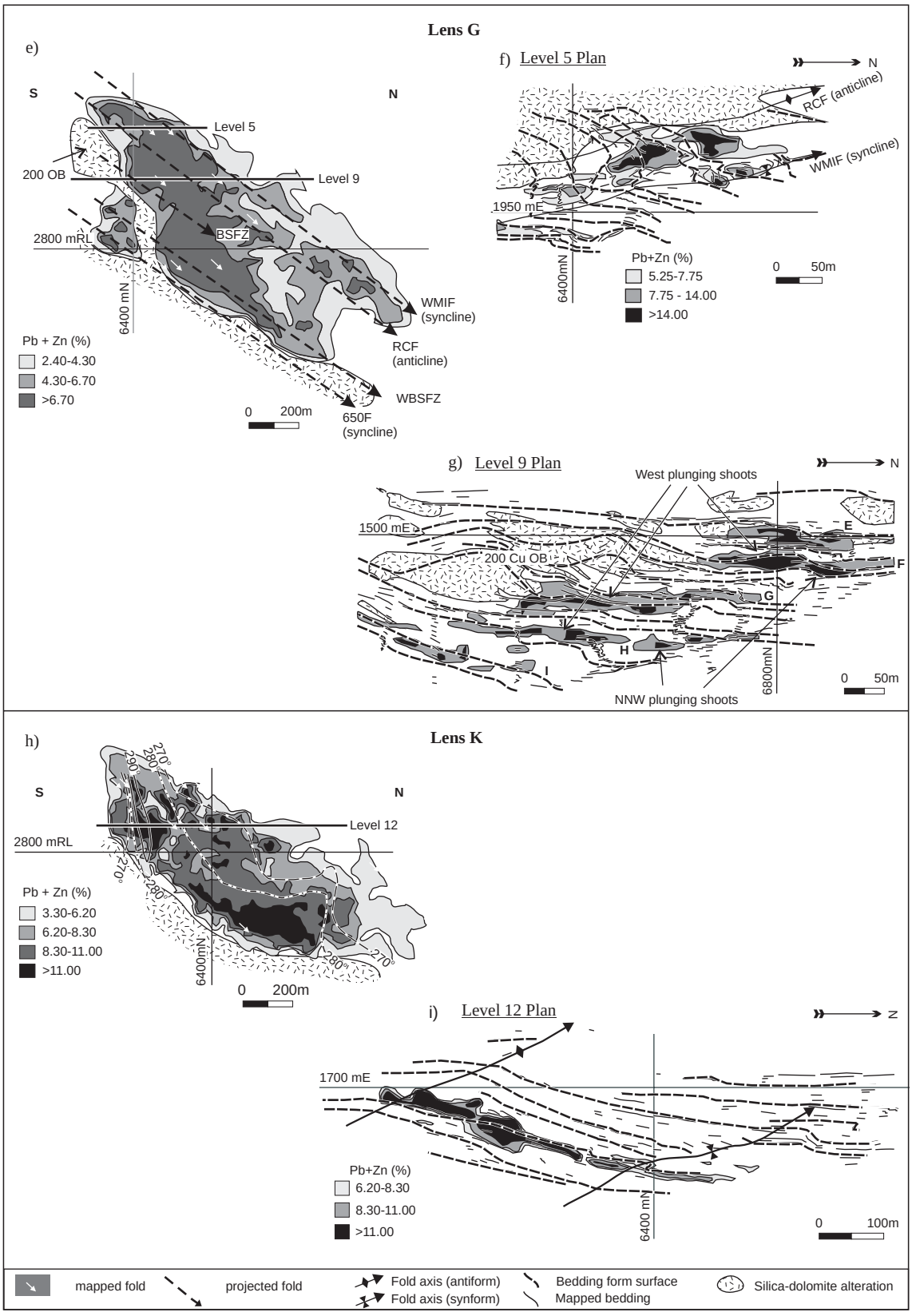
Lens G
e)
S
N
Level 5
200 OB
Level 9
2800 mRL
BSFZ
6400 mN
WMIF
(syncline)
RCF
(anticline)
WBSFZ
650F
(syncline)
0 200m
Pb + Zn (%)
2.40-4.30
4.30-6.70
>6.70
f) Level 5 Plan
N
RCF (anticline)
WMIF (syncline)
1950 mE
6400mN
Pb+Zn (%)
5.25-7.75
7.75 - 14.00
>14.00
0 50m
g) Level 9 Plan
N
West plunging shoots
1500 mE
200 Cu OB
E
F
G
H
I
6800mN
NNW plunging shoots
0 50m
Lens K
h)
S
N
Level 12
2800 mRL
270°
280°
290°
6400mN
0 200m
Pb + Zn (%)
3.30-6.20
6.20-8.30
8.30-11.00
>11.00
i) Level 12 Plan
z
1700 mE
6400 mN
Pb+Zn (%)
6.20-8.30
8.30-11.00
>11.00
0 100m
mapped fold
projected fold
Fold axis (antiform)
Fold axis (synform)
Bedding form surface
Mapped bedding
Silica-dolomite alteration

Figure 9. Longitudinal sections looking west (left column) and plans of mapped structure superimposed on modelled grade (right column) that demonstrate the geometries of the Zn-Pb-Ag orebody and grade relationships to the regional deformation structures. The locations of the plans are indicated on the longitudinal sections. The four Zn-Pb-Ag lenses shown are representative of the variety of external and internal geometries present. Fold axes are shown in sections including MIF (Mount Isa Fold anticline), WMIFZ (western Mount Isa Fold Zone), RCFZ (Racecourse Fold Zone); BSFZ (Black Star Fold Zone), WBSFZ (Western Black Star Fold Zone), 650F (650 Fold); anticlines or synclines are indicated. The white arrows indicate measured fold axes. Percentile values were used to define contours so that Zn-Pb-Ag lenses of different grades can be compared. The grade contours for a), c) and e) represent the 20, 40 and 60th percentile values for the modelled data, and for h), the 20, 40, 60 and 80th percentile values. Contours of bedding orientation in h) show the relationship between bedding orientation and the grade of the ores in lens K.

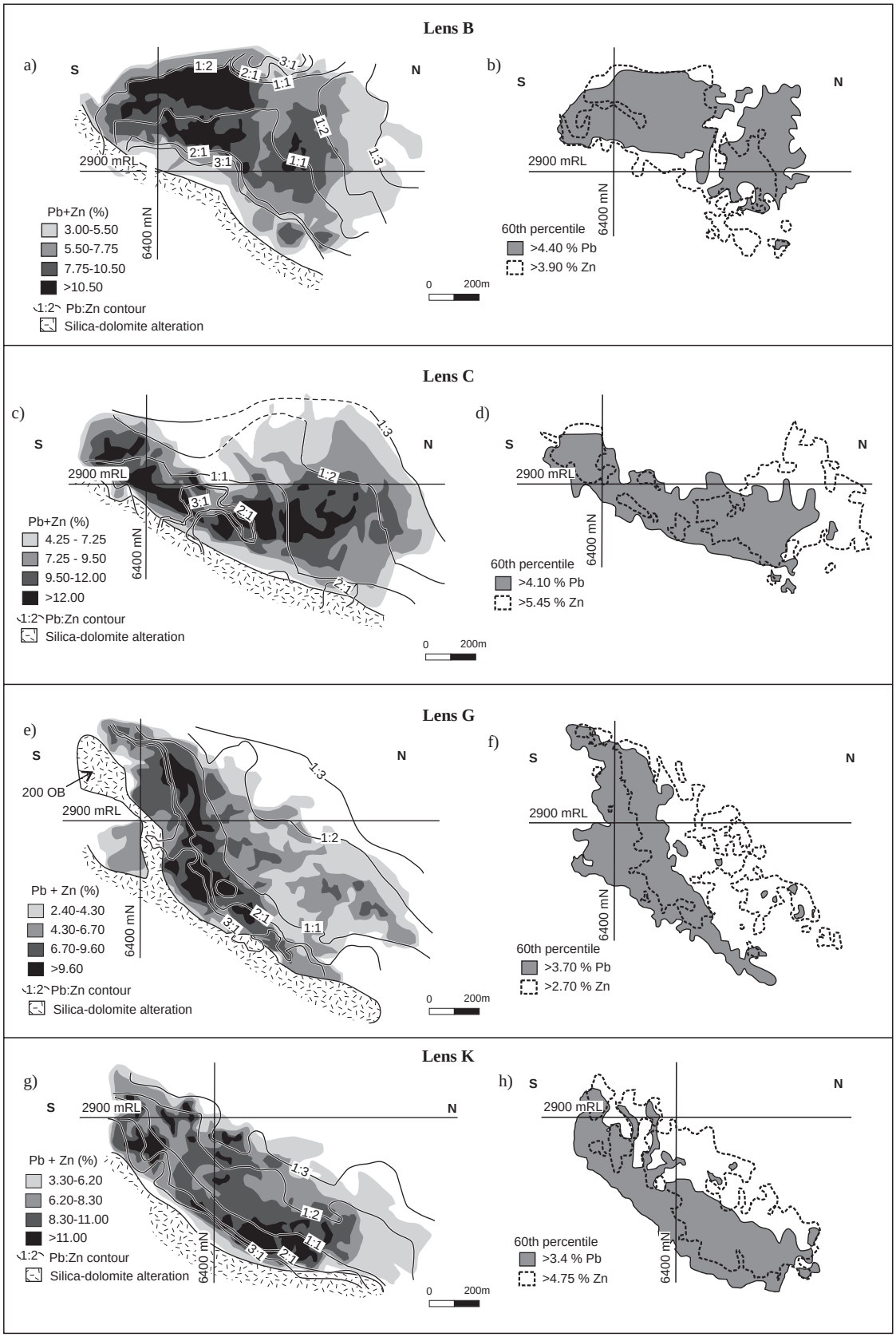
Lens B
a)
S
N
1:2
2:1
3:1
1:1
1:3
2900 mRL
6400 mN
Pb+Zn (%)
3.00-5.50
5.50-7.75
7.75-10.50
>10.50
1:2 Pb:Zn contour
Silica-dolomite alteration
0
200m
b)
60th percentile
>4.40 % Pb
>3.90 % Zn
Lens C
c)
4.25 - 7.25
7.25 - 9.50
9.50-12.00
>12.00
d)
>4.10 % Pb
>5.45 % Zn
Lens G
e)
200 OB
Pb + Zn (%)
2.40-4.30
4.30-6.70
6.70-9.60
>9.60
f)
>3.70 % Pb
>2.70 % Zn
Lens K
g)
3.30-6.20
6.20-8.30
8.30-11.00
>11.00
h)
>3.4 % Pb
>4.75 % Zn

Figure 10. Longitudinal sections illustrating Pb/Zn zonation patterns throughout the deposit (see also Figs. 12 b, c, f, g). Pb/Zn contours are superimposed on Pb+Zn grade and relative distributions of Pb and Zn (left column). Pb+Zn contours are the 20, 40, 60 and 80th percentile values for modelled data. In the right column longitudinal sections of the 60th percentile outlines lead (grey) and zinc (stippled) are used to compare their distributions. The similar shapes of the grade contours for the two metals suggests there is a systematic relationship between Pb and Zn in all cases.

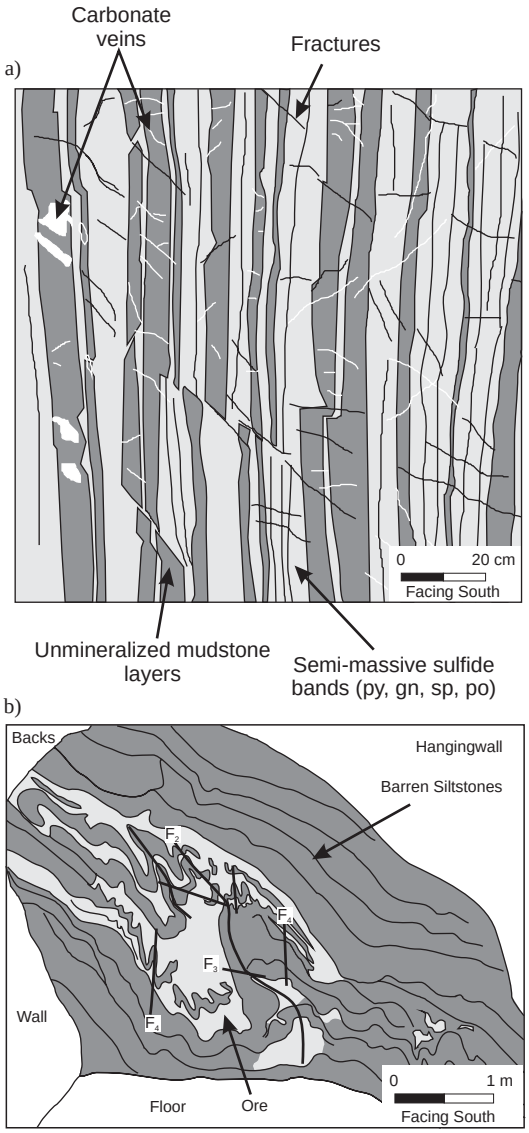

Figure 11. a) Sketch of unfolded Zn-Pb-Ag ore. Semi-massive sulfide bands (light grey) are interlayered with barren massive mudstones (dark grey). This exposure is within meters of the Mount Isa fold (0012 Orebody, M73 Decline, 17B Level, Mount Isa Lead Mine). b) Sketch of development face (14CA, 2445 mRL and 6527 mN) showing a high grade shoot cantered on large F_2 and F_4 folds that are situated between barren unfolded massive mudstones. This face is located in a NNW plunging shoot in orebody K and is typical of fold-cantered, high grade shoots that define the internal geometries of the Zn-Pb-Ag ores.

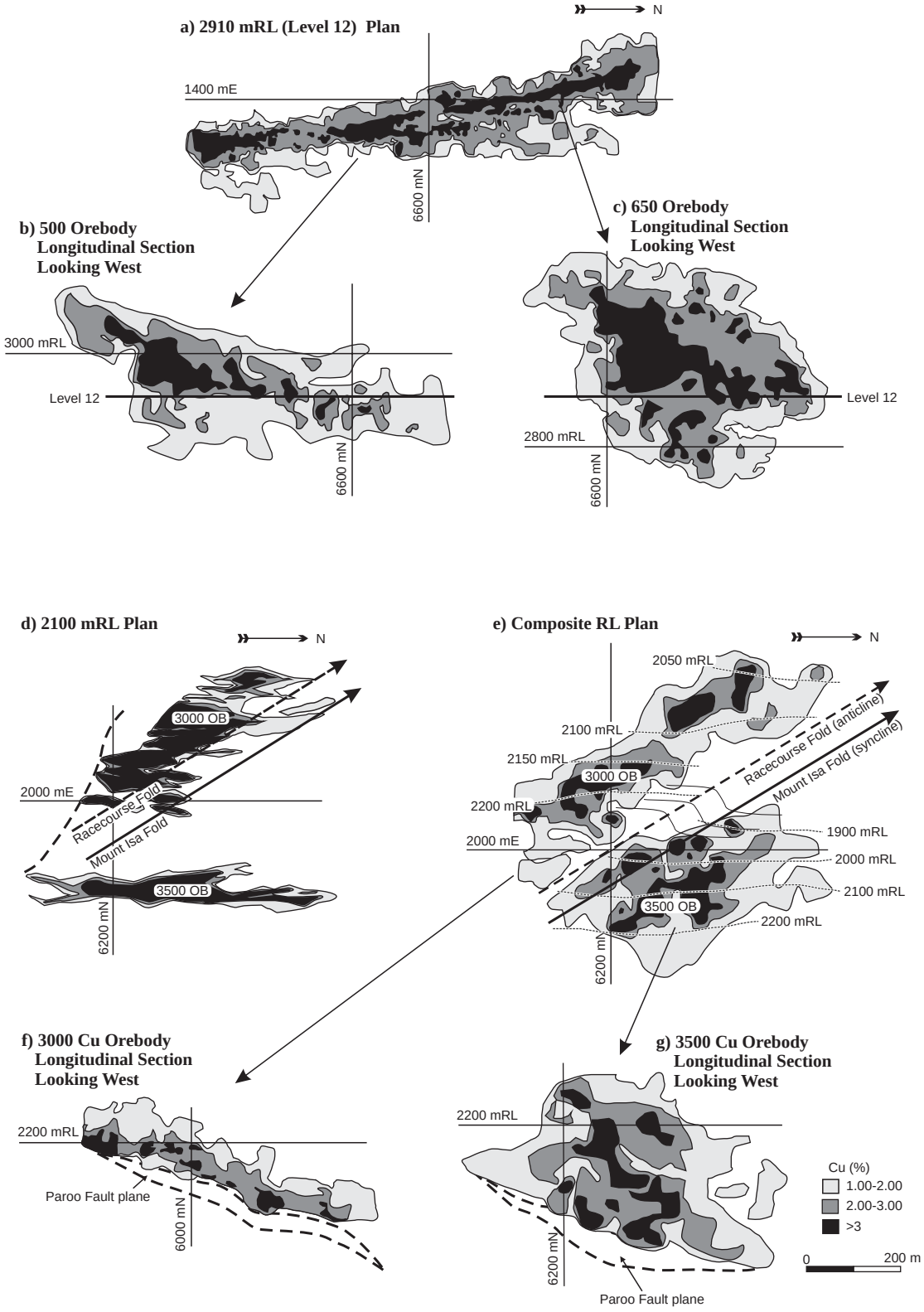
a) 2910 mRL (Level 12) Plan
N
1400 mE
6600 mN
b) 500 Orebody
Longitudinal Section
Looking West
3000 mRL
Level 12
6600 mN
c) 650 Orebody
Longitudinal Section
Looking West
Level 12
2800 mRL
6600 mN
d) 2100 mRL Plan
N
3000 OB
2000 mE
Racecourse Fold
Mount Isa Fold
3500 OB
6200 mN
e) Composite RL Plan
N
2050 mRL
2100 mRL
2150 mRL
3000 OB
Racecourse Fold (anticline)
Mount Isa Fold (syncline)
2200 mRL
1900 mRL
2000 mE
2000 mRL
2100 mRL
3500 OB
2200 mRL
6200 mN
f) 3000 Cu Orebody
Longitudinal Section
Looking West
2200 mRL
Paroo Fault plane
6000 mN
g) 3500 Cu Orebody
Longitudinal Section
Looking West
2200 mRL
6200 mN
Paroo Fault plane
Cu (%)
1.00-2.00
2.00-3.00
>3
0
200 m

Figure. 12. Level plans (a, d, e) and longitudinal sections (b, c, f, g) indicating the geometries of the copper orebodies. a) Individual level plan (2910 mRL) of the 500/650 orebody. b) Longitudinal section of the 500 orebody (N-S-striking). c) Longitudinal section of the 650 orebody (NNW-SSE-striking). d) Single level plan of the 3000 and 3500 orebodies at 2100 mRL (Enterprise Mine), and e) Composite level plan showing the dipping orebody from above. Broken lines are level contours. This plan differs from d) which shows the grade distribution of a slice at a specific level through the orebody. f) and g) Longitudinal sections of the 3000 and 3500 orebodies respectively. The copper deposits have NNW-plunging geometries similar to that of the Zn-Pb-Ag orebodies. See Figs. 2 and 4 for locations of the copper orebodies.

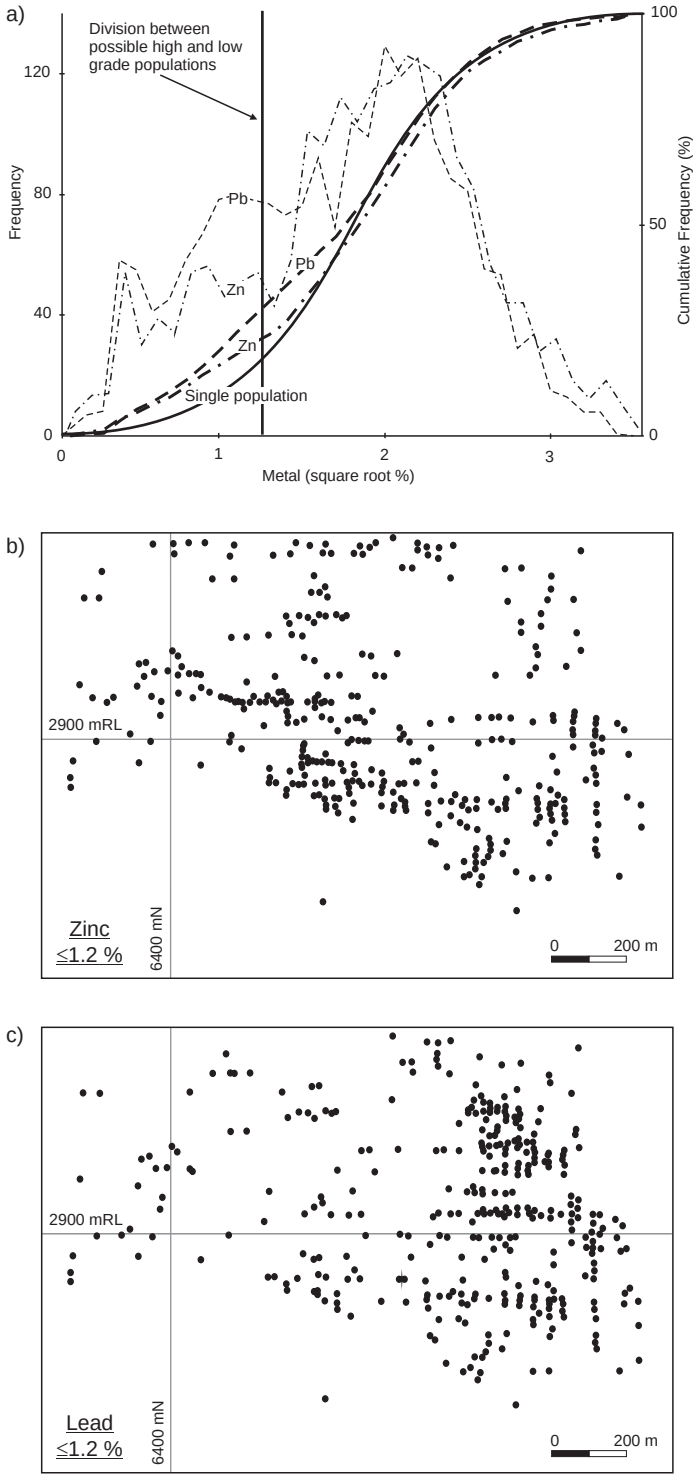
a)
Division between possible high and low grade populations
Frequency
Cumulative Frequency (%)
Pb
Zn
Pb
Zn
Single population
Metal (square root %)
b)
2900 mRL
6400 mN
Zinc
≤1.2 %
0
200 m
c)
2900 mRL
6400 mN
Lead
≤1.2 %
0
200 m

Figure 13. a) Cumulative frequency plots (heavy dashed lines) were examined to determine if multiple populations existed in the data that are not evident in the grade maps. The square root of metal values produces a close to normal distribution. Only the orebody B cumulative frequency curves are illustrated. The deviation of these from the solid curve, representing a single population, may indicate the presence of possible multiple populations in the data. Frequency histograms (light dashed lines) show peaks in the same area. The division between high and low grade populations is located where the histograms indicate the possible intersections of the populations, although there may be considerable overlap. Samples corresponding to a possible second population were plotted on indicator maps to determine their spatial distribution. b and c) show the distribution of the low grade samples (zinc and lead concentrations =1.2%) in longitudinal projections looking west. Zinc poor samples group as a north plunging cluster at deeper level and lead poor samples cluster in the north with a north plunging upper surface.

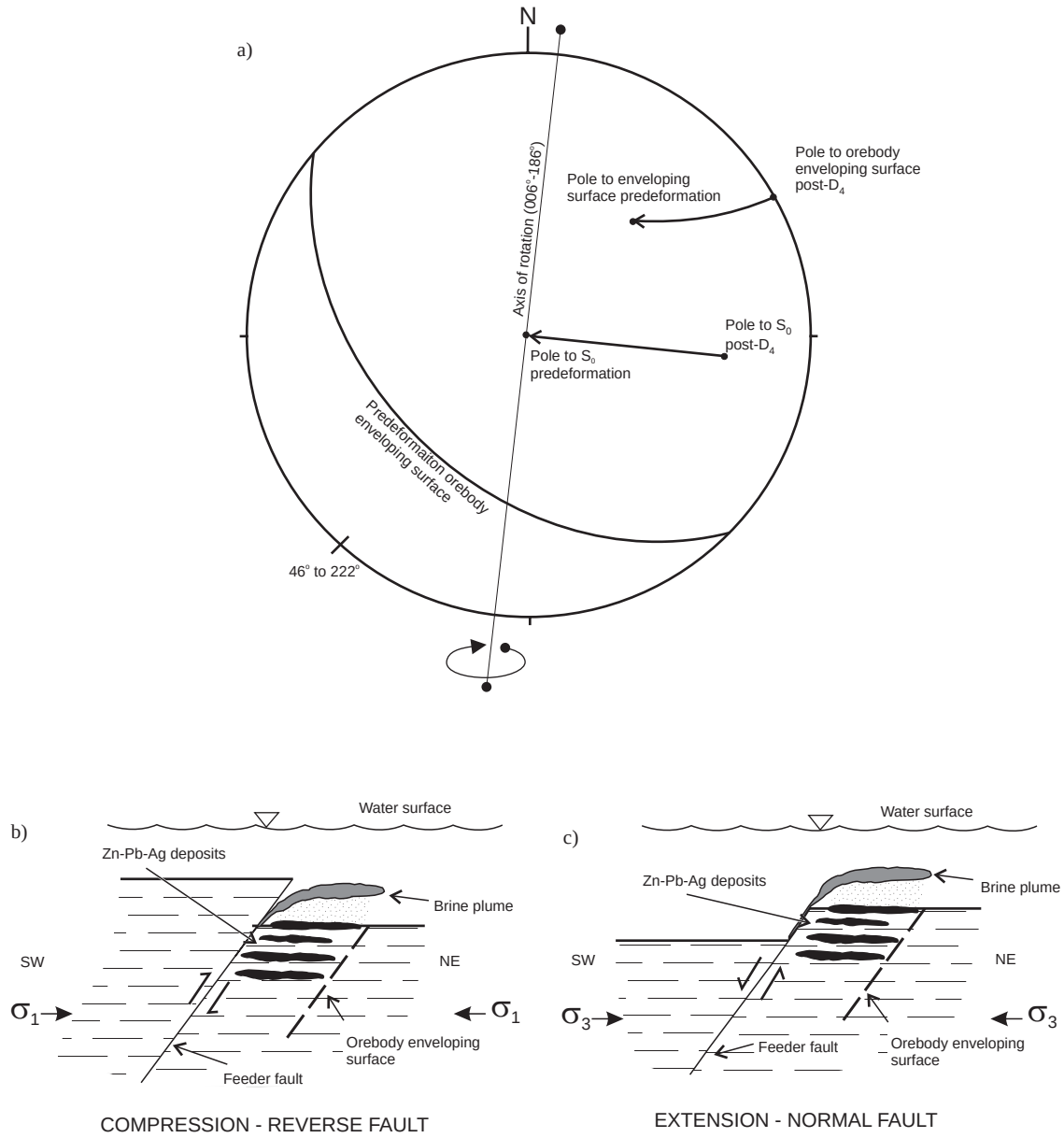

Figure 14. Reconstruction of hypothetical predeformation deposit geometries. a) Equal area projection of rotations applied to attain predeformation geometries. The great circle represents the enveloping surface of a hypothetical predeformation deposit and constrains the orientation of faults that might have controlled mineralisation. b and c) Illustrations of the two possible scenarios for predeformation mineralisation taking into account the geometric constraints imposed by deposit feeder geometry. The scenario in b) requires compression to form a basin, whereas in c) accumulation and preservation of the ores must occur on highs, both of which are considered incompatible with synsedimentary processes.

Part B

The formation of NNW-plunging, asymmetric folds implicated in the formation of the Mount Isa Cu and Zn-Pb-Ag orebodies.

The formation of NNW-plunging, asymmetric folds implicated in the formation of the Mount Isa Cu and Zn-Pb-Ag orebodies

Abstract

Asymmetric folds that are intimately associated with the development of the Zn-Pb-Ag and copper orebodies in the Mount Isa Lead Mine were examined and found to have formed over several deformations (D_3 and D_4). The mechanism of folding provides insights into dilation mechanisms that led to orebody formation. Folds with vertical NNW-SSE-striking axial planes were initiated from zones affected by localised horizontal shearing during an earlier deformation event. These initially horizontal folds were tightened significantly during D_4 by opposite shear senses operating on either limb along the actively developing axial planar foliation, S_4. Shearing along S_4 in the long limb domains reflects the bulk shear sense for this deformation. The shear sense operating along S_4 on the minor limbs of asymmetric folds was caused by the presence of a D_3 high strain zone. Reactivation of the D_3 high strain zone and bedding surrounding it in D_4, prior to establishment of the axial plane cleavage in the short limb domain, imposes a clockwise sense of rotation (looking north), which is opposite to that along the actively forming foliation in the long limb areas. The continuity of folds is related to the scale of competency domains controlling localisation of the fold initiating shear band in D_3. A general model for folding is presented in which alternate limbs of folds form in different deformations. Fold limbs should be viewed as shear domains with fold hinges forming from strain gradients near the margins of domains belonging to separate deformations with one determining the location of the fold.

Introduction

Folding is an important process in the formation of many ore deposits including Bendigo in Victoria (Forde and Bell, 1994), Ashanti in Ghana (Allibone et al., 2002), Elura in New South Wales (de Roo, 1989), and, Cosmo-Howley in Northern Territory (Matthäi et al., 1995). At Mount Isa folding has been found to have had an active role in the formation of the copper orebodies (Perkins, 1984; Swager, 1985; Bell et al., 1988) with a possible link to the Zn-Pb-Ag ores noted by Myers et al. (1986) and Perkins (1997). Recently, Davis (2004) was able to show that the formation of the Zn-Pb-Ag orebodies at Mount Isa was intimately linked to the development of NNW-SSE –striking folds, and not to pre-deformation processes as was previously thought (e.g. Love and Zimmerman, 1961; Neudert, 1981, 1986; Forrestal, 1990). Understanding the mechanism of formation of this fold should provide insights into mineralisation and ore forming processes at Mount Isa and may also be applicable to other ore deposits that are proximal to folds or high strain zones.

Recent studies by Adshead-Bell and Bell (1998) and Bell et al. (2003) have demonstrated that many large-scale folds form early in the deformation history and undergo continued development during all subsequent events. They found that cleavages folded around these structures do not necessarily indicate a late timing for the fold, but that such cleavages can form with the fold and be folded around it in the same event or subsequent deformations that tighten it. Interpretations based on large scale observations of simple fold geometries may overlook important steps in the deformation history. Microstructural studies can reveal complexity not apparent at a larger scale and are consequently extremely useful in determining the deformation history of an area.

The aim of this study was to determine how the folds that control the metal distribution in the Mount Isa base metal deposit formed, and to accurately link this to the deformation history using a microstructural analysis of the host rocks. This work focuses on the Mount Isa fold in particular, which is a large NNW-plunging, ENE-verging asymmetric fold situated along the northern margin of the Zn-Pb-Ag orebody. This fold is the best exposed example of a series of similarly oriented smaller folds that are implicated in orebody formation (Part A).

Background

Mount Isa is located on the western margin of the Leichhardt River Fault Trough in the Mount Isa inlier, Queensland, Australia (Fig. 1). Base metal ores are hosted by the Urquhart Shale, which is an early Mesoproterozoic fine grained and dolomitic sedimentary sequence.

Rocks in the study area are unmetamorphosed or at most metamorphosed to lower greenschist grades. Deformation of the Urquhart Shale occurred in the Isan Orogeny (1610-1500 Ma) and is well documented throughout the region (Page and Bell, 1986; Winsor, 1986; Xu, 1996; Bell and Hickey, 1998; Mares, 1998; Rubenach and Barker, 1998).

The nature of D_1 is controversial. Holcombe et al. (1991), Passchier (1986) and Passchier and Williams (1989) argue in favour of extensional style tectonics, whereas, Bell (1983; 1991) and Bell et al. (1992) propose N-S-directed horizontal compressional deformation involving thrusting. Bell and Hickey (1998) labelled D_1 a N-S-shortening orogeny to separate it from subsequent deformations that are grouped in to a E-W-shortening orogeny.

There is remarkable similarity between the remaining deformation sequences reported across the Mount Isa Inlier (e.g., Xu, 1996; Bell and Hickey, 1998; Mares, 1998; Adshead-Bell, 2000). This deformation sequence is characterised by a series of alternate horizontal and vertical shortening events that are interpreted to reflect cycles of repeated crustal thickening followed by gravitational collapse (Bell and Hickey 1998). The first horizontal shortening event after thrusting is D_2, which produced folds with vertical N-S-striking axial planes (Page and Bell, 1986; Winsor, 1986; Bell et al., 1988; Mares, 1998; Rubenach and Barker, 1998). D_3 produced folds with horizontal axial planes and axial planar cleavages (e.g., Xu, 1996; Bell and Hickey, 1998). Folds with NNW-SSE-striking, vertical axial planes and axial planar cleavages are attributed to renewed E-W-directed horizontal shortening in D_4 (Xu, 1996; Bell and Hickey, 1998). These main deformations are variably followed by further alternating horizontal and vertical compression events that are relatively weakly developed (Mares, 1998). The designation of deformations events varies slightly between workers. For example, Mares (1998) identified an event that produced a shallow-dipping cleavage after D_1 thrusting and before N-S folding, which she designated D_2. This deformation was not been identified in this study. Also, Bell and Hickey (1998) called the deformation forming a shallow-dipping cleavage between the N-S and NNW-SSE folding events $D_{2.5}$ because D_3 had already been assigned to the NNW-SSE fold forming event. Here the deformation corresponding to Bell and Hickey's $D_{2.5}$ is designated D_3 to avoid their cumbersome nomenclature and the later deformations are adjusted accordingly.

Host Rock Deformation Styles

The Urquhart Shale comprises interbedded carbonaceous shales, pyritic shales, massive siltstones and mudstones, base metal sulphide-bearing bands, and so-called tuffaceous marker beds (Fig. 2). The most abundant rock types are the carbonaceous shales, pyritic shales and

massive siltstones and mudstones. These are of interest to this study because they define competency domains that have implications for deformation localisation and, ultimately, folding.

Carbonaceous shales and pyritic shales have well developed closely spaced crenulation cleavages. These cleavages can be recognised through the wavy habit of the carbonaceous seams (Fig. 3a). Widespread recrystallisation or metasomatism, evident by the presence of neoform bands and nodules of carbonate and quartz with straight extinction, destroys the across layering continuity of cleavages in many places. Consequently, at micro-scales only single or groups of crenulation hinges are preserved, which can make it difficult to recognise crenulation cleavages and their overprinting relationships. However, correlation of these with well preserved cleavages in adjacent layers that lack neoform minerals confirms the overprinting relationships where continuity is disrupted by neoform nodules and bands.

Pyrite filled crenulation and crenulated cleavages in the pyritic shales form anastomosing seams in which several overprinting generations can be identified (Figs. 2c and 3b). As a result, it was found that these rocks preserve abundant crenulation cleavages that can be used to determine the deformation sequence. Linear seams consisting of 70-90% pyrite are differentiated crenulation limbs, and sigmoidal folia, 1-2 grains wide, between these correspond to crenulation hinges and contain less pyrite (30-70 %). The sigmoidal folia of pyrite are separated by fibrous quartz and carbonate. Some hinges contain patches of quartz and pyrrhotite. Pyrite in S_4 seams, which is the youngest cleavage to be overprinted by microcrystalline pyrite, is locally deformed.

Crenulation cleavages are rarely observed in the massive mudstone and siltstone rock types but where present they are faint and barely differentiated, which makes determination of the shear sense difficult (Figs 2d and 3c). Conversely, spaced disjunctive cleavages, mainly S_2, are well developed and correlate with crenulation cleavages in adjacent shales. Both morphological variant of S_2 lie axial planar to folds in interbedded siltstone and shale horizons (Fig. 4).

The main rock type groupings, shales (carbonaceous and pyritic variants) and the massive units (siltstones and mudstones), are the basis of the primary contrasting competency domains in the Urquhart Shale, which are best illustrated at hand specimen-scale (Fig. 4). The massive siltstones and mudstones are significantly less deformed, indicating they are the stronger rock types. Crenulation cleavages in less competent rock types curve into boundaries with the more competent massive siltstones and mudstones with which they are interbedded (Figs. 2c and 3).

Structural Relationships in the Mount Isa lead mine

Macro- to meso-scale relationships

The area contains N-S- to NNE-SSW-striking bedding traversed by numerous NNW-SSE-trending asymmetric folds (Fig 5). Some folds persist across the study area (through-going folds) and others do not (disharmonic folds). Through-going folds, such as the Mount Isa Fold, have very few or no mesoscale folds on their short limbs and tend to be located on the margins of the orebody. Disharmonic folds have abundant smaller scale folds on their short limbs and are located in the centre of high grade ore shoots (Fig. 6; Part A).

The Mount Isa fold is a NNW-plunging, NE-verging, asymmetric fold couplet with a vertical axial plane. It is located at the northern end of the Mount Isa Lead Mine where the anticlinal hinge is well exposed in the underground workings (Fig. 7). Extensive mine development in the Enterprise Mine, where copper ores are exploited vertically below the Lead Mine, exposes both the anticlinal and synclinal hinges of this fold (Fig. 8). In the Lead Mine, the Mount Isa fold has a short limb half-wavelength of 80 m, an interlimb angle of 64°, and S_0 on the short limb has an average orientation of 72E°/304°. There is a large (>5 m wide) NNW-SSE-striking high strain zone situated on the short limb (Fig. 7). In the Enterprise Mine, the distance between the hinges across the short limb of the Mount Isa fold is, for the majority of the exposed fold, at the higher end of the range of 80 to 135 m and the average orientation of S_0 is 52°W/037°. The interlimb angle is between 115° to 148°.

Four dominant fold orientations are present in the area. The rarest are folds with E-W-striking axial surfaces (Fig. 9). The other fold orientations are folds with vertical-dipping N-S- or NNW-SSE-striking axial planes and folds with near horizontal axial planes. An equal area projection of fold axes measured on the short limb areas of non through-going NNW-SSE-striking folds (Fig. 10a) displays a cluster between the NW-SE- and NNE-SSW with a few data outside of this range. Plunges range between 0-80º with a clustering around intermediate values. Two trends are subtly discernable in the main cluster of points of the equal area plot, but are more pronounced in a rose diagram, which shows folds with N-S- or NNW-SSE-striking axial planes (Fig. 10b). E-W-striking and NE-SW-striking folds form two populations in which there are only a few fold axis measurements.

The macro- to mesoscopic fold overprinting sequence, as determined from underground exposures, comprises D_1 folds with E-W-striking axial planes overprinted by N-S-striking F_2 folds (Fig. 9a). F_2 folds formed with vertical axial planes that were overprinted by the effects of D_3 and D_4 (Fig. 11). F_3 axial planes were initially horizontal and formed by localised top to the east shearing along S_3 on one limb, which rotated F_2 fold axial planes to west-dipping

orientations. F_4 axial planes remain vertical across the F_3 fold (Fig. 11) revealing their later timing. East-dipping F_3 axial planes were rotated by east block down shearing along S_4 at the locality illustrated in figure 11, which is several metres to the east of the anticlinal hinge of the Mount Isa Fold. The D_2-D_4 sequence of deformations formed during the E-W shortening orogeny as described by Bell and Hickey (1998).

High strain zones

Discrete zones of intense shearing strain are located throughout the mine sequence (Fig. 12). These structures are either N-S- or NNW-SSE-striking, and always steeply-dipping. Shear senses are difficult to determine because foliations within the high strain zones are commonly parallel to their walls. However, east block down displacements are common where shear sense can be determined. The largest of these shear bands are the Urquhart and Racecourse high strain zones. NNW-SSE-striking zones of shearing have only been mapped on the short limbs of the NNW-SSE striking folds, whereas N-S-striking ones are located on both the long and short limbs (Fig. 7).

Microstructural relationships

The Mount Isa fold was mapped and samples were collected for microscopic examination from numerous sites in the underground workings including the 7350 XC drives on the 17 and 17B levels and the M73, and P70 inclines which run between these levels (Fig. 7). The Racecourse fold (Fig. 6) is an example of a non through-going NNW-SSE-striking fold with numerous folds having various orientations on its short limb. Samples were collected across the short limb from an exposure in the S61NE cross cut on Level 5 of the mine. Three sequentially overprinting cleavages corresponding to D_2-D_4 were identified in the long and short limb domains with the main cleavage being S_4. Weak deformation post-dating these main cleavages includes rotation of S_4 by a vertical cleavage with east block down movement (S_6).

The orientations of cleavages were determined by measuring the pitch of each cleavage in a radial series of vertical thin sections (Fig. 13). On the long limbs bedding has an average orientation of 71W/000°, and the main cleavage, S_4, is 90°/338° with an east block up shear sense indicated by the differentiation asymmetry (e.g. Bell et al., 2003). The cleavage-bedding asymmetry indicates anticline to the east and overprints west-dipping and east-dipping cleavages. The west-dipping cleavage is S_3 and has an average orientation of 45°W/020°, a top to the east shear sense, and a shallower dip than bedding (Figs. 13a and 14). It is crenulated by S_4 and crenulates east-dipping S_2 cleavage. S_2 has the most variable orientation of all the cleavages identified but shows an east block up movement in long limb areas and an anticline to

the east vergence (Fig. 13a). Two planes fit the east pitching cleavage data, 48°E/165°and 65°S/189°. S_2 crenulates a bedding parallel foliation in shaly units and forms a prominent disjunctive cleavage in massive siltstones and mudstones and lies axial planar to folds with east dipping axial surfaces (Figs. 4 and 14).

The main cleavage on the short limb of the Mount Isa fold, S_4, is steeply west-dipping and NNW-SSE-striking with an east block down shear sense and cleavage-bedding vergence indicating an anticline to the west (Figs. 13b-c and 15). It crenulates two older east-dipping cleavages, S_2 and S_3. S_2 displays east block up movement and an anticline to the east vergence. S_3 shows an east block down displacement and an anticline to the west vergence. S_3 has the same shear sense and vergence as S_4. S_2 and S_4 are the shallowest and steepest dipping cleavages on the short limb of the Mount Isa fold with S_3 located between them. On the short limb of the Racecourse fold S_4 is west-dipping with a top to the east shear sense (Fig. 3a) and is rotated into a vertical cleavage with an east block up movement.

Discussion

Deformation history

The deformation history at Mount determined in this study is similar to that reported by Bell and Hickey (1998) and other workers throughout the region. Table 1 compared the deformation histories in the Mount Isa Inlier reported by selected previous, and that found in this study. Regional deformation commenced with N-S-shortening orogenesis as indicated by the oldest folds having E-W-striking axial planes and appears to support the thrusting model of Bell (1983, 1991). No evidence was found to corroborate the early extensional style tectonics proposed by Passchier (1986), Passchier and Williams (1989) and Holcombe et al., (1991). Folds with E-W-striking axial planes that are overprinted by F_2 folds were produced at this time. Subsequent E-W-shortening orogenesis was characterised by an alternating series of horizontal and vertical compressional events. This pattern of deformation indicates crustal thickening followed by gravitational collapse (Bell et al., 2003).

N-S-striking asymmetric folds with vertical axial planes formed in D_2. Consistent east block up shear sense along S_2 and cleavage-bedding vergence throughout the mine indicate a regional D_2 anticline to the east of Mount Isa. The cleavage identified as S_2 in this study differs from that of Swager (1985) and Perkins (1997). These workers labelled a bedding parallel carbonaceous seam S_2, but here it was found to be east-dipping, crenulated by S_3 and crenulating a bedding parallel seam, but is also commonly found to be rotated in to bedding parallel foliations indicating reactivation of bedding has occurred. The cleavage identified as S_2

in this study is axial planar to folds with east-dipping axial surfaces that are overprinted by F_3 and F_4. Observed orientations of S_2 and F_2 axial planes indicate they are deformed, but D_2 folds with vertical axial planes do occur in areas that are relatively unaffected by the younger deformation events.

The third regional deformation involved vertically directed compression and formed a horizontal crenulation cleavage with a top to the east shear sense. Reactivation, or shearing along a pre-existing foliation is a sense antithetic to the bulk shear sense (Bell, 1986), of bedding in D_3 rotated S_2 to an east-dipping orientation. This is an important detail because it allowed S_4 to form as a separate cleavage. If S_2 had been still vertical at the onset of D_4 it would have been reused and S_4 would not have developed. Reuse is when progressive shearing strain along an already existing foliation is synthetic is the same a the bulk shear sense. This definition of reuse is slightly different to that of Davis and Forde (1994), who first defined reuse as occurring

> "when the progressive shearing strain component in a subsequent deformation operates in a synthetic sense along pre-existing foliations in subsequent events."

D_4 involved the formation of a cleavage that is axial planar to the NNW-SSE-striking folds. S_4 has opposite shear senses on either limb of these folds. On the short limbs of the NNW-SSE-striking folds S_4 had east block down displacement with the opposite shear sense on the long limbs. Deformation after D_4 was much weaker than in the preceding events and was largely restricted to the short limbs of the NNW-SSE-striking folds. S_4 was first rotated to an intermediate west-dipping orientation by D_5, which involved vertical compression with bulk a top to the east shear sense. Then D_6 developed a local vertical cleavage, S_6, with an east block up shear sense.

Folding mechanism

Two mechanisms can explain the features of the NNW-SSE-striking folds. The first has the folds initiating in D_4 through the opposite shear senses acting along the actively forming axial planar foliation, S_4, on either limb during bulk shortening. During D_4, S_3 on the short limb was rotated by about 90° from its original horizontal orientation to be steeply east-dipping. However, S_2 was rotated more than this from a near vertical orientation to be overturned and steeply east-dipping at the end of D_4. In this model the high strain zone on the short limb forms by localization of D_4 strain.

An alternative to initial fold formation by shearing along S_4 only, is fold initiation in an earlier deformation involving localised rotation of bedding and S_2 into a shallow west-dipping or horizontal orientation in a shear band followed by rotation of this structure during D_4, and

significant tightening of the fold. In this model a horizontal high strain zone with top to the east shear sense formed during D_3 and was responsible for the rotation of d bedding plus S_2 to a shallower west-dipping orientations to a low angle with S_3 (Fig. 17). This is the preferred model for folding because it accounts for the shear sense on S_4 on the short limbs and the S_2 and S_3 relationships across the fold as well as the location of the fold. In the first model described, where the fold is initiated in D_4, there is no particular reason why shearing along S_4 should change from east block up to east block down across the hinge. The lack of heterogeneities in this model should either produce homogenous deformation or at most localised shear bands with an east block up displacement in the area of the fold, but neither these will produce the required fold geometry.

There are two distinct phases in the formation of the NNW-SSE-striking folds in the combined D_3/D_4 model (Fig. 17). The first is the development of horizontal D_3 shear bands in which S_2 and S_0 were rotated into a shallow west-dipping orientation
at a low angle to S_3 by top to the east shearing along that foliation in the high strain zone. Outside of the D_3 shear band, deformation was more coaxial with S_2 and S_3 remaining nearly orthogonal and concurrent east block down shearing on bedding rotating S_2 to be steeply east-dipping. This meant that S_4 was able to develop rather than simply reusing S_2 as D_2 and D_4 are closely oriented, being separated by only 15-20°.

Any structural model needs to account for the restricted distribution of the D_3 high strain zones to the short limbs of the NNW-SSE-striking folds. A lack of west-dipping high strain zones on long limbs indicates that S_3 shear bands are limited in extent and were not simple tabular structures indiscriminately folded in D_4 by east block up shearing along S_4. Rather, development of the short limbs of the folds id related to the presence of the horizontal high strain zones that are controlled competence domains in the rock. Competency domains are readily identifiable between the different rock types at the scale of individual beds to entire exposures with the shales, or shale dominated packages, being more deformed than the massive siltstones and mudstones. Domains are characterised at these scales by folding in the lower competency domains lying between unfolded stronger units. Different strain rates between contrasting competency domains causes strain incompatibilities along their boundaries that result in mechanical instabilities and the nucleation of shearing along domain margins (Goodwin and Tikoff, 2002). As a result the high strain zones curve into the boundary between adjacent competency domains as shearing along bedding increases. An interpretation of the D_3 high strain zone prior to D_4 is illustrated in figure 17. In this case the shear band is horizontal in the centre of the lower competency domain and rotated into the domain boundaries to form a sigmoidal structure. The same type of structure as that just described can be seen at a hand

specimen-scale between pyritic shale and massive siltstone in figure 2c.

Fold initiation in D_3 was followed by opposite shear senses on S_4 on either limb as was observed in the microstructural analysis. The short limb of the NNW-SSE-striking folds was formed by east block down displacement along S_4, which rotated the shear band to a steeply east-dipping orientation. East block up movement along the same cleavage created the long limb. The shear sense of S_4 on the short limb resulted from the presence of the D_3 high strain zone. In areas of steeply west-dipping bedding east block up shearing along S_4 dominates because this shear sense is most compatible with west block up shearing along S_0, resulting from its orientation relative to a horizontal maximum principal stress, plus the fact that it is the dominant anisotropy in the rock. However, from the onset of bedding reactivation deformation was partitioned producing two distinct domains of different deformation styles. In the vicinity of the D_3 high strain zone, bedding and S_2 are shallowly-dipping, at a high angle to the shortening direction and less likely to partition shearing strain. In these areas deformation will be largely coaxial so that there will be roughly equal numbers of opposite shear senses along the actively forming cleavage. As a result, the horizontal high strain zone will crenulate. Two domains will exist as a result of this partitioning. At this stage the this area was deforming more or less coaxially and is surrounded by rock experiencing non-coaxial deformation. Reactivation of bedding in the area outside of the coaxially deforming domain will impose a clockwise rotation, looking north, on the high strain zone. This rotation will enhance an east block down shear sense on S_4 in the vicinity of the D_3 shear band resulting in the formation of the short limb of the NNW-SSE-striking folds.

Post-D_4 deformation may have slightly tightened the NNW-SSE-striking folds in a manner similar to that described by Adshead-Bell and Bell (1998) and Bell et al. (2003). These workers found that large asymmetric folds underwent continued development through out the deformation history. At Mount Isa, deformations subsequent to D_4 are spatially partitioned into the short limbs of the NNW-SSE-striking folds, which may reflect the presence of a competency reducing feature.

This model accounts for large high strain zones, like the Racecourse Shear Zone, on the short limbs of NNW-SSE-striking folds. Localisation of shearing strain is a common feature of deformation at Mount Isa and is recognisable at a range of scales. N-S-striking, steeply-dipping high strain zones on the long limbs of the NNW-SSE-striking folds are interpreted to be D_2 structures and would have would have undergone reactivation from the onset of D_4 preventing them from being rotated in that deformation. The misorientation of these structures means that they would have been dilatant in D_4, which can explain the base metal mineralisation and alteration associated with them. Consequently, these structures may also have been significant

conduits in the transportation of fluids from the Basement fault.

The continuity of the folds was determined by the extent of the initiating shear bands and thereby defines the competency domains that were influential during folding. Folds that are continuous over shorter distances define competency domains at smaller scales than folds that are continuous over a greater distance. In this case, the Mount Isa fold represents a competency domain at least on the scale of the Urquhart Shale because it is continuous across this unit. Folds on the long limb of the Mount Isa fold, which host Zn-Pb-Ag high grade shoots, define competency domains within the Urquhart Shale. This relationship can be demonstrated down to microscale folding (cf. Figs. 4 and 5). The variability of the interlimb angle of the Mount Isa fold can be attributed to the varying effects of the D_3 shear band and shearing along S_4. Hinges are located close to the boundaries of the D_3 shear band. The larger interlimb angle close to the Paroo Fault suggests a decreased influence of the D_3 high strain zone and a position close to the edge of the competency domain.

NNW-SSE-striking folds hosting high grade ore shoots within the deposit are disharmonic at the mine-scale and contain older folds on their short limbs. Conversely, there is a paucity of smaller scale folds on the short limbs of NNW-SSE-striking folds at the periphery of the orebody, which are continuous at the scale of the orebody. These features can be explained by the size of the D_3 high strain zone. If the fold initiating shear band is significantly larger than pre-existing folds in the vicinity it will destroy them. On the other hand, a high strain zone smaller than the folds with which it overlaps will not be able to obliterate these folds in which case they will be preserved, though they will be at least partially deformed. Older folds will be preserved in more or less their original orientation distal to the shear bands and on the short limb of the fold where the horizontal shear band contained low strain areas, with the least deformation occurring near the hinges (Fig. 17). This also accounts for small high strain zones associated with high grade shoots, as illustrated in figure 6, compared to the much larger shear zones on the short limb of the Mount Isa fold. The preservation of older folds will result in variously oriented surfaces with the potential to dilate and form orebodies in D_4, whereas in the D_3 shear bands, rotated foliations and structural heterogeneities would be destroyed.

Evolution of the Paroo fault

The angle between S_2 and bedding is between 46° and 74° suggesting that bedding was dipping between 16°and 44°W at the beginning of D_2, which would have also been the dip of the western lateral ramp of the Kokkalukkanurker Duplex was identified by Bell (1991) (Fig. 16). This means bedding in the Urquhart Shale was steepened and the portion of the Meerenurker Thrust corresponding to the Paroo Fault below the deposit, against which the

Urquhart Shale terminates, was rotated to a shallower orientation subsequent to D_1 (Fig. 16). NNW-SSE-striking folds in the Paroo Fault under the Mount Isa deposit reported by Law (1999) indicate that D_4 played a major role shaping of the fault in this location.

The large interlimb angle of the Mount Isa fold close to the Basement fault, as mapped in the Enterprise mine, suggests that this locality is near to the end of the D_3 high strain zone. This may have implications for the generation of the shape of the Paroo Fault. It has already been shown that this structure had a steeper dip to the east prior to D_2, suggesting that the present shape of the Paroo Fault, shallowly east-dipping below the orebodies and changing to steeply west-dipping in the west, was not attained in D_1 as proposed by Bell (1991). The portion of the Paroo Fault below the mine containing NNW-SSE-striking folds reveals areas corresponding to the long limb domains are shallowly dipping to the NE, whereas short limb areas are steeply dipping. The microstructural kinematics of the NNW-SSE-striking folds suggests that the flat portions of the Paroo Fault have been rotated into their present orientation by east block up shearing along S_4. Conversely, the areas below the mine where the Paroo Fault is steeper correspond to the short limb domains where the opposite displacement along S_4 took place. Bell (1991) noted that the steeply west-dipping portion of the Paroo Fault on the western side of the deposit was folded by an F_4 fold, as was the flat section below the deposit, indicating that the steeply west-dipping orientation was attained before D_4. This model requires adjustment because bedding was shallower dipping before D_2. Specifically, the Meerenurker Thrust along the western lateral ramp of the Kokkalukkanurker duplex, which is actually the Paroo Fault, was steeply east-dipping after D_1 and only slightly overturned, and not greatly so as suggested by Bell (1983, 1991). Instead the extremely overturned nature was produced by the accumulation of later deformations. The steeply west-dipping orientation of the fault west of the deposit would not have eventuated in D_2 because the bulk shear sense in that event would have produced a shallower east dip. This points to this orientation being the result of clockwise rotation (looking north) in D_3 by top to the east shearing along the actively forming foliation with deformation being localised at a higher structural level than the flexure where the Paroo Fault changes from west- to east-dipping (Fig. 16c). This also indicates that the deposit is located in large D_3 strain domain at least at the scale of the mine, which contains localised areas fo higher strain represented by the folds already discussed. Further shallowing of the east dipping portion of the fault occurred in D_4.

Conclusions

NNW-SSE-striking asymmetric fold couplets with vertical axial planes, such as the Mount Isa fold, formed by the development of a horizontal shear band in D_3 that was rotated to a steep orientation in D_4 to form the short limb. The opposite shear sense on the axial planar foliation, S_4, on either limb could be interpreted to be the sole cause of folding but the restriction of the low angle relationship between S_2 and S_3 to the short limb is a critical feature in determining the origin of this fold. The small angle between these foliations suggests that a D_3 shear band is located on the short limb. The lack of a west-dipping high strain zones on the long limb suggests it was restricted to the minor limb. Without a heterogeneity in the vicinity of the short limb there would be no reason for S_4 to develop the opposite shear sense to that of the long limb.

The degree of continuity of the folds and the preservation of older folds on the short limbs is dependant on the dimensions of the horizontal shear band. The comparative sizes of the high strain zone and pre-existing folds will determine whether the earlier folds are destroyed by the shear band, or locally deformed, but on the whole preserved. Localisation of deformation and high strain zone development was controlled by competency domains in the rock, and, because of this the folds are ultimately a reflection of these zones. At Mount Isa, carbonaceous shales and pyritic shales, or domains where the rheology is dominated by shales, are more deformed than massive mudstone or siltstone units. As a result, folds are intrafolial between the less deformed rock types. The fold-initiating shear bands rotate into the margins of the competency domains. Consequently, the fold has a higher interlimb angle at the ends of the D_3 shear band.

The restriction of S_3 shear bands to the short limbs of the NNW-SSE-striking folds indicates that shear sense on S_4 was influenced, but not wholly determined, by the high strain zone. The shear sense of S_4 on the short limb is caused by the rotation imposed from the reuse/reactivation of the D_3 shear band and bedding outside of it. This reactivation of bedding would have rotated the shear band clockwise, looking north, which would also have contributed to the east block down shear sense on S_4 on the short limb. Post-D_4 deformation is localised in short limbs rather than long limbs of the NNW-SSE-striking folds, indicative of a feature giving these areas a lower competency and is consistent base metal mineralisation at Mount Isa in D_4. Post-D_4 deformations tightened these folds.

Determination of the mechanism by which the NNW-SSE-striking folds formed has implications for the evolution of the Paroo Fault, which is interpreted as the primary structural control on copper mineralization. The shallow and steep dipping portions of the Paroo Fault

below the orebodies match the long and short limbs of the NNW-SSE-striking folds respectively, suggesting that these orientations are related to deformation in D_4. East block up shearing along S_4 on the long limbs rotated the Paroo Fault to a shallow orientation before mineralization. The high angle between the fault and S_4 resulted in dilation of this structure as initially proposed by Bell et al. (1988).

Fold formation by overprinting of shear bands in successive deformations best accounts for the microstructural characteristics of the asymmetric folds at Mount Isa and may be applicable elsewhere. This process shows how folds are influenced by competency domains at a range of scales, and how the interaction between these and the variation in localisation of deformation can form ore deposits.

Acknowledgements

This project was supervised by Prof. Timothy Hampton Bell and his contribution as supervisor is gratefully acknowledged. Funding was provided by MIM Limited, Mount Isa Business Unit. Steve Law and Alice Clarke are especially thanked for setting up the project. Company geologists are thanked for providing logistical assistance in the field. Chris Bell and Tom Blenkinsop provided stimulating discussions and useful insights. Their suggestion were greatly appreciated.

Table 1. Correlation Between Deformation Sequences of Selected Previous Workers

This Study	Bell & Hickey (1998), Perkins (1997)	Bell et al. (1988)	Holcombe et al. (1991)	Passchier & Williams (1989)
			D_1: Horizontal shear zone	**Alligator phase:** Listric faults and breccias
D_1: Folds with E-W-striking axial planes.	**D_1:** N-S thrusting, E-W-striking folds	**D_1:** N-S thrusting, E-W-striking folds		**Malbon phase:** Minor thrusting and isoclinal folding
D_2: Folds with N-S-striking and variably dipping axial planes. S_2, crenulation and disjunctive cleavages depending on rock type. Variations in orientation due to later deformation	**D_2:** N-S-striking folds and axial planar foliation.	**D_2:** N-S-striking folds and axial planar foliation.	**D_2:** N-S striking upright folds	**Duchess phase:** Steeply west-dipping cleavage, N- or S-plunging folds
D_3: Sub-horizontal shear bands at all scales down to the S_3 crenulation cleavage. Folds with sub-horizontal axial planes.	**$D_{2.5}$:** Folds with sub-horizontal axial planes			
D_4: NNW-SSE-striking, vertical cleavage, S_4. Dominantly NNW-plunging folds.	**D_3:** N-S to NNW-SSE trending folds and axial plane foliation, S_4	**D_3:** NNW-plunging folds and axial planar foliation		**Fountain Range phase:** Brittle NE-SW faults
D_5: Deformation of S_4. Weak horizontal cleavage.				
D_6: Vertical N-S-striking cleavage.				

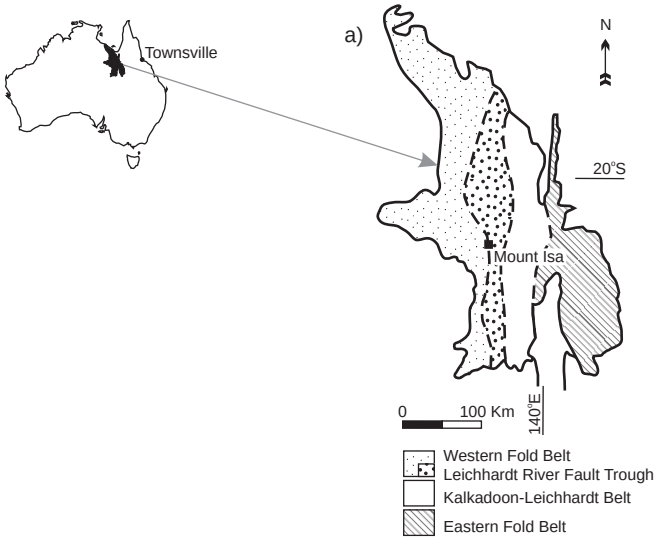

Figure 1: Locality map of Mount Isa Inlier in Northern Australia. Mount Isa is located on the western margin of the Leichhardt River Fault Trough in the Western Fold Belt.

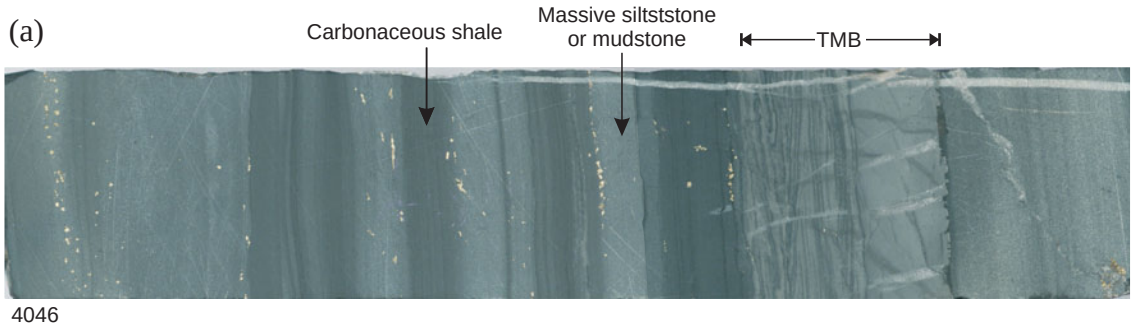
(a)
Carbonaceous shale
Massive siltststone
or mudstone
TMB
4046

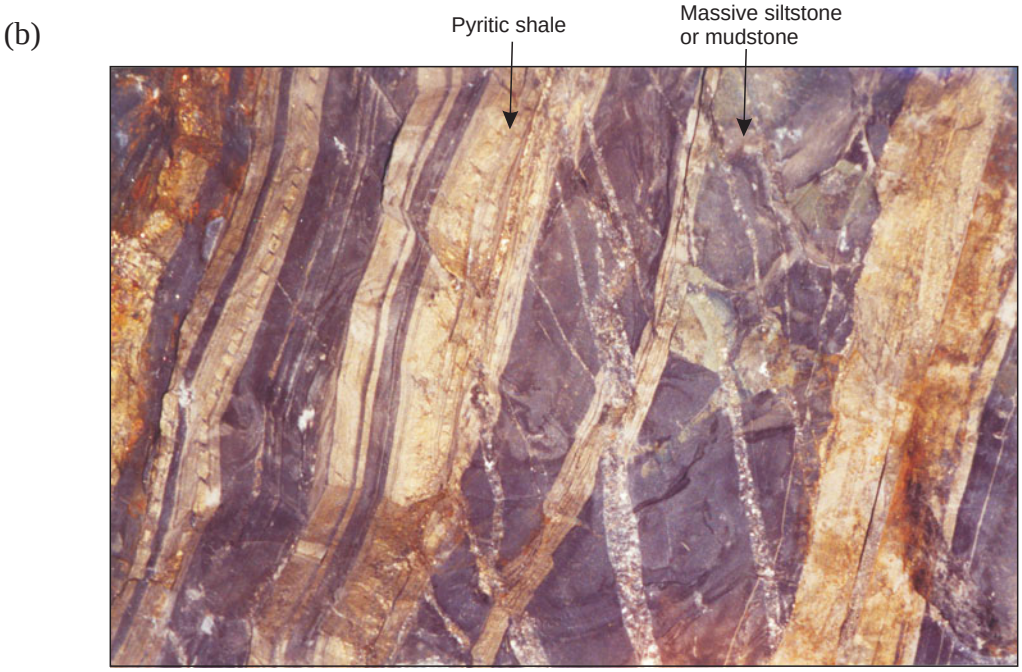
(b)
Pyritic shale
Massive siltstone
or mudstone

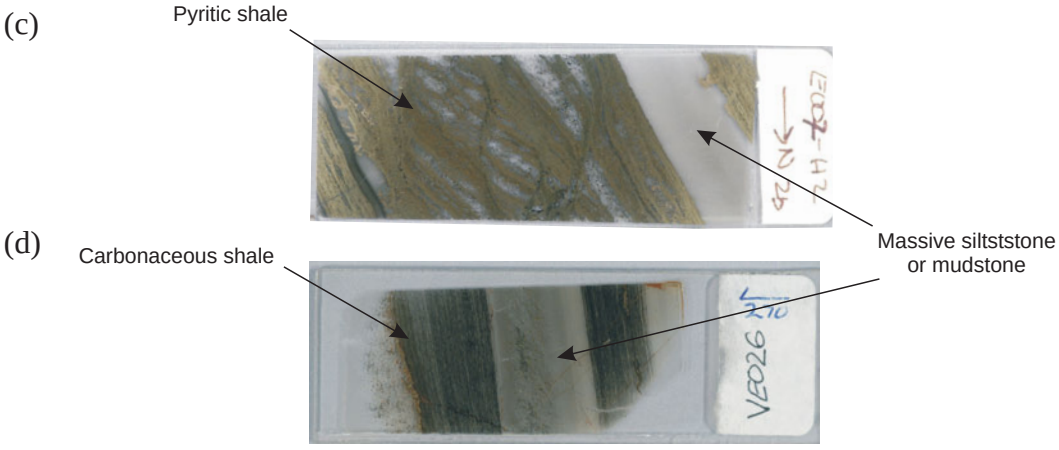
(c)
Pyritic shale
(d)
Carbonaceous shale
Massive siltststone
or mudstone

Figure 2: Illustration of the main rock types at Mount Isa. a) Photograph of drill core of interbedded carbonaceous shales and massive rock types including siltstone and mudstone, which impart a banded appearance at the centimetre scale. Tuffaceous marker beds (TMB's) occur sporadically throughout the sequence and may be massive or banded. Core is 35 mm wide. b) Photograph of an underground exposure of pyritic shales (light bands) interbedded with massive siltstone. Width of view is approximately 50 cm, looking north (6904 XC level, Lead Mine). c) Photograph of a thinsection (2.5 x 7.5 cm) containing anastomosing pyrite seams in pyritic shale. The clear areas between pyrite seams are coarse grained carbonate and quartz. See also figure 3b. d) Photograph of a thinsection (2.5 x 7.5 cm) of interbedded carbonaceous shale and massive mudstone and siltstone. Dark seams in the carbonaceous shale are anastomosing graphic cleavage seams. Weak cleavages are discernable in the massive siltstone. See also figure 3c.

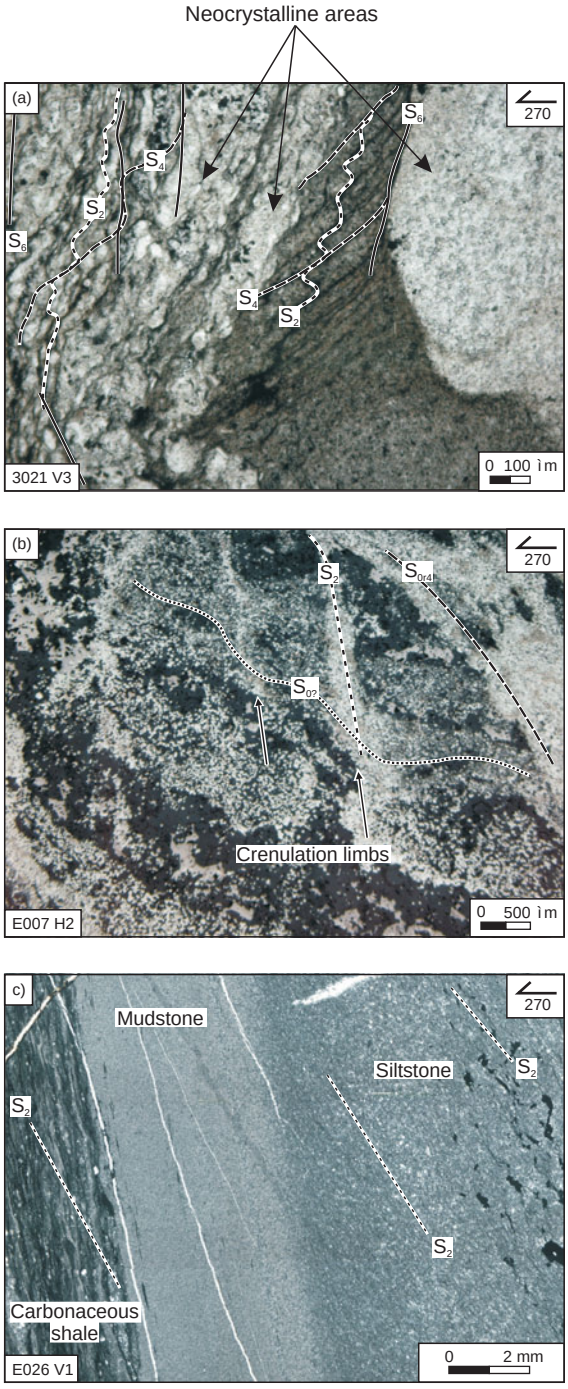
Neocrystalline areas
(a)
270
S_6
S_4
S_2
S_6
S_4
S_2
3021 V3
0 100 µm
(b)
270
S_2
S_{cc4}
S_{cc2}
Crenulation limbs
E007 H2
0 500 µm
c)
270
Mudstone
Siltstone
S_2
S_2
S_2
Carbonaceous shale
E026 V1
0 2 mm

Figure 3: Cleavages in the different rock types. a) Photomicrograph of crenulation cleavages in carbonaceous shale. Metasomatism has destroyed much of the continuity of the cleavages across layering. The dark vertical band right of the centre has not been effected by metasomatism and contains well preserved differentiated cleavages. In contrast to this, the area to the left has widespread metasomatism with a few crenulation hinges preserved between neoform patches (transmitted, plane polarised light; Lead Mine, S61 NE XC level 5). b) Photomicrograph of pyritic shale. Pyrite alteration occurs along crenulation, and to a less extent, crenulated cleavages. S_2 is rotated into bedding in the top of the image, see also figure 2c. (Reflected light photomicrograph; Lead Mine, P70 incline, 17a level). c) Photomicrograph that demonstrates cleavages in massive mudstone and siltstone, which have only weakly developed cleavages compared to carbonaceous shale on the left that has a distributed and well developed crenulation cleavage (transmitted, plane polarised light; Lead Mine, M73 incline 17B level).

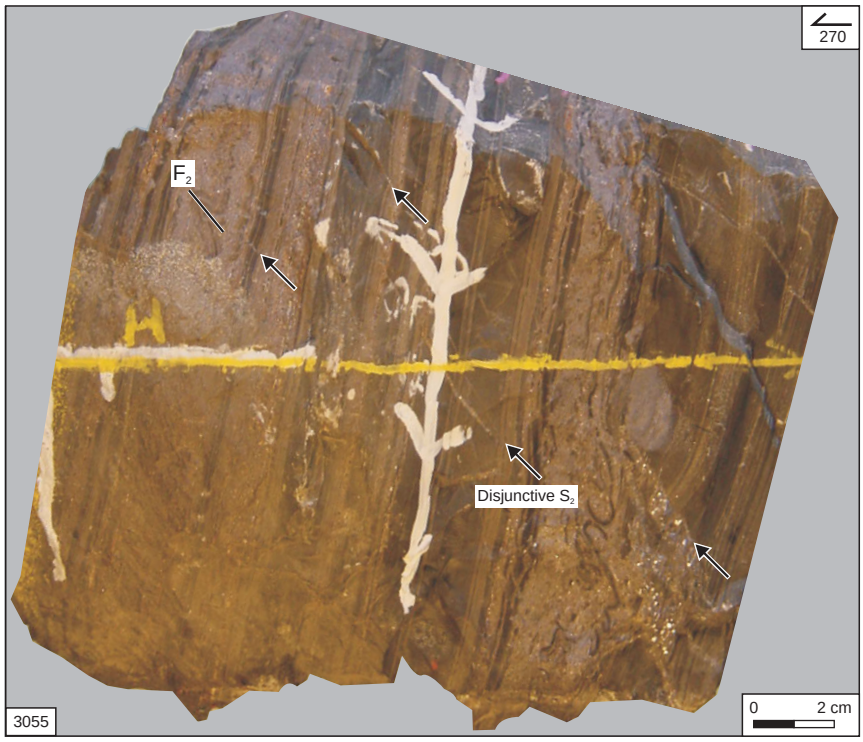

Figure 4: Photograph oriented hand specimen containing a disjunctive cleavage in massive rock types interbedded with shales. This sample illustrates S_2 forms a disjunctive cleavage in massive lithologies, which is parallel to F_2 axial planes of folded thin siltstone beds in massive sulphide bands (Sample locality: Lead Mine, 6904 XC, 5 level).

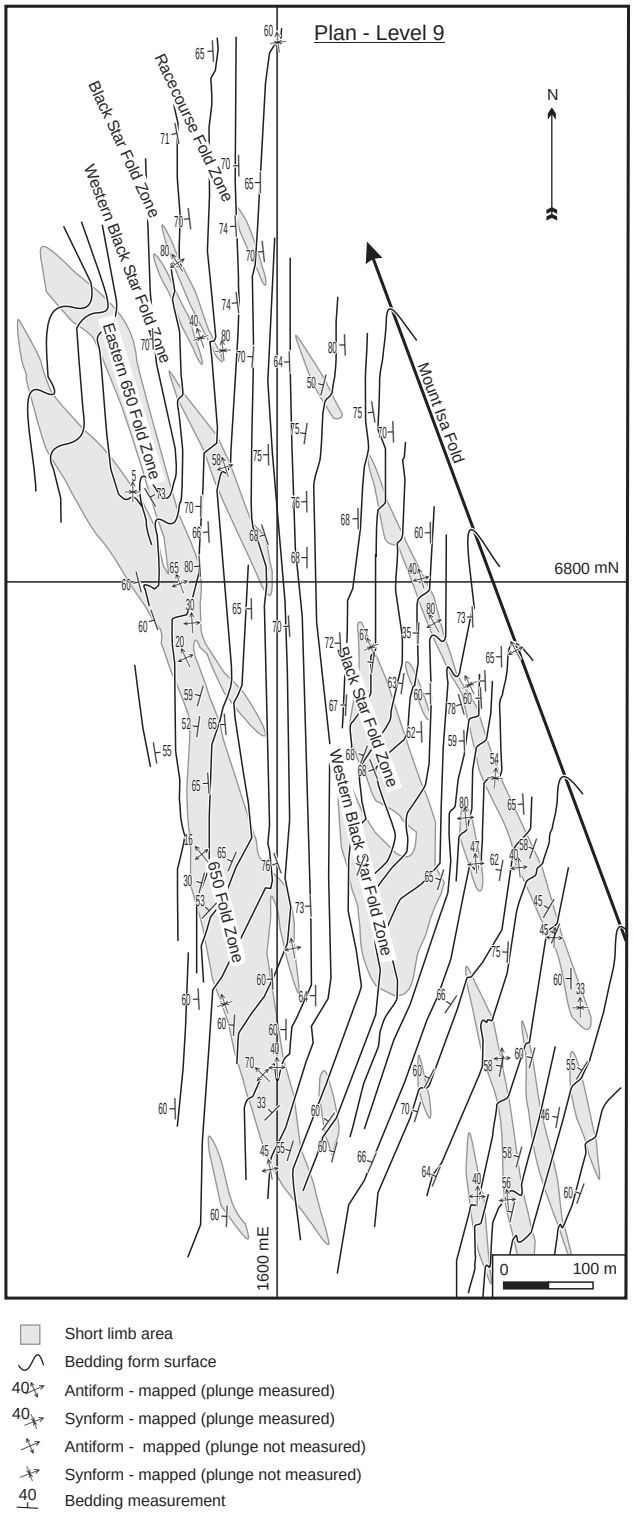

Figure 5: NNW-SSE-striking fold zones in the Lead Mine at Level 9 (3080 mRL).

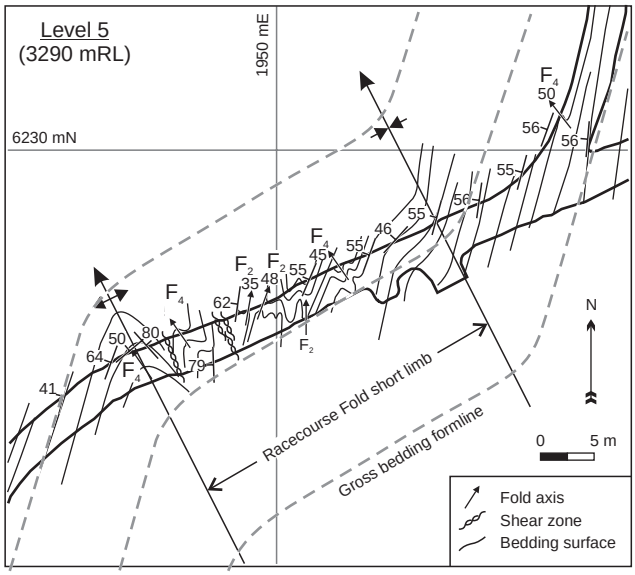

Figure 6: Cross cut (S61 NE XC) map of the Racecourse fold in the 0011 orebody on level 5. Macro-scale folds of various orientations are preserved on the short limb of the NNW-SSE-striking fold couplet. Note several NNW-SSE-striking high strain zones near the anticlinal hinge.

Figure 7: a) Map of the Mount Isa fold (anticline) on level 17. A prominent high strain zone is located on the short limb. b) Detail of the box in a) of the Mount Isa fold on levels 17 and 17B around 7350 mN. Structural measurements from oriented thinsections are presented in the shaded boxes. Sample sites are indicated by the black diamonds and sample numbers are located next to them. The Mount Isa fold is characterized by a paucity of smaller folds on the short limb. Other large F_4 short limbs contain numerous folds, compare to Figure 6. c) Lower hemisphere equal area projection of bedding around the Mount Isa Fold between the 17 and 16D levels.

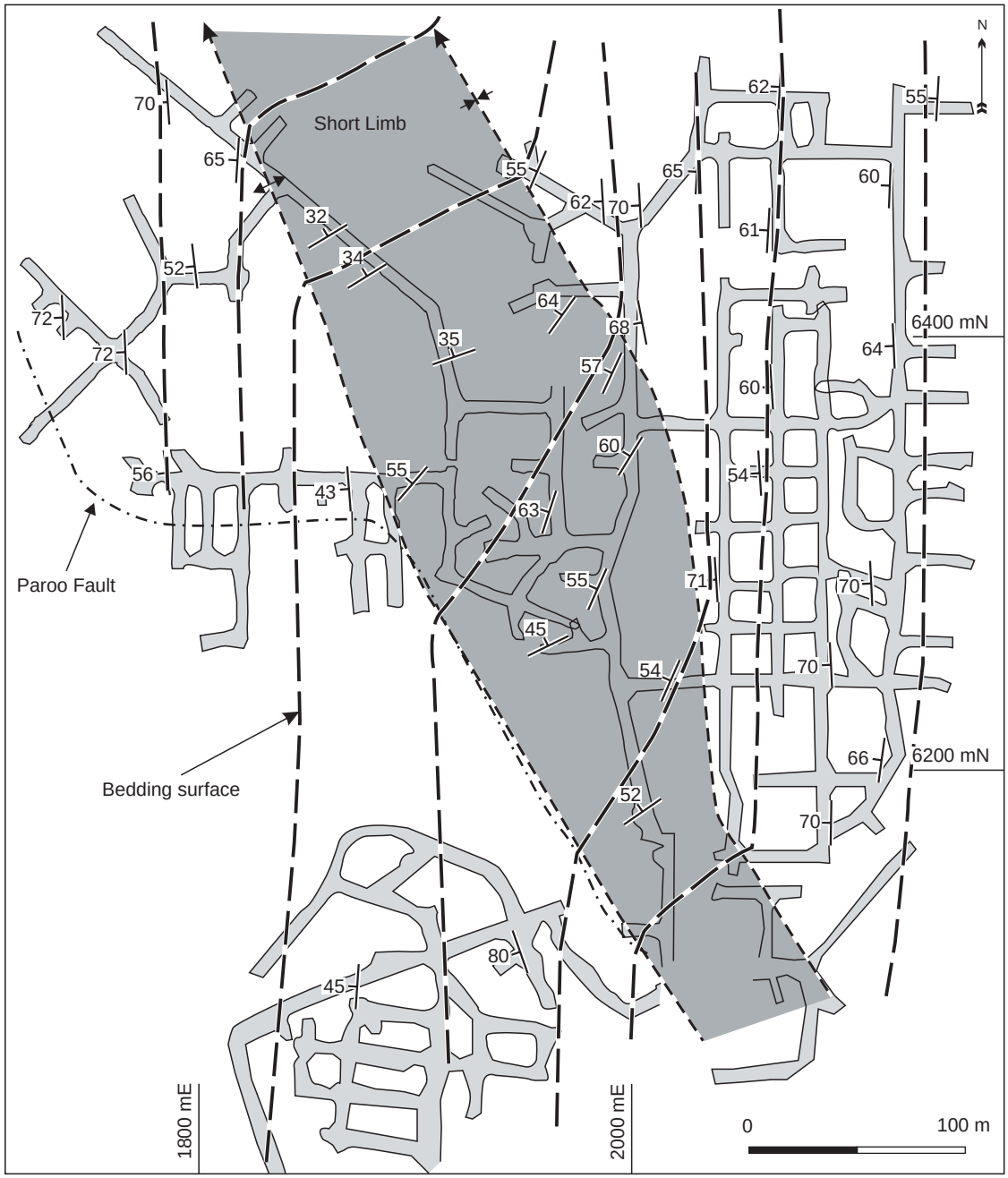

Figure 8: Plan of the Mount Isa fold on level 27c of the Enterprise Mine. Both hinges (dashed lines) are exposed by the underground workings. The short limb is highlighted by the shaded area. The interlimb angle at this locality is significantly larger than in the Lead Mine, (cf. figure 7). The 3000 copper orebody is located west of the Mount Isa fold and the 3500 to the east. The dashed and dotted line is the Paroo Fault in the basement location. The Urquhart Shale is north of the Paroo Fault.

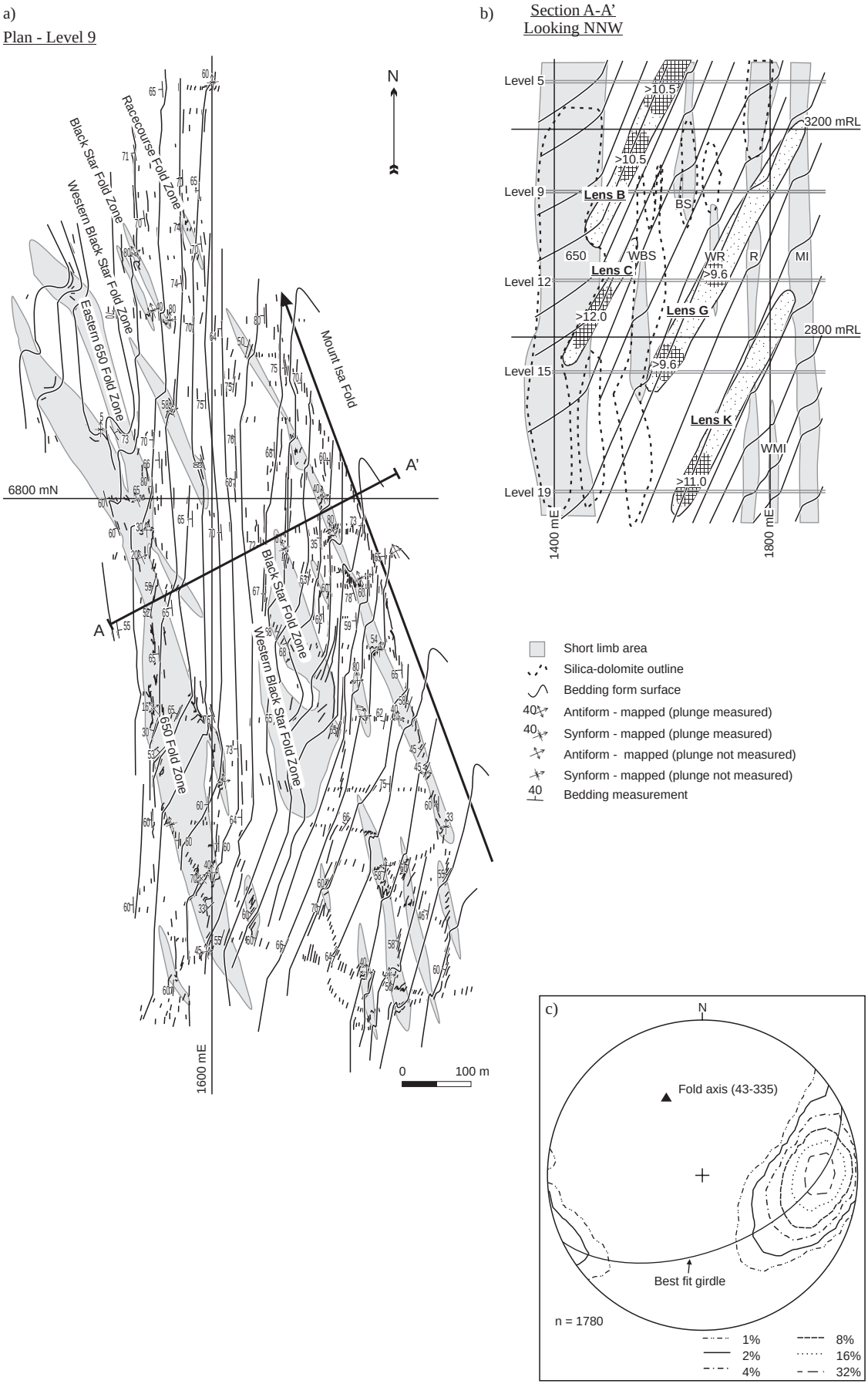
a)
Plan - Level 9
N
Racecourse Fold Zone
Black Star Fold Zone
Western Black Star Fold Zone
Eastern 650 Fold Zone
Mount Isa Fold
A
A'
6800 mN
650 Fold Zone
Black Star Fold Zone
Western Black Star Fold Zone
1600 mE
0
100 m
b)
Section A-A'
Looking NNW
Level 5
Level 9
Level 12
Level 15
Level 19
3200 mRL
2800 mRL
>10.5
>10.5
Lens B
BS
650
WBS
WR
R
MI
Lens C
>9.6
>12.0
Lens G
>9.6
Lens K
WMI
>11.0
1400 mE
1800 mE
Short limb area
Silica-dolomite outline
Bedding form surface
Antiform - mapped (plunge measured)
Synform - mapped (plunge measured)
Antiform - mapped (plunge not measured)
Synform - mapped (plunge not measured)
Bedding measurement
c)
N
Fold axis (43-335)
Best fit girdle
n = 1780
1%
2%
4%
8%
16%
32%

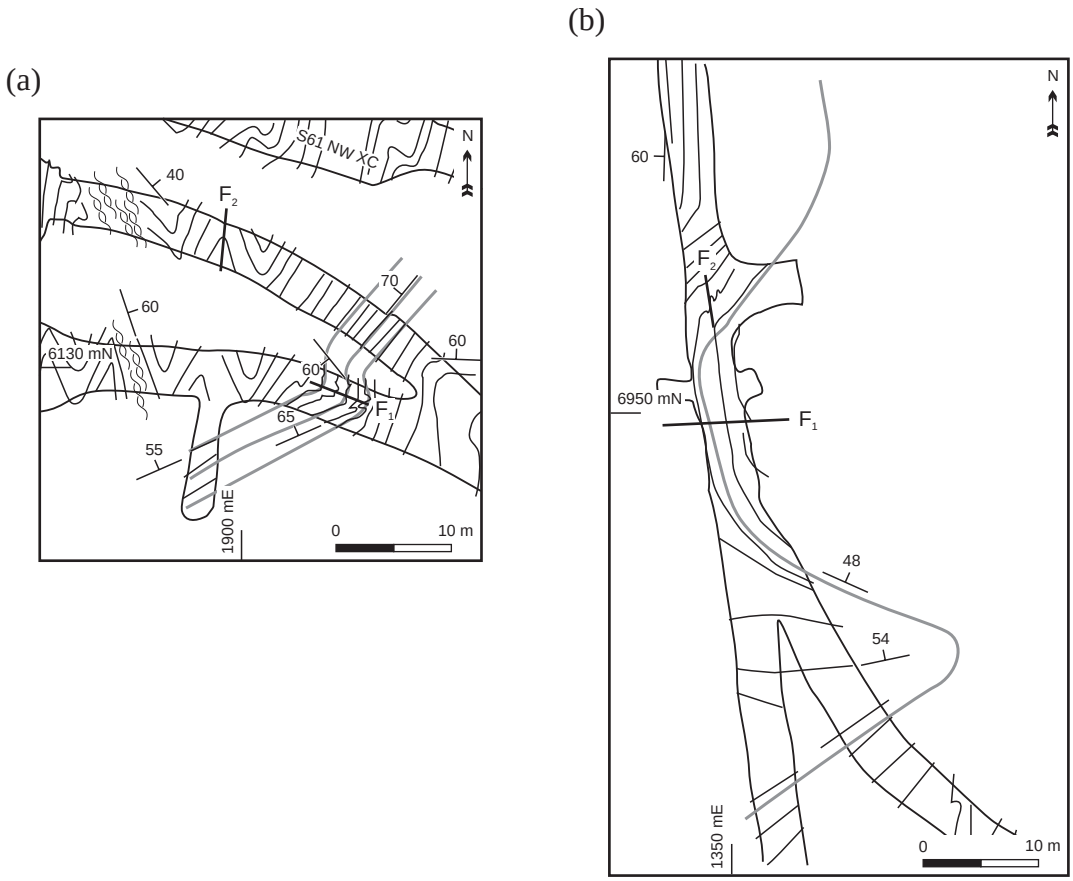

Figure 9: Mapped bedding shows F_1 folds on the 15 level. Thick grey lines are interpreted bedding surfaces. a) Near the S61 NW XC. b) L 61 N DR. At this locality the large F_1 fold is overprinted by F_2 folds.

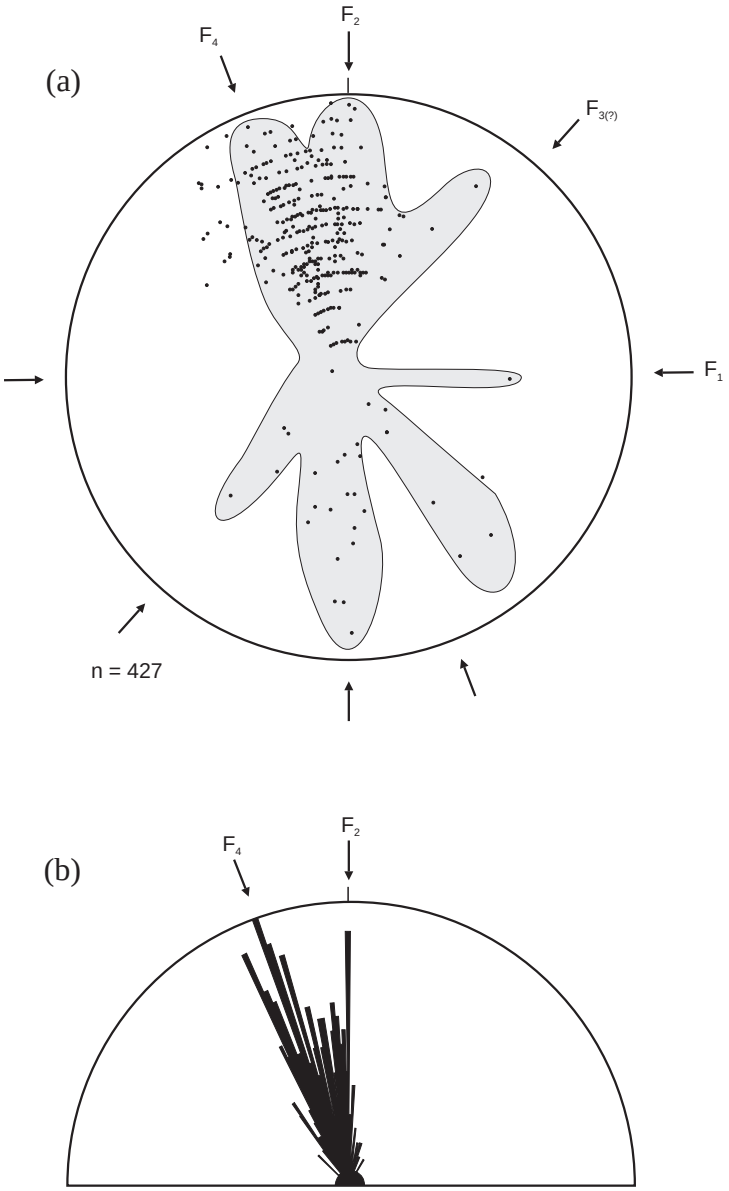

Figure 10: a) Lower hemisphere equal area projection of fold axes in the mine. The data was derived from historical mapping by company geologists. Clustering of plunges in small circles at 5° degree intervals is an artifact of data collection reduced to the closest 5°. N-S-, NNW-SSE-, NE-SW- and E-W-striking trends in the data are highlighted by the shaded area and the arrows along the margin of the projection. The main cluster is spread between N and NNW-plunging. Trends that make up this cluster are clearly illustrated by in b) below. B) Rose diagram of F_2 and F_4 fold axes.

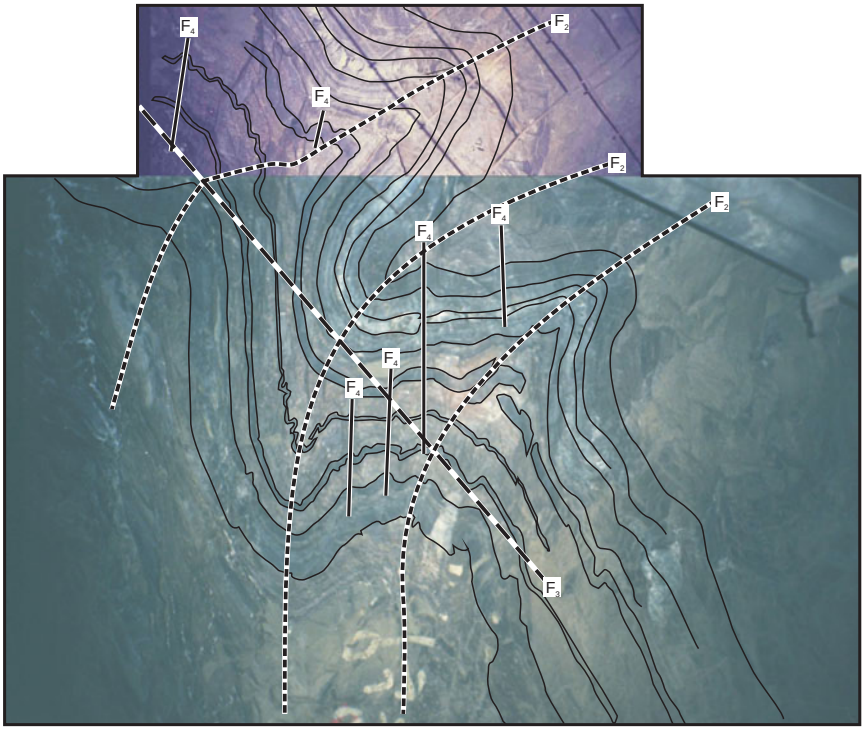

Figure 11: Photograph of polyclinal fold exposed in the underground development illustrating fold overprinting relationships looking approximately to the north. Large F_2 folds and are folded by the shallow east-dipping F_3 folds. Small F_4 folds with vertical axes are located on both limbs of the F_3. This locality is several metres east of the anticlinal hinge of the Mount Isa fold and were the only folds observed on the short limb of this fold. This image is a collage of two photographs taken at slightly different angles so there is a small mismatch between them. Looking south, width of view approximately 5 metres, 7350 XC, level 17B.

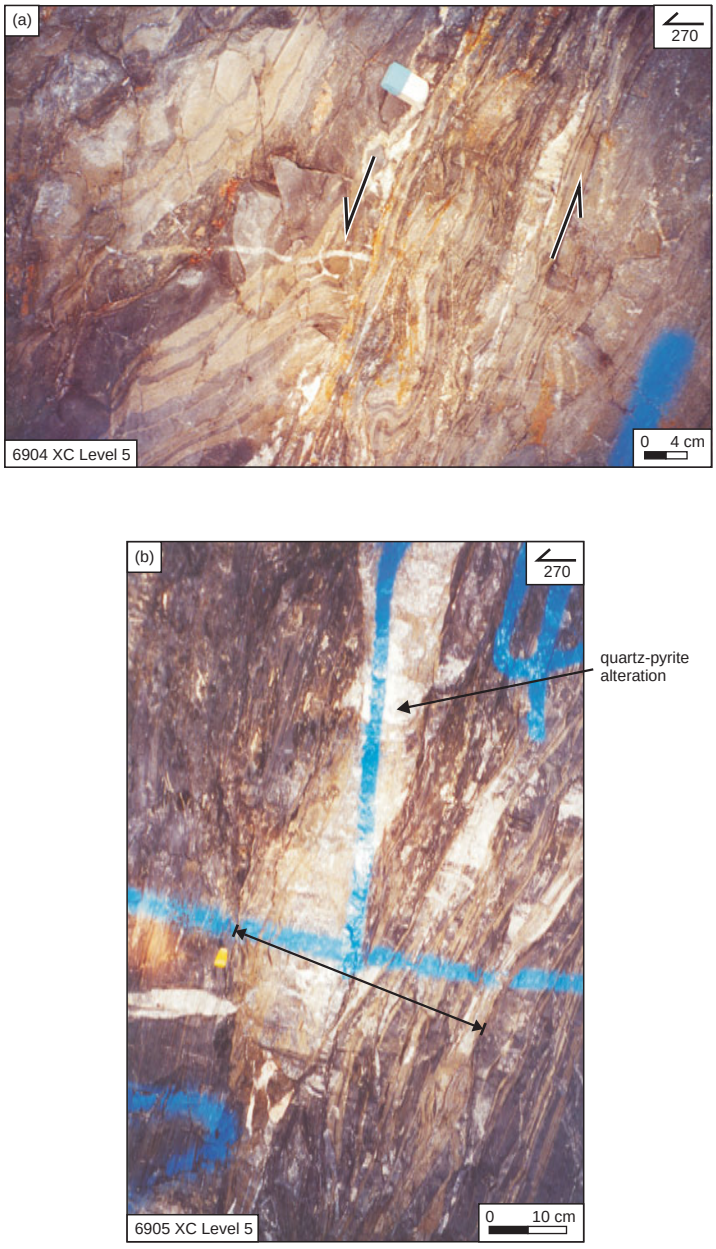

Figure 12: Photographs of underground exposures of high strain zones in the Lead Mine on the 6904 XC, level 5 . High strain zones typically contain quartz, carbonate and sulphide mineralisation. Reactivation and dilation of N-S-striking D_2 high strain zones occurred in D_4 and was probably important in providing channelways for mineralising fluids.

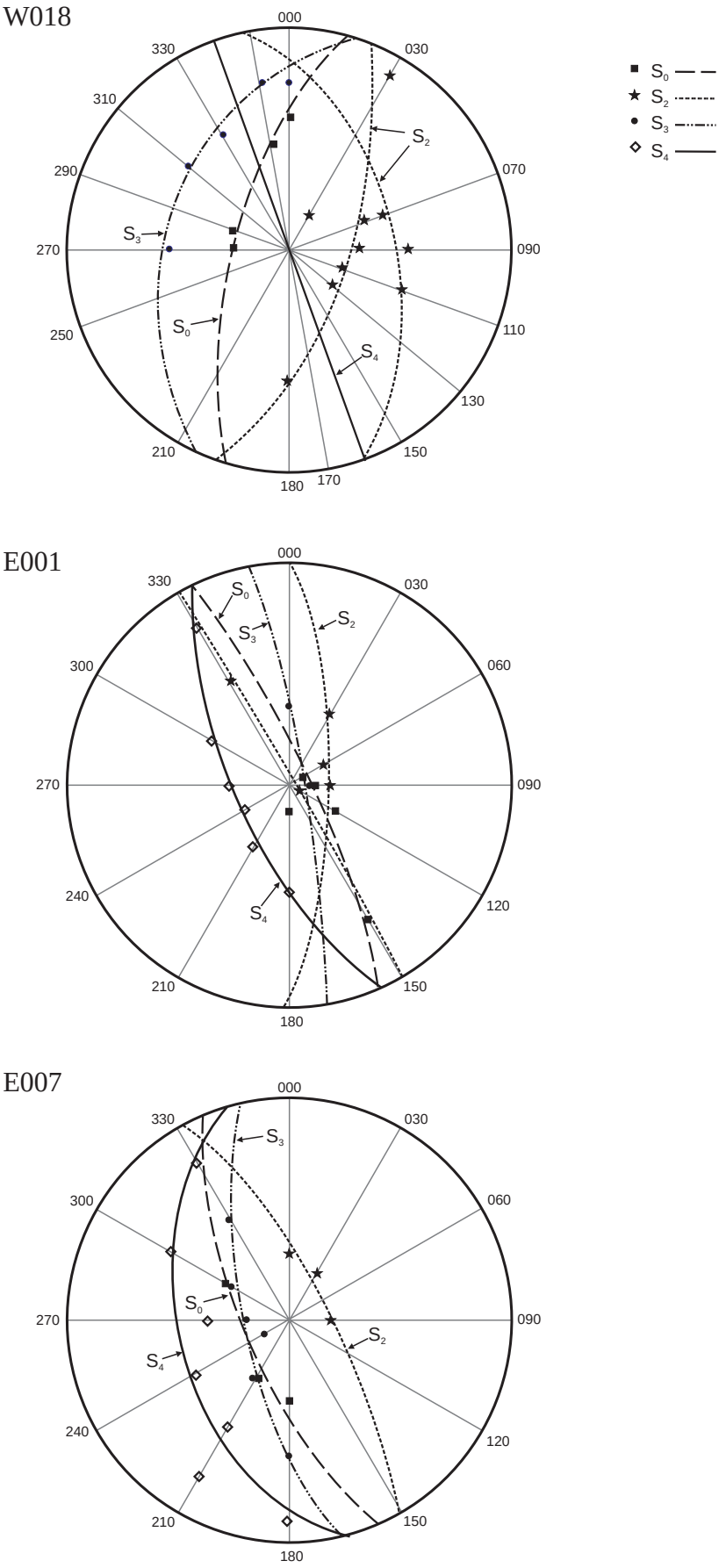
W018
000
030
070
090
110
130
150
170
180
210
250
270
290
310
330
S_0
S_2
S_3
S_4
E001
000
030
060
090
120
150
180
210
240
270
300
330
S_0
S_2
S_3
S_4
E007
000
030
060
090
120
150
180
210
240
270
300
330
S_0
S_2
S_3
S_4

Figure 13: Equal area projections of cleavage pitches from in a radial series of vertical thin sections. Sample W018 is on the western long limb of the Mount Isa fold. S_2 is an east-dipping crenulation, with east block up asymmetry into zones of differentiated cleavage indicating east side up shear, and has the most variable orientation. Two planes can be fitted to the S_2 data. S_3 is a west-dipping crenulation with top to the east movement. (sample locality: Lead Mine, 7350 XC, level 16, 1130 orebody). E001 (sample locality: Lead Mine, M73 inc. level 17a) and E007 (sample locality: Lead Mine, P70 inc. level 17a) are on the short limb of the Mount Isa fold. S_4 steeply west-dipping because of later deformations. S_2 is steeply east-dipping and S_3 is between it and S_4. The low angle between S_2 and S_3 indicates high D_3 strain on the short limb.

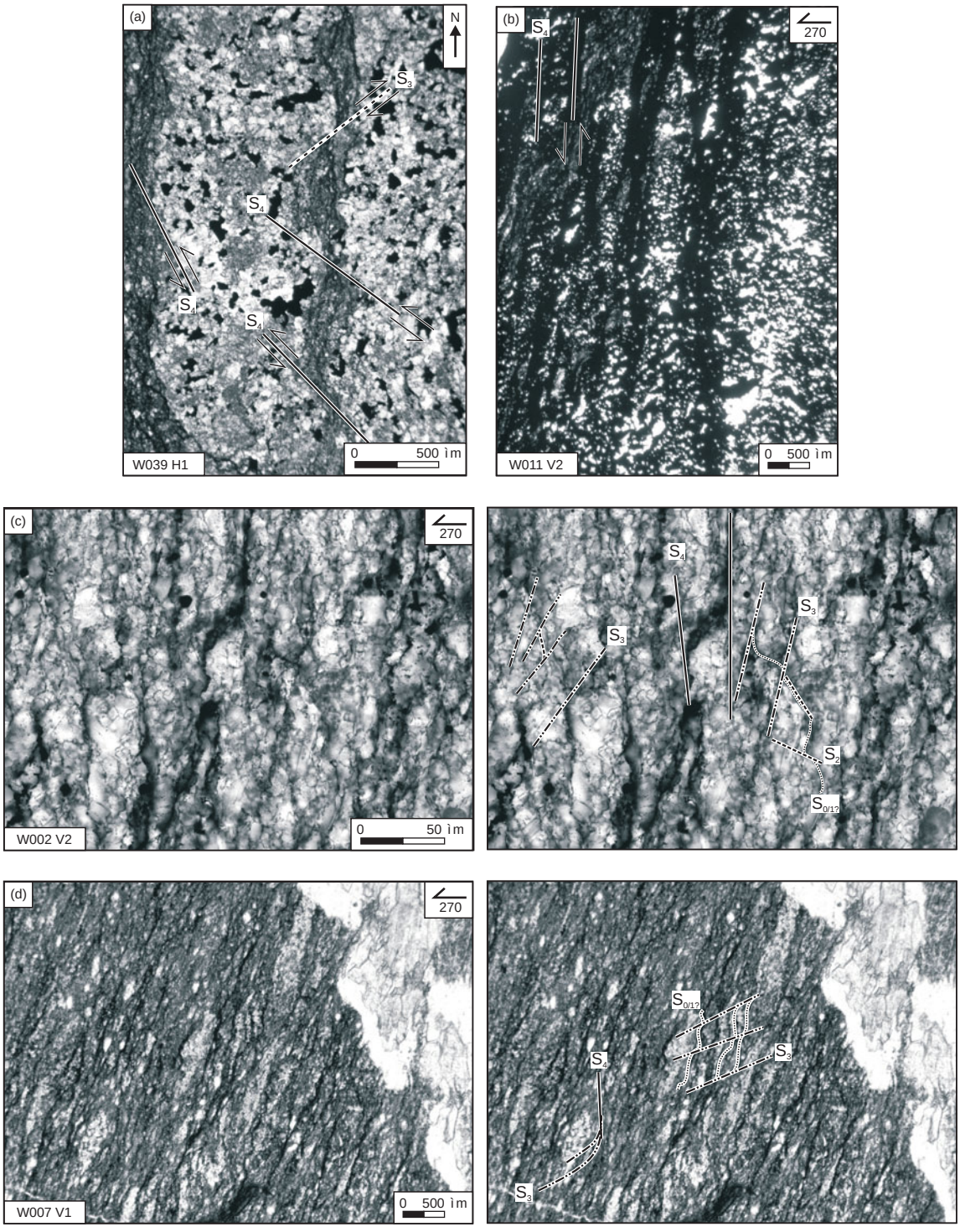
(a)
N
S3
S4
S4
S1
0 500 µm
W039 H1
(b)
S1
270
0 500 µm
W011 V2
(c)
270
0 50 µm
W002 V2
S4
S3
S3
S2
S0/1?
(d)
270
0 500 µm
W007 V1
S0/1?
S4
S3
S3

Figure 14: Photomicrographs (ppl) of cleavages in long limb areas of macro scale NNW-SSE-striking folds. a) Horizontal section showing NW-SE- to NNW-SSE-striking S_4 displaying a sinistral shear sense and NE-SW-striking S_3 with a dextral shear. N-S-striking neoform bands interrupt the across layering continuity of the cleavages. b) Vertical section. Vertical S_4 crenulation cleavage has east block up movement and is the main cleavage. c) Vertical sections illustrating the most common three cleavages found in the carbonaceous shales and their relative overprinting relationships. S_3 is a weak, spaced, west-dipping cleavage with a clockwise shear sense. It overprints S_2 which is an east dipping crenulation with anticlockwise movement. d) Vertical section. This carbonaceous shale sample shows S_3 as an west-dipping crenulation with top to the east shear sense and is crenulated by east block up movement on S_4.

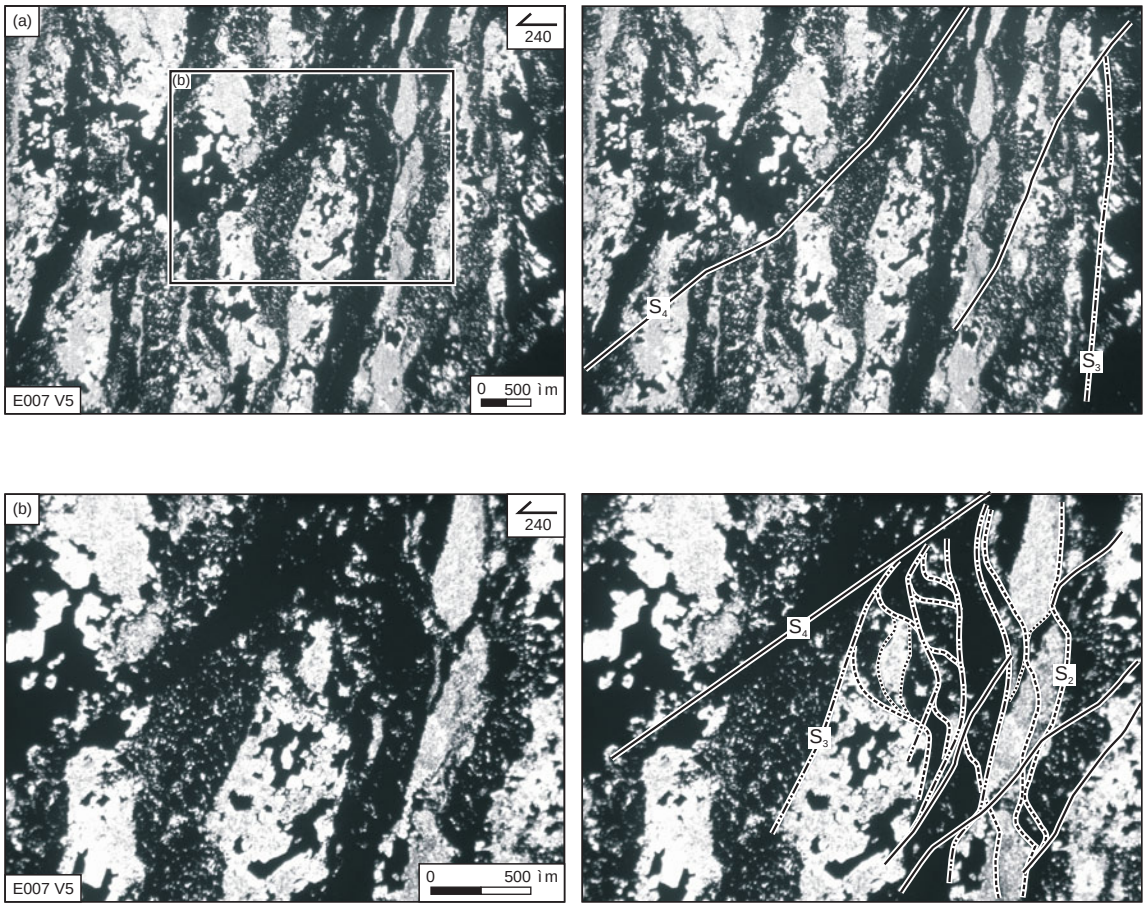

Figure 15: Photomicrographs (ppl) of vertical thinsection (E007-V5), looking north, from the short limb of the Mount Isa Fold (sample locality: Lead Mine, P70 inc, level 17a) of pyritic shale with pyrite alteration along foliations. Cleavage line diagrams are in the right column. a) Steep west-dipping S_4 crenulates near-vertical S_3, both cleavages have east-block-down displacement. The box in the left image indicate the positions of the photomicrographs in (b). b) S_4, east-block-down shear sense, crenulates S_3, also with east-block-down movement, and both fold S_2, which has east-block-up displacement.

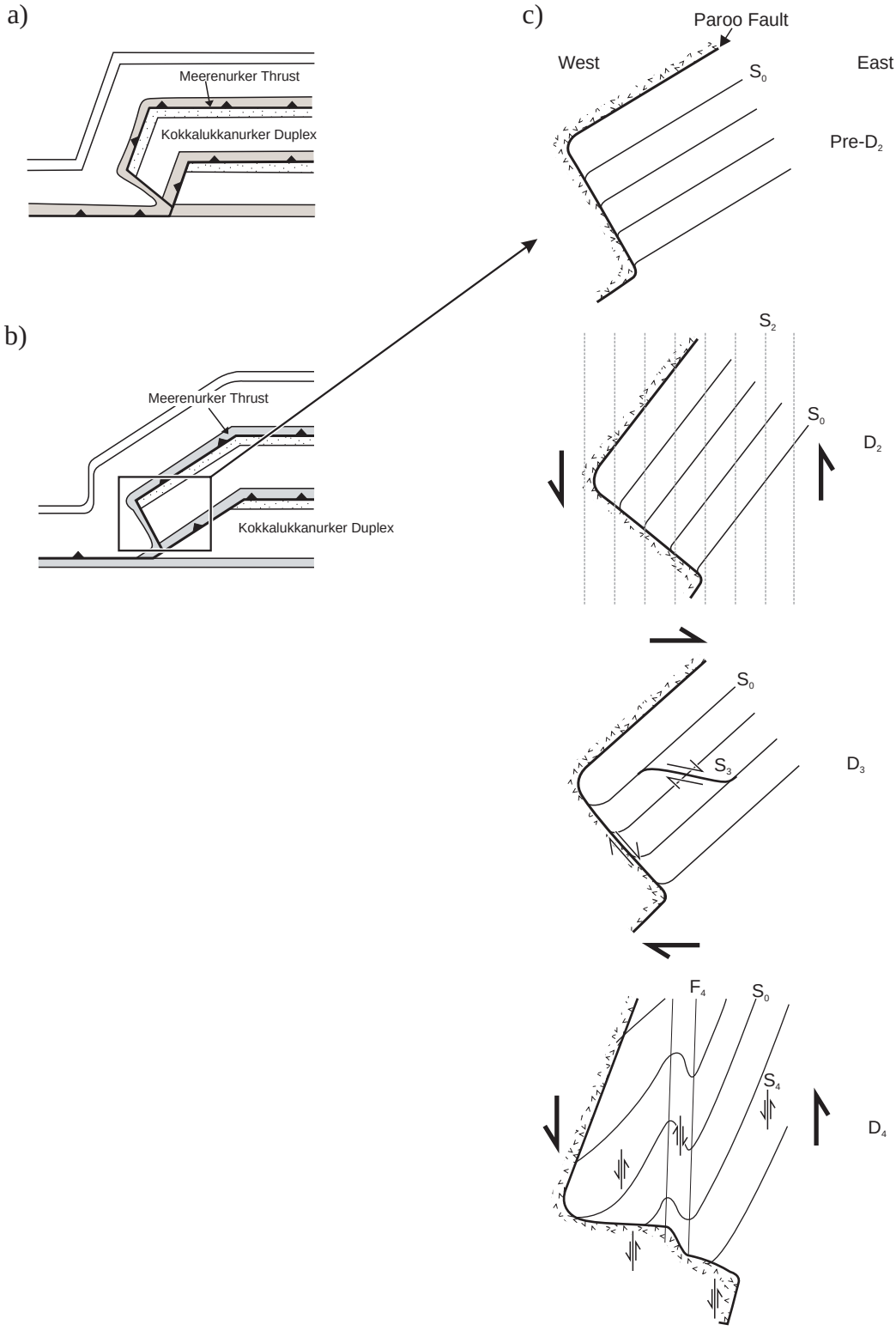
a)
Meerenurker Thrust
Kokkalukkanurker Duplex
b)
Meerenurker Thrust
Kokkalukkanurker Duplex
c)
Paroo Fault
West
East
S_0
Pre-D_2
S_2
S_0
D_2
S_0
S_3
D_3
F_4
S_0
S_4
D_4

Figure 16: Evolution of the Paroo Fault. a) Cross section through the Kokkalukanurker Duplex, looking north (Bell, 1991). In this model bedding in the lateral ramp area is steeply west-dipping at the end of D_1 as shown. The Meerenurker Thrust is synonymous with the Paroo Fault. b) Same view as a) but bedding in the lateral ramp section is shallow-dipping. This geometry is indicated by the high angle between S_2 and S_0. c) Series of illustrations demonstrating the evolution of the structure of the Paroo Fault. The west-dipping and east-dipping portions of the Paroo Fault are rotated to steeper and shallower orientations respectively in D_2. The effect of D_3 on the Paroo Fault is uncertain. Top to the east shearing along S_3 may have partially countered the effects of D_2 rotation or this may have been reduced by reactivation along the fault. In D_4 east block up shearing along S_4 on F_4 long limbs steepened the west dipping portion of the Paroo Fault and made the east-dipping segment shallower. However, in short limb areas the opposite displacement on S_4 steepened shallow east-dipping parts of the Paroo Fault, or at least they kept their pre-D_4 orientation.

a) D_3 high strain zone formation

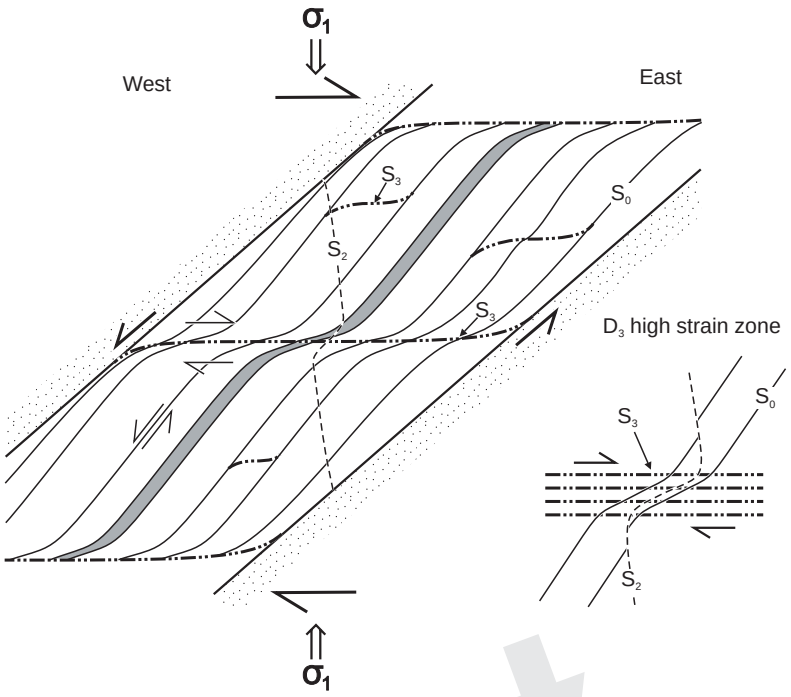

b) D_4 early, S_4 establishment

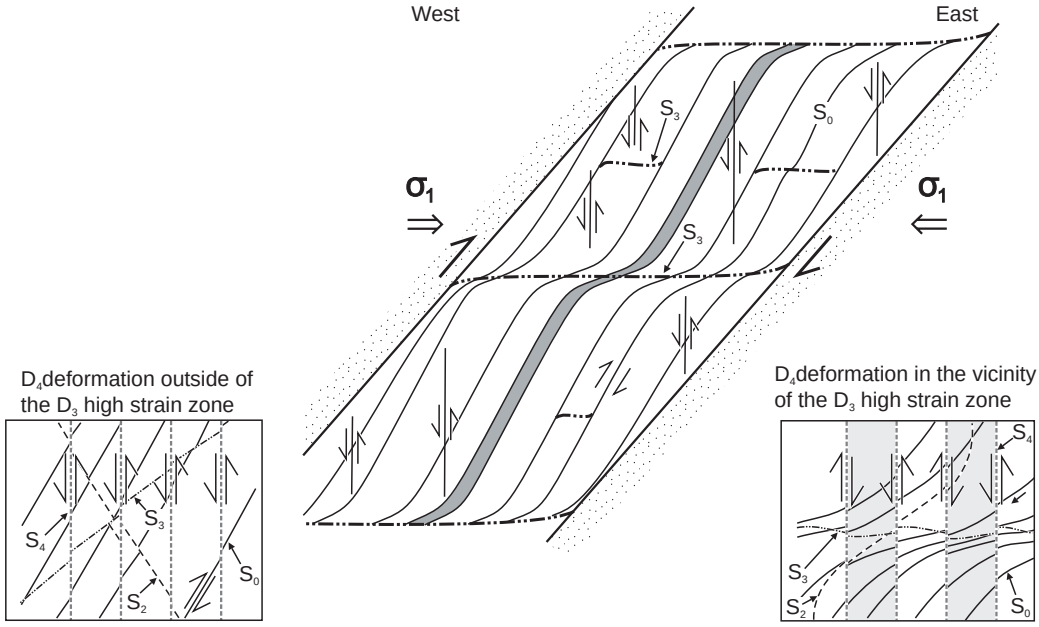

c) D_4 bedding reactivation and shear band rotation

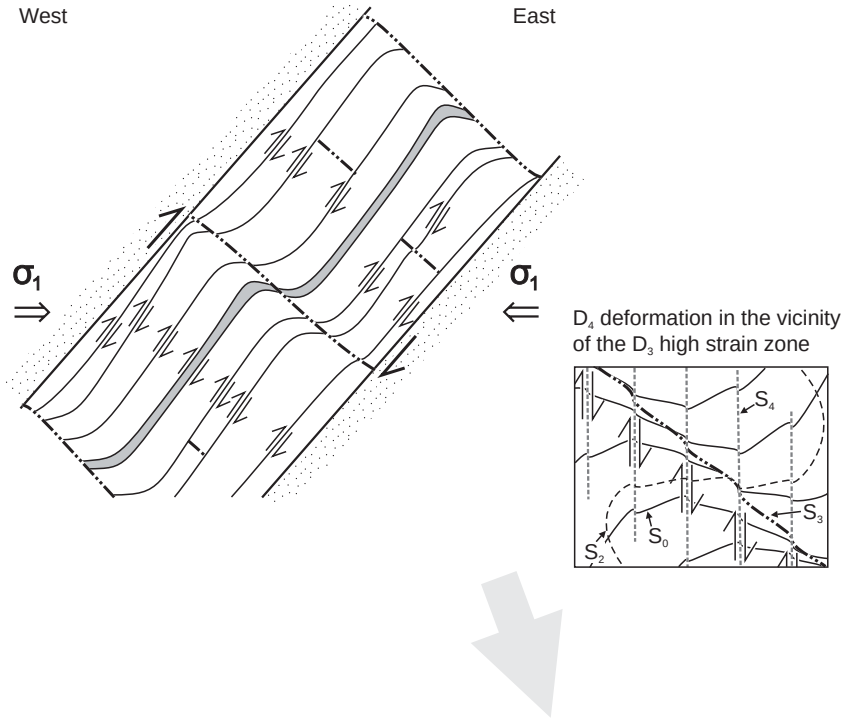

d) D_4 finite structure with cleavage relationships

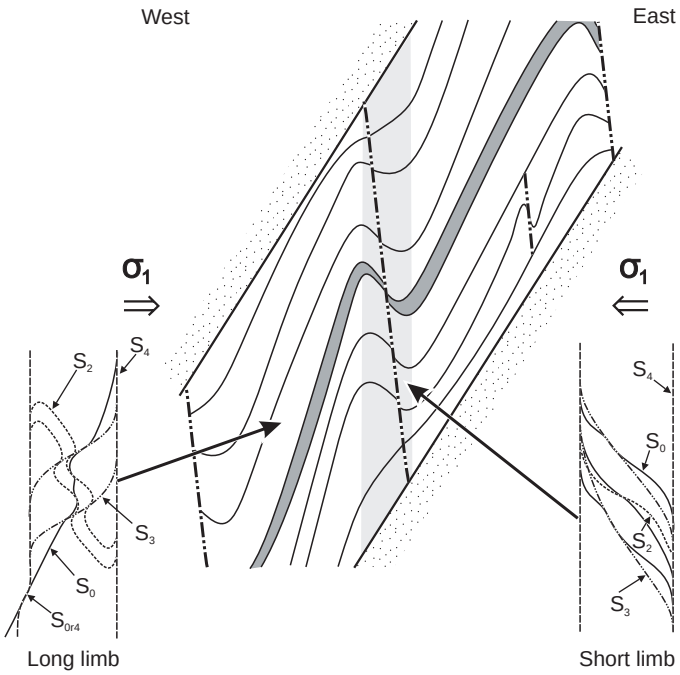

Figure 17: Formation of the NNW-SSE striking folds. Line diagrams show the main cleavage relationships. a) Folds are initiated by a horizontal high strain zones in D_3 low competency domains. The stippled area represents a higher competency domain. Shear bands rotate into competency domain margins. Within the high strain zone S_2 and S_0 are rotated into low angles with S_3. External to the shear band reactivation rotated S_2 to an east-dipping orientation. b) During D_4 east block up shearing in long limb domains rotates S_0, S_2 and S_3. The inset on the left illustrates the deformation outside of the shear band, where bulk deformation was non-coaxial with dominantly east block up shearing along S_4. Inset on the right; in the vicinity of the D_3 shear band deformation is was more coaxial with approximately the same amount of either shear sense along S_4. c) Reactivation of layering in D_4 rotated the D_3 shear bands clockwise (looking north). This caused a bias to east block down shearing along S_4 in the vicinity of the shear bands (inset). d) Final disharmonic fold showing the observed short and long limb cleavage relationships. The most open parts on the fold are close to the margin of the competency domains because this was where an more of the progressive shearing strain was accommodated by reactivation of bedding in D_3.See also Figs 16 c and d.

Part C

Microstructural analysis of asymmetric boudins and flanking structures from Mount Isa

Microstructural analysis of asymmetric boudins and flanking structures from Mount Isa

Abstract

New mechanisms for the formation of asymmetric boudins and flanking structures are linked to the deformation history by examining these structures from exposure to microscopic-scales. It was found that these structures formed by overprinting deformations, so they can only be used as kinematic indicators when their precise relationship to the deformation history is known. The processes of determining this relationship reveals much information about the deformation of the volume in which the structures are situated.

The development of asymmetric boudins commenced with D_2segmentation of competent layers interbedded with weaker rock types. Disjunctive cleavages in massive siltstones and mudstones formed interboudin planes at the same time as distributed crenulation cleavage was produced in adjacent shale beds. Rotation and separation of boudins occurred to some degree in all subsequent deformations, but the bulk of these effects are attributed to D_4. The formation of the interboudin planes during cleavage formation demonstrates that the maximum principal stress was perpendicular to them and at a low angle to bedding.

Flanking structures at Mount Isa formed by dilation of S_2 shear bands in D_4 followed by rotation of the external host element by shearing along S_4. Dilation of the shear band occurred to accommodate D_4 deformation in the surrounding rocks. Relative rotation between the external and internal host element domains is caused by more intense deformation in the former, as shown by the density of S_4 seams. In this process the internal host element remains more or less stationary, which is substantially different from present models.

Flanking structures and asymmetric boudins preserve details of deformation that may have been destroyed or largely masked by ongoing deformation in the rocks around them and as such can be useful in understanding the deformation history. These structures should therefore be given significant attention when attempting to determine the deformation history of an area, especially in high strain areas where few other heterogeneities are preserved.

Introduction

Kinematic indicators are structures that show how the rock has deformed and because of this are of great interest to structural geologists. Their usefulness depends on the accuracy of interpreted formation mechanisms that are applied to them. Accordingly, significant effort is invested in modelling structures with the potential to be kinematic indicators (e.g. Strömgård, 1973; Goldstein, 1988; Mandal and Khan, 1991; Kidan and Cosgrove, 1996; Mandal et al. 2000; Passchier and Druguet, 2002). This paper examines two potential kinematic indicators, asymmetric boudins and flanking structures developed in the dolomitic siltstones and shales that host the Mount Isa Zn-Pb-Ag and copper orebodies that the mechanism of their formation can be determined. The evolution of these structures is linked to a deformation history containing multiple events that are well defined by earlier independent studies (Bell, 1991; Perkins, 1997; Bell and Hickey, 1998). Microstructural studies revealed relationships not obvious at larger scales. For both flanking structures and asymmetric boudins, the formation of individual features that make up these structures can be linked to separate deformations. The results obtained have implications for the structural evolution of the orebodies in the Mount Isa Cu-Zn-Pb-Ag deposit.

Boudins are portions of a segmented rock layer surrounded by a continuous less competent matrix (Ramberg, 1955; Strömgård 1973; Hanmer, 1986; Goldstein, 1988; Passchier and Druguet, 2002). Segmentation occurs on spaced zones of brittle, brittle-ductile, or ductile deformation that take the form of diffuse or discrete planes of shearing, or tensile factures, known as interboudin planes, or localised layer attenuation, termed boudin necks (Ramberg, 1955; Hanmer, 1986; Goldstein, 1988; Mandal and Khan, 1991; Jordan, 1991; Swanson, 1992; Price and Cosgrove, 1990; Kidan and Cosgrove, 1996; Mandal et al., 2000). Goscombe and Passchier (2003) and Goscombe et al. (2004) give a clear description of the geometric features of asymmetric boudins (Fig. 1; Table 1). Segmentation, shearing along the interboudin plane, boudin rotation, separation and deformation are widely proposed as occurring when the maximum principal stress is normal or at a high angle to layering and the bulk shearing strain is parallel to layering or the enveloping surface of the boudin train (Ramberg, 1955; Strömgård, 1973; Platt and Vissers, 1980; Hanmer, 1986; Goldstein, 1988; Mandal and Khan, 1991; Jordan, 1991; Kidan and Cosgrove, 1996; Mandal et al., 2000; Passchier and Druguet, 2002; Goscombe and Passchier, 2003). Goscombe et al. (2004) have created a classification scheme that encompasses a wide range of boudin styles based on the layer parallel shearing model. Layer parallel compression has been proposed as a stress state that could form these structures by some workers but it is not widely reported (e.g., Price and Cosgrove, 1990).

The present understanding of asymmetric boudinage is derived from a combination of observation of natural structures (Hanmer, 1986; Goldstein, 1988; Jordan, 1991; Swanson, 1992; Goscombe and Passchier, 2002) and a variety of modelling studies, including rock analogue (Kidan and Cosgrove, 1996; Mandal et al., 2000), photoelastic (Strömgård, 1973), and numerical modelling (Passchier and Druguet, 2002). Formation of these structures has been found to be influenced by interrelated factors including contrasting characteristics between layering, for example, the viscosity ratio (Ramberg, 1955; Strömgård, 1973), strength ratio (Mandal et al., 2000), aspect ratio (Strömgård, 1973), layer-thickness ratio (Mandal et al., 2000), and stress field related factors such as applied stress (Strömgård 1973) and the orientation with respect to the boudin train (Passchier and Druguet, 2002). To date there have been few microstructural studies of these structures.

A variety of mechanisms have been proposed for the formation asymmetric boudins (Hanmer, 1986; Goldstein, 1998; Jordan, 1991; Swanson, 1992; Passchier and Druguet, 2002; Goscombe and Passchier, 2003). Rhombic shaped boudins have been interpreted as commencing angular, with the interboudin plane (S_{ib}) oblique or normal to the boudin surface (S_b) with either or both surfaces being rotated by later deformation (Goldstein 1988; Jordan, 1991). Ductile deformation after initial formation may convert planar boundaries to curviplanar and produce a range of shapes (Hanmer 1986).

Classification schemes indicate the relative importance placed on specific features, components or mechanisms during the formation of structures. Shear sense along S_{ib} and rotation of boudins relative to shearing in the surrounding less competent rocks parallel to layering or the enveloping surface form the basis of recently proposed classification schemes (Jordan, 1991; Passchier and Druguet, 2002; Goscombe and Passchier, 2003; Goscombe et al., 2004). The implication of these schemes is that shearing along S_{ib} and rotation of the boudins are related and synchronous processes. Goscombe and Passchier (2003) and Goscombe et al. (2004) divided asymmetric boudins into two groups according to slip along S_{ib} being either synthetic or antithetic to the interpreted bulk shear sense parallel to the enveloping surface (Fig. 1b). Shear band boudins have synthetic slip, or S-slip, and those with antithetic slip, or A-slip are termed domino boudins.

Flanking structures have been recently defined by Passchier (2001) as deflections in a penetrative fabric element, termed the host element, around a cross-cutting element such as a vein, termed the cutting element (Fig. 2). Passchier (2001) lists the mechanisms proposed to date for the formation of these structures and points out that, because at least three and possibly five mechanisms may form flanking structures, their use as kinematic indicators is limited. Grasemann and Stüwe (2001) and Grasemann et al. (2003) have modelled these structures to

gain a better understanding into their formation and assess their use as kinematic indicators. The host element is divided into internal and external domains (Fig. 2). The internal host element is located between the cutting element and the external host element and is interpreted to contain deflected fabric that defines the flanking structure (Passchier, 2001; Grasemann and Stüwe, 2001). Two types of flanking structures are defined by the nature of this deflection, flanking folds and flanking shear bands (Fig. 2). For flanking folds the angle between the host element fabric and the cutting element increases from the external host element towards the internal host element and the cutting element. Conversely, the angle between the host element and the cutting element decreases in a flanking shear band. Recent work has endeavoured to resolve uncertainty about flanking structure formation so that their potential as kinematic indicators can be assessed (e.g. Passchier, 2001; Grasemann and Stüwe, 2001; Goscombe and Passchier, 2003). At Mount Isa flanking structures are located around carbonate ± quartz ± sulphide veins that are concentrated in the barren rocks along the margins of conformable Zn-Pb-Ag mineralised packages. Dilation of these veins appears to have been important in base metal mineralisation (Perkins, 1997; Part D).

Background

Mount Isa is located on the western margin of the Leichhardt River Fault Trough in the Western Fold Belt of the Mount Isa Inlier (Fig. 3). The metamorphic grade of the rocks at Mount Isa is no higher than lower greenschist facies so there has been good preservation of structures from a series of deformations. The structures examined are located in the Urquhart Shale, which is part of the Mount Isa Group. The Urquhart Shale is a fine grained dolomitic sedimentary sequence of interbedded, carbonaceous shale, pyritic shale, massive mudstone and massive siltstone. According to Neudert (1996) the average bed thickness in the Urquhart Shale is 11.6 mm. Aphanitic potassium feldspar marker horizons are sporadically distributed throughout the sequence. The area hosts the Mount Isa Zn-Pb-Ag orebody which comprises massive sulphide bands.

Six deformation events are recognised at Mount Isa as presented in Part B. D_1 produced folds with E-W-striking axial planes. Deformations subsequent to D_1 produced alternately horizontal and vertical cleavages. Bell and Hickey (1998) interpret this series of deformations as reflecting overall E-W shortening orogenesis punctuated by gravitational collapse of the thickened crust that formed horizontal foliations. The carbonaceous shales and pyritic shales have well developed distributed crenulation cleavages. Conversely, the massive siltstones and mudstones have only weakly formed crenulation cleavages or disjunctive cleavages (Figs 4 and

5). Steeply east-dipping carbonate, quartz and sulphide veins are a common feature in the host rocks beside the conformable Zn-Pb-Ag bodies (Fig. 6a). Veins are commonly to be parallel to F_2 axial planes and generally terminate against bedding-parallel base metal bands.

Asymmetric Boudins

Boudins are common in layered rocks where a competency contrast exists between adjacent layers (Hanmer, 1986; Mandal et al., 2000). Asymmetric boudinage has occurred in the massive mudstones and siltstones interlayered with continuous carbonaceous shales, pyritic shales or base metal sulphide bands. Thin beds of massive pyrite surrounded by pyritic shale with a laminated appearance may be also boudinaged. The boudinaged massive siltstone and mudstone layers range in thickness from a few millimetres to several tens of centimetres. The massive pyrite layers are typically less than a centimetre thick. The boudins examined in this study are domino boudins according to the classification scheme of Goscombe and Passchier (2003; Figs 5a and 7).

Interboudin planes between asymmetric boudins in the massive mudstone layers are N-S-striking and east-dipping (Figs 5a and 7). They are to parallel F_2 axial planes and S_2 crenulation cleavages, which have the same shear senses, in the carbonaceous shales (cf. Figs 6a and b). There is generally a higher abundance of S_2 crenulation cleavages in the carbonaceous shales next to an interboudin plane. Interboudin planes may host fibrous veins of carbonate, quartz, sulphides and mica. Fine sphalerite and carbonate are common along S_{ib} where fibrous habit are absent. Interboudin planes are curved where traversed by S_4 (Figs 7c and d). The shales surrounding the boudin train are more deformed than the segmented massive siltstone and mudstone layers, which is an indication of the strong competency contrast between the main rock types (Fig. 7).

Flanking Structures

An oriented sample (sample no. W002) containing structures resembling flanking structures as defined by Passchier (2001) was collected from the footwall of the 9 orebody exposed in the 7350 XC on level 17B of the Mount Isa Lead mine (Fig. 8). It consists of interlayered pyritic shale and mudstone cut by several carbonate veins around which deviations of bedding are centred. Two episodes of movement along the cutting element with opposite shear senses are displayed by the displacement of bedding (Fig. 8). East block up displacement is displayed between the lower wall rock block and the large clast in the cutting element. There

is east block down offset between the hangingwall block of the vein and the large clast, as well as between the wall rocks on either side of the vein. The amount of east block down offset is greater in the cutting element with the more pronounced flanking structure.

Three episodes of veining are recognised in the cutting element vein (Fig. 9). An initial breccia vein with wall rock clasts in an ankerite matrix is overprinted by a second breccia vein with a lower abundance of clasts. These are overprinted by a carbonate (calcite to ferroan dolomite), quartz, galena and sphalerite vein recognisable as the central white band in the lower vein depicted in Figure 9. The oldest breccia clasts are angular and dominantly shale or mudstone. Shale clasts of this generation have similar fabrics to the pyritic shales but contain anastomosing graphite seams in place of pyrite (Fig. 10a). The second generation of breccia clasts are located along the margins of the vein adjacent to pyritic shale wall rock and comprise angular pyritic shale fragments (Fig. 10b). A thin line of inclusions in the carbonate matrix separating the different generations of clasts is interpreted to represent an increment of vein opening. Neither generation of breccia clasts have been transported far as they are angular and appear to have come from the adjacent wall rocks. The presence of two generations of clasts with the same fabric with only the second containing pyrite alteration indicates that they are separated by the pyrite alteration event.

Bedding dip isogons show that the orientation of bedding is linked to its proximity to the cutting element veins (Fig. 11b). There are three distinct domains defined by the orientation and spacing of dip isogons. The first is located adjacent to the veins and contains closely spaced dip isogons that are parallel to the cutting element veins. The dip isogon gradient in this domain defines progressively shallowing westwards bedding towards the cutting element vein. Dip isogons in the second domain are also parallel to the cutting element veins but have a gentler gradient compared to the first domain, defining decreasing westward dip of bedding away from the cutting element vein. In the third domain the dip isogon gradient is shallow and parallel to the cutting element vein. The separation of the host element into internal and external partitions based on the delineation of a fold or shear band adjacent to the cutting element produces boundaries between the internal and external partitions that closely match the borders of dip isogon domains. The internal host element closely correlates with the first dip isogon domain described. The other two dip isogon domains, which have a much gentler gradient, correspond to the external host element.

The host element contains numerous east-dipping S_2 shear bands at a low angle to the cutting element veins and with an east block up shear sense (Fig. 11). Where the shear bands intersect the cutting element the two are parallel for a short distance. Figure 11 shows the intersection of an S_2 shear band and a cutting element vein. Shear bands produce local

anomalies in the dip isogon pattern. The presence of the S_2 shear bands complicates the dip isogon pattern, and they occur in areas where the above correlation between the dip isogon domains and host element divisions does not hold. Above the upper vein in Figure 11, and below the lower vein, the pattern of dip isogons is difficult to determine because of the physical limits of the samples. There is a higher density of S_4 in the external versus the internal host element (Fig. 12). S_2 shear bands are more common in the internal host elements and largely absent form the external host element.

Discussion

Incremental steps in the formation of asymmetric boudins and flanking structures can be attributed to a combination of deformations. An important feature of D_2 is the influence of competency domains on the localisation of deformation microstructures, such that in competent rock types, discrete disjunctive planes of shearing formed, whereas crenulation cleavages were produced in less competent units.

An overview of deformation localisation

Deformation localisation or inhomogeneous deformation is the process of higher strain developing in some parts of the rock compared to surrounding areas (Bell et al., 1989; Hobbs et al., 1990). Deformation of heterogeneous material is characterized by different strain rates between the various competency domains. Competency domains can be caused by inherent characteristics such as grain size (Goodwin and Tikoff, 2002) or grain size distribution (Montési and Hirth, 2003). Localisation can also be caused by features such as the stability or bifurcation of the deforming system (Hobbs et al., 1990; Jiang, 1994) or as the result of physical modification during deformation due to cataclasis or dynamic recrystallisation that decreases the grainsize (e.g., Tullis and Yund, 1985; Handy 1989; Goodwin and Wenk, 1995; Jin et al., 1998).

Rock competency has been shown to play an important role in the localisation and partitioning of deformation with weaker domains found to partition more non-coaxial strain compared to more competent domains (Bell et al., 1989; Jiang, 1994; Goodwin and Tikoff, 2002). At Mount Isa there is a distinct competency contrast between the shales and the massive siltstones and mudstones. This is manifest as a distinct morphological difference between S_2 cleavages in the different rock types including a distributed crenulation cleavage and shear bands in shales and a disjunctive foliation in massive siltstones and mudstones. Localisation of deformation into the shales was favoured because of their uneven grainsize distribution and the fine-grained nature of the matrix with internal competency domains between detrital clasts and

the matrix. Montési and Hirth (2003) note that a wider grainsize distribution enhances diffusion creep. The reason for this could be that competency domaining occurs between the different sized grains. Goodwin and Tikoff (2002) show that shear bands initiate along the boundaries of competency domains because of mechanical instabilities arising from differential deformation between them. In comparison, massive siltstones and mudstones are equigranular and lack internal competency domains causing deformation to be more coaxial. The influence of this rheological contrast is best displayed by D_2 structures, suggesting it was the strongest deformation event. Conversely, in D_4 localisation occurred after a period of more homogenous deformation. The most recognisable feature of localisation in this deformation are shear bands. Localisation in both D_2 and D_4 had important influences on the development of asymmetric boudins and flanking structures.

Asymmetric boudinage

Models for the formation of asymmetric boudins have all aspects of boudin formation developing in the same deformation event by shearing parallel to layering in surrounding less competent units (Goldstein, 1988; Jordan, 1991; Swanson, 1992; Goscombe and Passchier, 2003). In this deformation the maximum principal stress is at a high angle, close to normal, to the layering (Strömgård, 1973; Jordan, 1991; Passchier and Druguet, 2002). The recently proposed classification schemes of Goscombe and Passchier (2003) and Goscombe et al. (2004) are intended to assist in the application of these structures in kinematic analysis and are based on such deformation models. The formation of asymmetric boudins at Mount Isa can be shown to have occurred over several deformations in different relative stress field orientations to that described by Passchier and Druguet (2002). Consequently, the application of existing classification schemes and the ensuing kinematic interpretations that follow from them are not appropriate in this case.

Four key features of asymmetric boudins are, 1) segmentation of layering, 2) displacement along the interboudin plane, 3) deformation of the boudin including boudin rotation, and 4) extension across the interboudin plane or separation of segments. Segmentation of more competent massive rock types occurred by either shearing or dissolution along a plane during the formation of disjunctive axial planar cleavages, rather than tensile failure (Fig. 13). S_2 has been identified as the structure that most frequently formes the interboudin plane from their orientation parallel to the axial planes of F_2 folds as well as parallelism to D_2 crenulation cleavages in the rocks surrounding the boudin train. The different style of S_2 between rock types is explained by variation of strain rates between them, which in turn reflects lithological differences such as grainsize and mineralogy. Competency domains are defined according to

rock type with the shales being weaker than the massive siltstones and mudstones. Recognition of the origin of the interboudin planes as axial planar cleavages means the maximum principal stress during segmentation was perpendicular to the interboudin plane and at a much lower angle to layering than suggested in present models. This is a major departure from these models but is the most appropriate interpretation of the features observed. The bulk of displacement along the interboudin plane probably occurred during cleavage formation as the sense of the movement is the same as that on S_2 differentiated crenulation cleavages in the surrounding incompetent layers. Layer normal compression models suggest minor displacement during segmentation with the most significant contribution to offset along the interboudin plane occurring after it was established (e.g., Ramberg, 1955; Strömgård, 1973; Platt and Vissers, 1980; Hanmer, 1986; Goldstein, 1988; Mandal and Khan, 1991; Jordan, 1991; Kidan and Cosgrove, 1996; Mandal et al., 2000; Passchier and Druguet, 2002; Goscombe and Passchier, 2003).

Deformation and rotation of the boudins occurred in D_4, the second deformation after formation of the bulk of the observed interboudin planes. Extension across S_2 interboudin planes could have occurred in either D_3 or D_4 but the latter is most likely because the composition of the material in the interboudin planes is the same as in veins forming in that event (i.e. carbonate, quartz and sulphides; Part D). Localised shearing late in D_4 caused folding of boudin surfaces where they are overprinted by shear bands as is shown by the folding of the boudin surfaces at the microscale (Fig. 7d), or as the relative rotation of boudins at larger scales, as shown in Figure 9a by the variation in the dip of the interboudin plane.

The formation of asymmetric boudins during multiple deformations, with segmentation occurring while the maximum compressive stress is normal to S_{ib}, is highly significant. Previous models (Ramberg, 1955; Strömgård, 1973; Hanmer, 1986; Goldstein, 1988; Jordan, 1991; Kidan and Cosgrove, 1996; Mandal et al., 2000; Passchier and Druguet, 2002; Goscombe and Passchier, 2003) proposed layer-parallel shearing in the incompetent units adjacent to the boudin train as a major component of the deformation that produced the asymmetric boudin structures. This can lead to the interpretation that the maximum stress was at a high angle to layering, which in this case would be erroneous. Here it is shown that there are more components to the formation of these structures and that shearing along layering is not a major contributing factor. Conversely, shearing along layering, or reactivation of bedding can mask the deformation in the less competent units that is related to segmentation. This will give the false impression that layer parallel shearing is the causative process in boudinage. Shearing along layering occurs because deformation is localised into the less competent domain. Bell (1986) showed that during progressive deformation, shearing can switch from the actively

forming axial planar foliation to reactivation of older foliations. The shear sense on the reactivating foliation is opposite to that of the axial planar foliation. In this case, reactivation of weaker layers will rotate differentiated S_2 crenulation cleavages, which are the shale hosted equivalent of the disjunctive S_2 in the competent beds, into parallelism with bedding making them difficult to recognise. If the boudinaged layer and those immediately surrounding it were the only layers observed, then the bulk of the shearing strain would appear to be parallel to layering. Figure 14 demonstrates this process and shows that if the scale of observation is limited to a zone of reactivation, then misinterpretations of the bulk shear sense and stress field can easily occur.

The possibility of segmentation during a different deformation event to that causing boudin rotation and separation, shows how models and classification schemes that interpret these processes to occur in the same deformation may be oversimplified. Kinematic interpretation based on such models may be misleading and detailed microstructural analyses of these structures is required to account for their formation in a deformation history that may contain a series of events before a kinematic interpretation can be made.

Flanking structures

A general sequence for the formation of flanking structures can be linked to the deformation history, which is determined from independent means (Part B). Cutting element veins formed in D_4 by dilation of structures that formed in D_2. Formation of the flanking structures is intimately linked to D_4 shearing strain and its progression from being distributed to localised.

The initial structural discontinuity that defines the cutting element originated in D_2 and experienced at least two distinct shear displacements and three dilational events. The correlation of the vein hosting structure with S_2 is based on overprinting relationships, common orientations, shear sense and vergence. Displacement initially took place during progressive shearing strain along the actively forming S_2 cleavage. Veins not surrounded by flanking structures still exhibit this displacement. The second displacement along the cutting element, displayed by the overall east block down offset along bedding, is opposite to the first and occurred in D_4 to accommodate rotation of bedding caused by east block up shearing along S_4 in localised domains.

Vein formation in the cutting element resulted from extension across S_2 at several periods in D_4. Veins overprint S_2 and breccia clasts contain an unidentified crenulation cleavage. The first extension probably occurred as S_2 cleavages experienced rotation due to the effects of progressive east block up shearing on S_4. The stepping of vein margins between

adjacent seams indicates that opening was not along individual seams. Rather, they opened at several locations that joined, resulting in an overall pinch and swell morphology. The timing of the extension is constrained by near vertical sigmoidal fibres in some veins. Brecciation occurred during reactivation of the cutting element involving east block down movement that was antithetic to localised shearing along S_4 in the external host element. The two brecciation episodes are separated by the pyrite alteration event. The final veining episode involved quartz and base metal sulphides that overprinted the earlier vein materials and included the formation of coarse grained carbonate in the vein by either deposition or recrystallisation.

The flanking fold formed by shearing along S_4, which was unevenly distributed between the internal and external host elements (Fig. 15). The progression to localisation of S_4 in the external host element produced discrete shear bands and amplified the flanking structure. The steepening of bedding caused by the localisation of S_4 is best illustrated around the vertical shear bands. The gradient in the density of S_4 between the internal and external host elements matches the variation in the orientation of bedding that defines the fold and is a compelling feature supporting this mechanism. There is a correlation between the internal host elements having the lowest density of S_4 and shallow dipping S_0 while the external ones have the highest density of S_4 and steeper S_0. The establishment of the internal host element may have in part been in response to a strain shadow produced by the vein. The progressive shearing component of deformation in the external host element deflected S_0 relative to the internal host element and the cutting element and not the other way round that was proposed by Passchier (2001) and Grasemann et al. (2003). The offset along the cutting element and the formation of the flanking structure are related. Reactivation of the cutting element occurred to accommodate the rotational component of the shearing strain that produced the flanking structure nearby.

Flanking shear bands formed by overprinting the vein on earlier S_2 shear bands, which is similar to the late-cutting element model of Passchier (2001). However, in this case the vein in this cutting element is locally parallel to the shear band but overall they are slightly incongruent. This occurred by joining different segments in adjacent bands so that the vein and the shear bands have slightly different orientations, and means the flanking shear band is only developed along part of the vein. The shear band may have been intensified by progressive shearing along S_4. Strain accumulation long the vein margin alone could produce flanking shear bands. However, the continuation of shallow dipping shear bands across the internal host element indicates that the shear band is overprinted by the vein and the flanking fold. S_2 shear bands are best preserved in the internal host element of the flanking fold which is consistent with these areas being of overall lower strain than the external areas.

The classification schemes for flanking structures contain assumptions about structure formation that may not always be valid. Passchier (2001) and Grasemann et al. (2003) interpreted a causal relationship between displacement along and rotation of the cutting element, and deflection of the host element structure, which is reflected in their classification scheme. Passchier's (2001) system relates displacement along the cutting element to the rotational movement of the internal host element. Passchier (2001) defines a-, n-, and s-type structures where the offset is antithetic, none, and synthetic respectively relative to the hypothetical rotation of the internal host element. This cannot be applied to the structure examined here because the external rather than the internal host element rotates to form the flanking fold (Fig. 15). Rotation of the cutting element host structure preceded flanking structure formation. Passchier (2001) is not clear as to the cause of flanking structure formation or why the internal host element is interpreted to be deflected in preference to the external host element. This classification scheme is misleading because it incorrectly infers the former element is deflected. The feature with a demonstrated causal relationship to the flanking structure is shearing along S_4, termed here the bulk shearing element. It is more appropriate to compare the displacement along the cutting element to this. Additionally it is necessary to note that the sample contained at least two displacement episodes along the cutting element and the first of these was not related to the flanking structure-forming bulk shearing event.

Grasemann and Stüwe (2001) and Grasemann et al. (2003) added to Passchier's classification. They based their schemes on shearing along, and rotation of, the cutting element with drag on the host element, relative to causative shearing that they interpreted to be parallel to the latter. The terms co- and counter-shearing, co- and counter-rotating, and normal and reverse drag are used to describe the relationships between shearing along and rotation of the cutting element and drag of the host element relative to causative shearing. These workers also interpreted the deviation forming the flanking structure to have occurred in the internal host element. This scheme is not directly applicable in this study because causative shearing is not parallel to the host element and the deviation occurred outside its internal partition. However, a co-rotating, counter shearing, normal drag, s-type flanking fold classification can be obtained by modifying the Grasemann et al. (2003) system. In their scheme such a classification could be used to get an idea of the type of flow that may have formed the structure, but this can not be done here because of the fundamental differences already outlined.

Flanking structures are potential kinematic indicators and have been used as such by several workers (e.g., Hudleston, 1989; Grasemann et al., 1999, Grasemann and Stüwe, 2001; Grasemann et al., 2003). In assessing their potential as shear sense indicators Passchier (2001) concluded that such use may be premature and highlighted the need for more modelling and

detailed field observational studies. Modelling studies such as undertaken by Grasemann et al. (2003) simulate a range of conditions under which these structures form. The present study shows that some of the assumptions in these studies may not always by valid because of the differences already mentioned. Before these structures can be applied as kinematic indicators, several important aspects of flanking structure formation must be determined, including 1) whether the internal or external host element has changed orientation, 2) whether the observed displacement along the cutting element is related to the deviation of the host element, 3) the pre-flanking structure history of the cutting element, and 4) how the flanking structure formation fits into to overall deformation history. This study has been able to address these points because of the high degree of preserved deformation owing to the low metamorphic grade in the study area. Further work needs to concentrate on determining these parameters using microstructural analysis for a range of flanking structures, such as those presented by Passchier (2001) and use the results to guide modelling studies.

The formation of flanking structures and asymmetric boudins occurred over multiple deformation events, and because of this, is too complex to be useful as kinematic indicators. However, microstructural examination of these structures in conjunction with knowledge of the individual events that comprise the deformation history of the volume has made it possible to determine their formation. Although these structures cannot be used easily as kinematic indicators, they do contain important information regarding the deformation history of a volume and should attract appropriate attention in the field.

Conclusions

The low metamorphic grade of the rocks that host the Mount Isa base metal deposit meant it was possible to link the formation of a range of structures and metasomatism to individual deformation events by using a combination of meso- and microstructural analysis. The mechanisms of formation that account for semi-incremental strain paths have been determined and have significant implications for the use of potential kinematic indicators such as asymmetric boudinage and flanking structures.

Strain localisation can be identified in three deformations as having an important role in the formation of these structures. Segmentation occurred when deformation localisation between competency domains defined by rock type in the second deformation formed interboudin planes when a discrete structure developed in higher competency units compared to weaker surrounding rocks where deformation was more distributed. During segmentation shortening was normal to the interboudin plane rather than layering. Deformation, rotation and

separation of boudins occurred in D_4 and possibly in D_3 as well. This is a departure from established theories of boudinage that assert shortening at a high angle to layering. The finite structure is the result of several deformations so it cannot be used as a kinematic indicator for a single deformation event.

The flanking structures formed over several deformations. The cutting element vein occupies S_2 shear bands that were reactivated in D_4 when the flanking fold formed. The flanking fold was produced by an uneven distribution of shearing strain between the internal and external host elements with higher deformation and rotation of bedding occurring in the latter. This is different from currently established mechanisms that advocate deviation of the internal host element.

The formation of asymmetric boudinage and flanking structures over multiple deformations makes it difficult to use them as kinematic indicators because the finite structures represent more than one stress field orientation. The value of these structures is that they preserve important structural information that may be destroyed by deformation in the more homogenously deformed parts of the rock. Further work is required on a range of these structures in rocks with higher metamorphic grades to investigate if they are related to the deformation history in a similar manner to that found here.

Acknowledgements

This work form part of a study to determine the structural controls on the Mount Isa Zn-Pb-Ag Deposit with funding provided by MIM Limited (now Xstrata plc), Mount Isa Business Unit. Supervision of this project by Prof. Tim Bell is gratefully acknowledged, as are suggestions regarding presentation by Tom Blenkinsop. Funding and permission for publication from MIM, and field assistance from company geologists is greatly appreciated.

Table 1. Description of the Geometric Features of Asymmetric Boudins as (Goscombe and Passchier, 2003)

Feature	Description
L_b	Boudin long axis.
S_b	Surface of the boudinaged layer.
S_{ib}	Interboudin surface or plane.
S_e	Enveloping surface of the boudin train.
D	Displacement measured parallel to S_{ib} between adjacent boudins.
N	Dilation normal to S_{ib}.
L	Cross sectional boudin length parallel to S_b.
W	Width normal to S_b.
θ	Angle between S_{ib} and S_b.

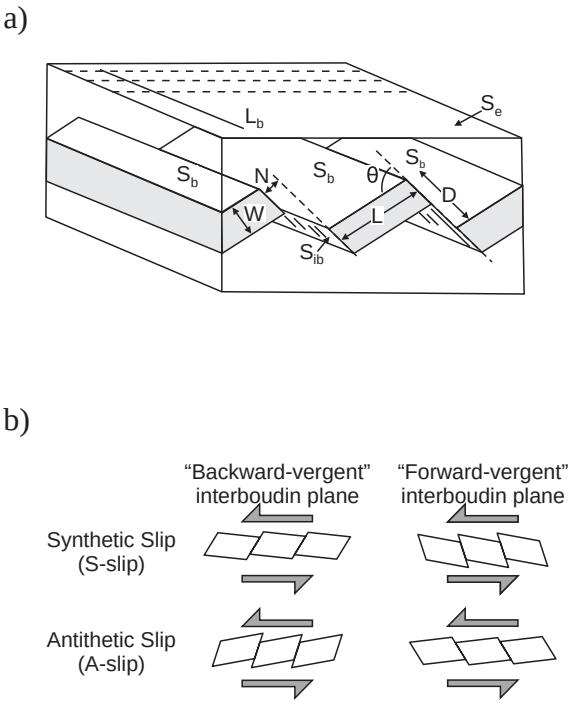

Figure 1: a) Illustration of the geometric features of asymmetric boudins from Goscombe and Passchier (2003). A description of the elements is given in Table 1. b) Goscombe and Passchier's classification of asymmetric boudins based on the relationship between shearing parallel to layering and the orientation and displacement of the interboudin plane.

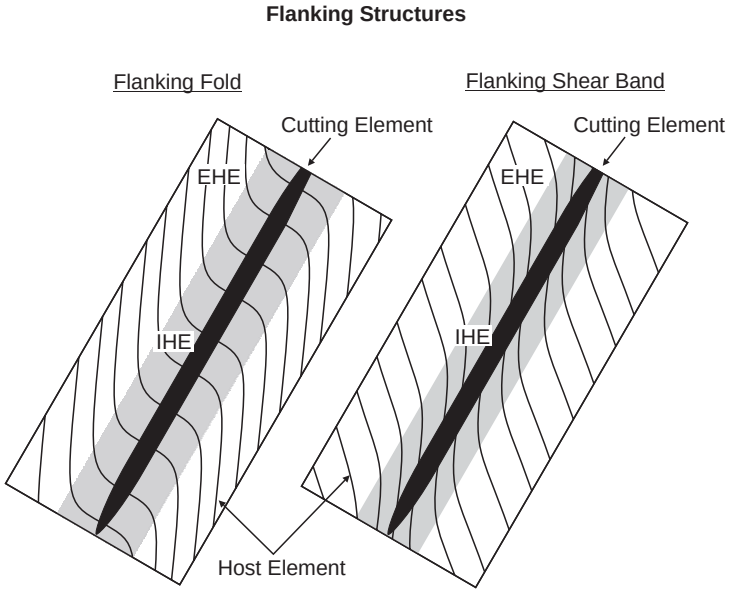

Figure 2: Schematic illustration of flanking structures. The solid line represents the host element foliation. The blank is the external host element (EHE) and the shaded area is the internal host element (IHE). (a) Flanking fold. (b) Flanking shear band. The internal host element is defined by a different fabric orientation to the external host element.

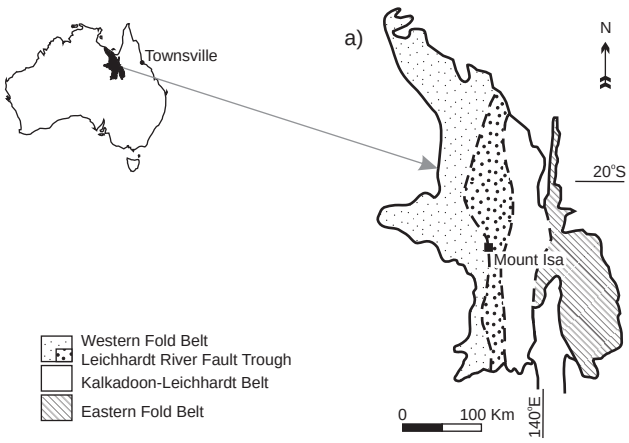

Figure 3: Locality map of Mount Isa Inlier in Northern Australia. Mount Isa is located on the western margin of the Leichhardt River Fault Trough in the Western Fold Belt.

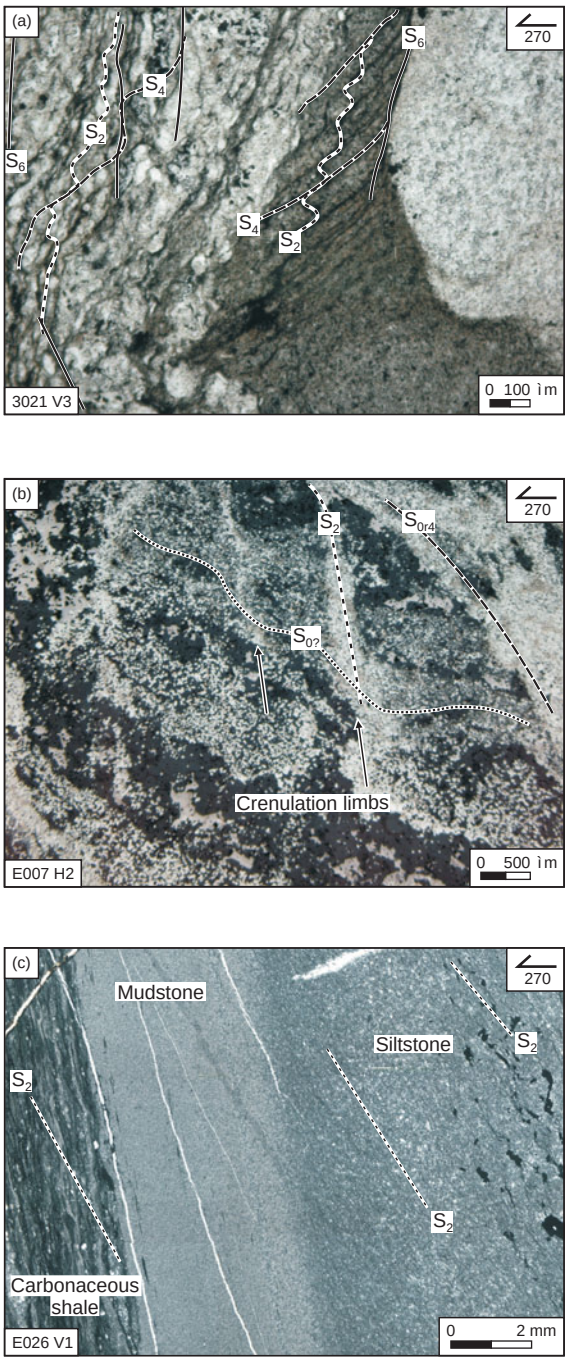

Figure 4: Photomicrographs displaying the different styles of deformation in the main rock types. a) Carbonaceous shale with well developed crenulation cleavage. Vertical E-W thinsection, arrow indicates horizontal and orientation of section. b) Pyritic shale in which pyrite overprints crenulation cleavages. Horizontal section. c) Massive mudstone and siltstone with only a weak cleavage recognisable. The carbonaceous shale on the left provides a striking comparison of the deformation in the different rock types. Vertical E-W thinsection.

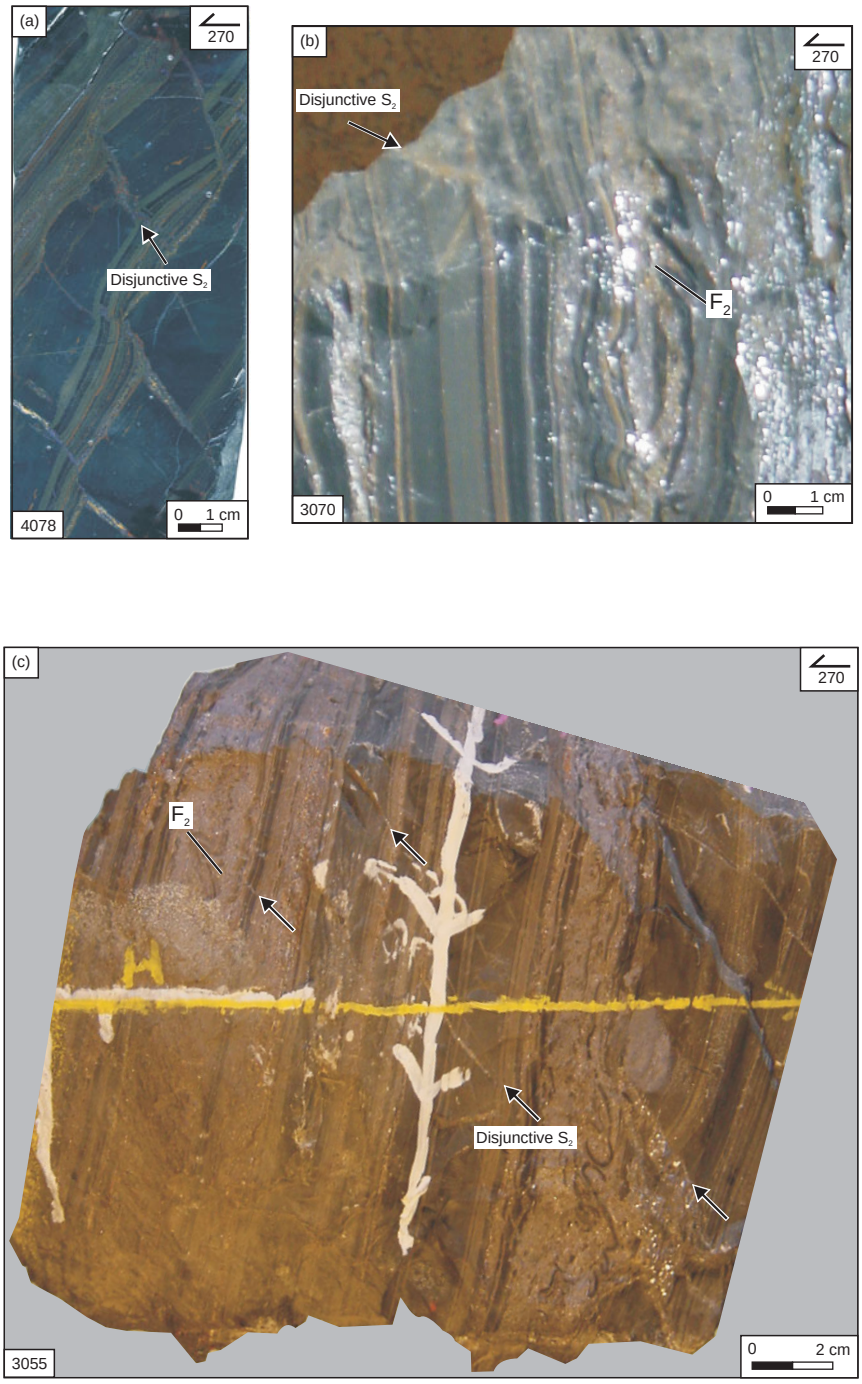

Figure 5: Disjunctive cleavage in massive rock types interbedded with shales. a) Photograph of oriented drill core illustrating disjunctive cleavage in the massive siltstones and mudstones. In this sample the disjunctive cleavages form the interboudin plane to an asymmetric boudin train. Sample width is 6.25 cm (Hole T618 V1). b) Photograph of oriented hand specimen (sample is wet). Disjunctive S_2 is axial planar to F_2 in a folded siltstone bed. (6904 XC, level 5). c) Photograph of oriented hand specimen. This sample illustrates the disjunctive nature of S_2 in massive lithologies. It also demonstrates this cleavage is parallel to F_2 axial planes of folded thin siltstone beds in massive sulphide intervals (6904 XC, level 5).

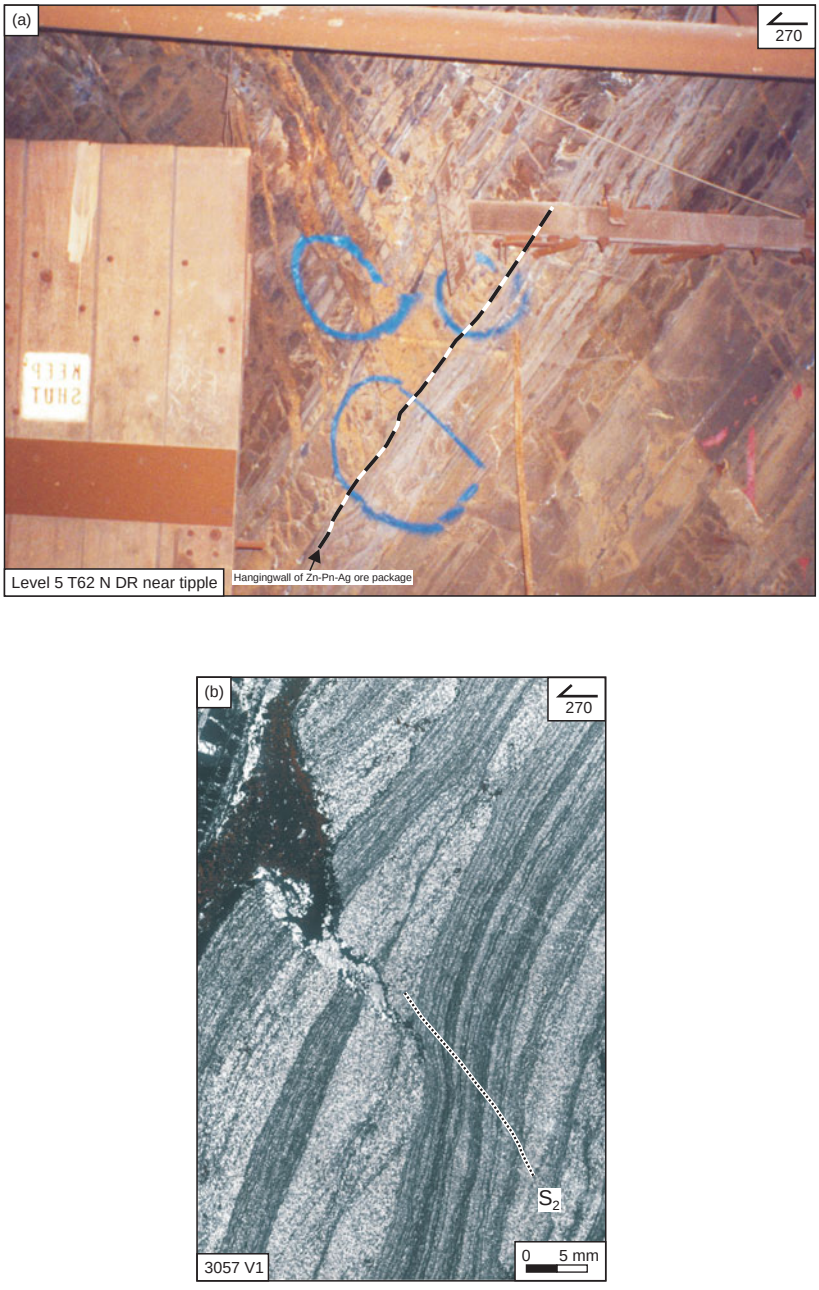

Figure 6: a) Underground exposure photograph, looking to the NNE, of east-dipping carbonate veins, right of the broken line, in the barren host rocks in the hangingwall of the 0011 Zn-Pb-Ag orebody (T 62 N DR, level 5). b) Photomicrograph of vertical section illustrating carbonate, quartz and sulphide vein in a S_2 shear band.

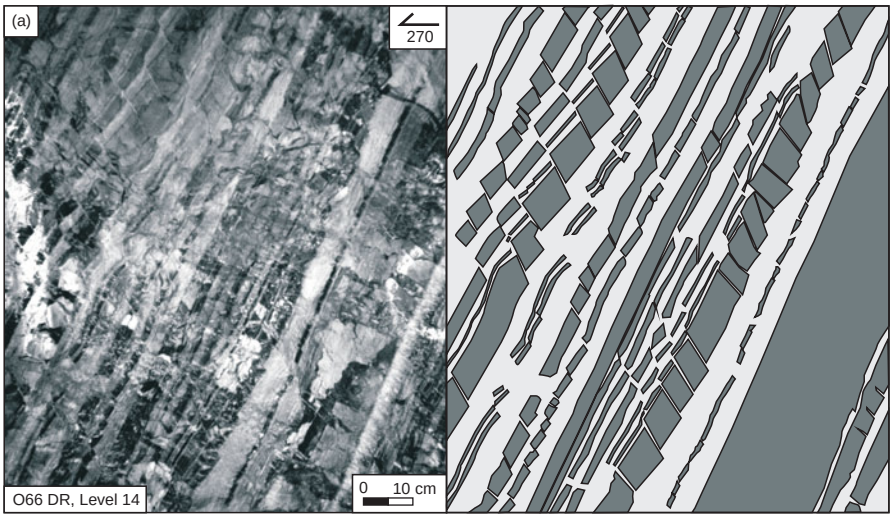

Figure 7: Asymmetric boudins. a) Photograph and sketch of exposure of asymmetric boudins (O66 XC level 14). Dark grey shaded units are massive siltstone and mudstones and the lightly shaded areas are shales. b) Drill core (Hole T618 V1, 197.5 m) through interbedded shales and siltstones containing asymmetric boudins. c) Photomicrograph of the area indicated in b). Deformation in the shales that corresponds with the interboudin plane in the siltstone is more dispersed. d) Close up photomicrograph of the area marked in c), illustrating deformation of the boudin by an S_4 shear band. More dispersed deformation will cause the rotation of entire boudins, see Fig 5a.

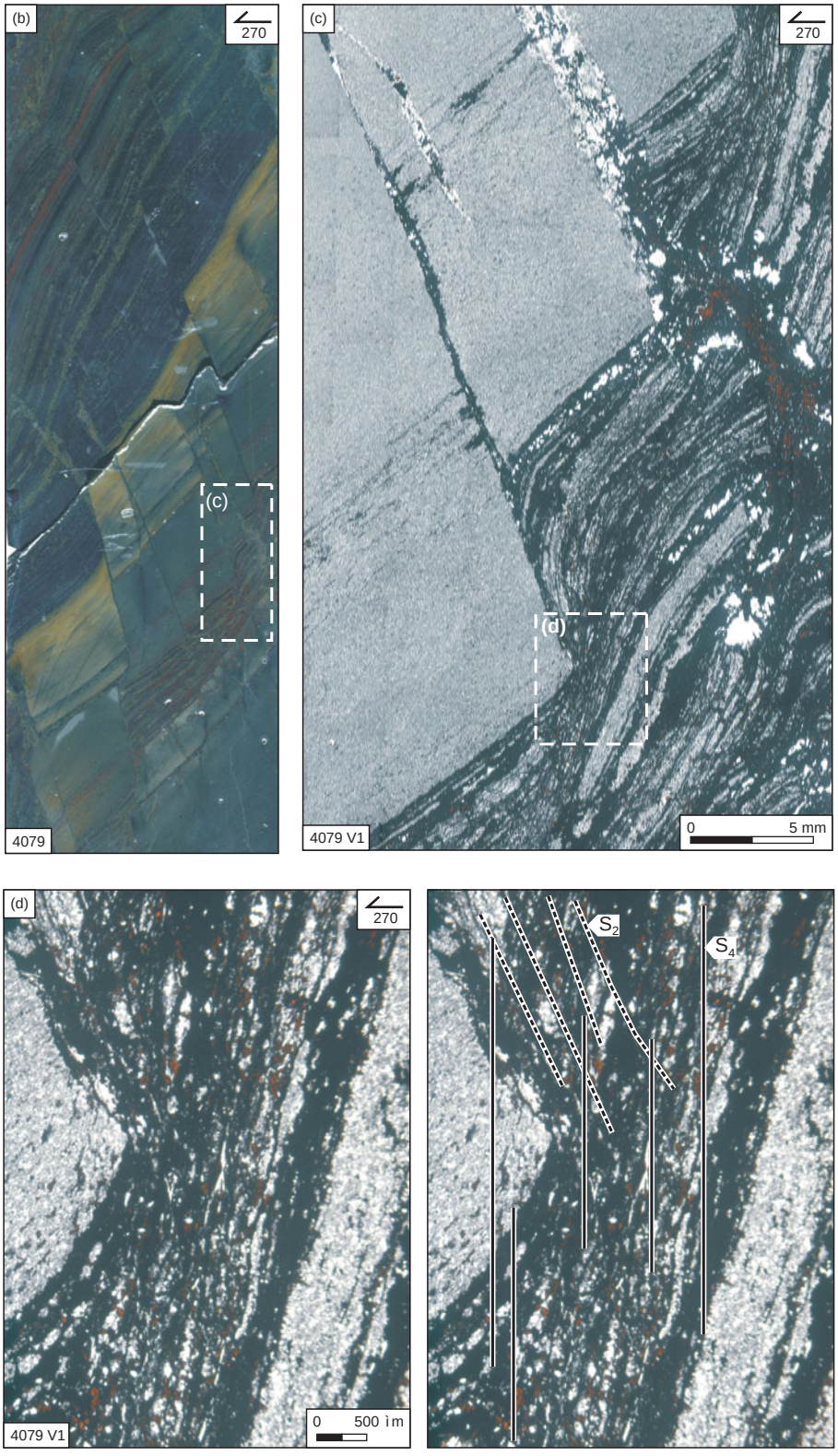
(b)
270
(c)
4079
(c)
270
(d)
4079 V1
0 5 mm
(d)
270
4079 V1
0 500 im
S2
S4

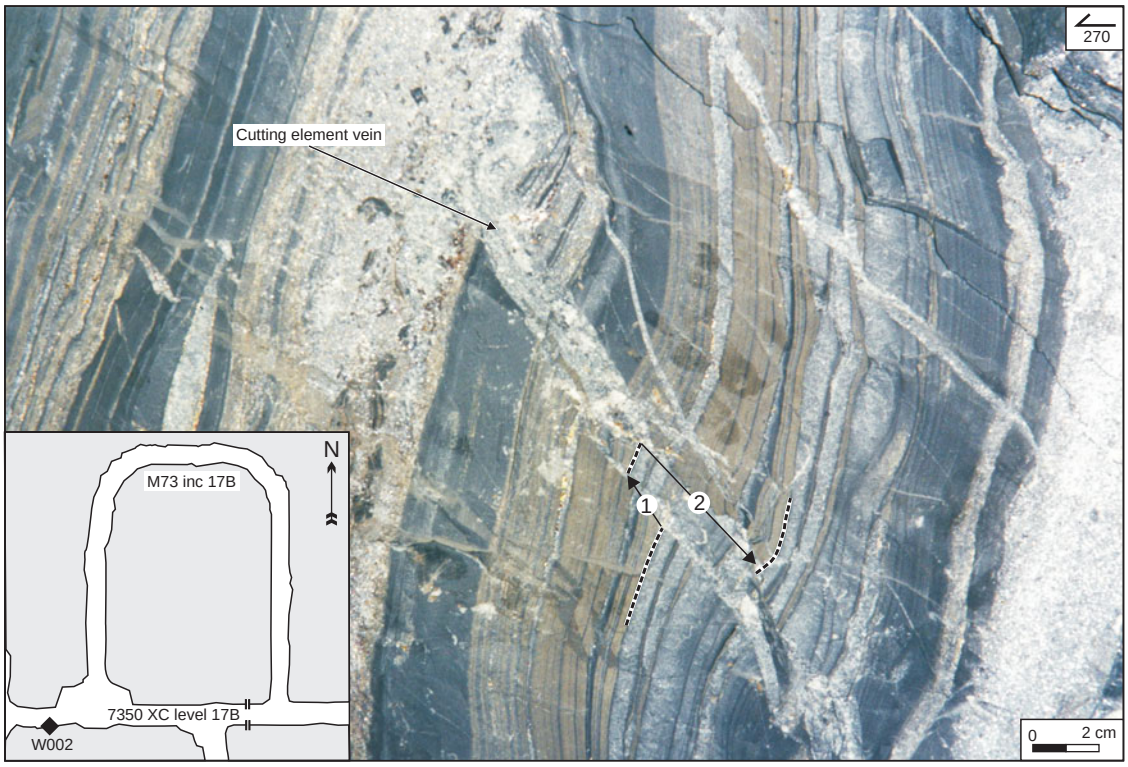

Figure 8: Flanking structure exposed in the underground workings. Two episodes of movement along the cutting element structure, labelled 1 and 2, can be discerned from displacement. Looking south, width of view is approximately 30 cm. Inset, plan of underground workings on levels 17 and 17b indicating the location of the sample

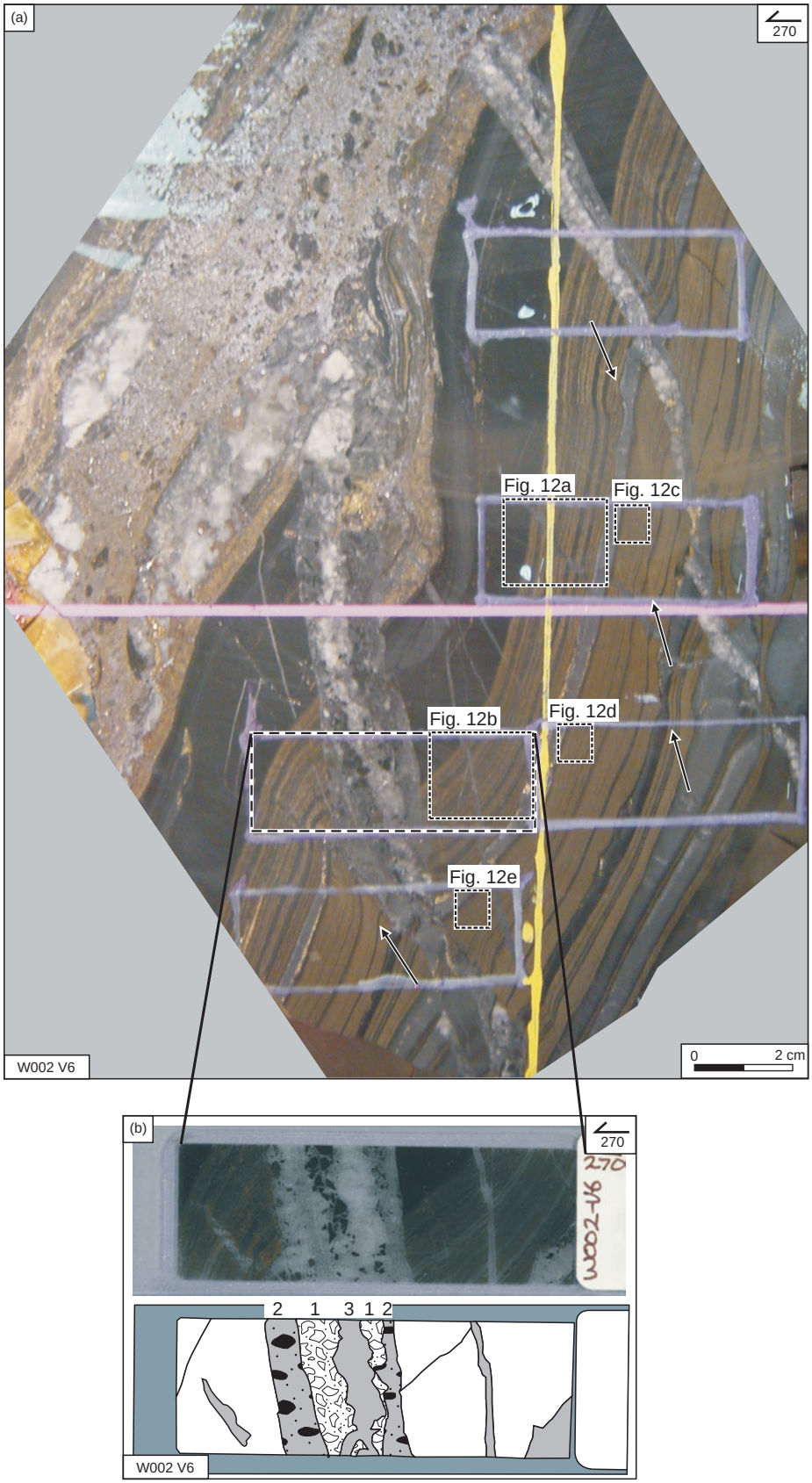
(a)
270
Fig. 12a
Fig. 12c
Fig. 12b
Fig. 12d
Fig. 12e
W002 V6
0
2 cm
(b)
270
270
W002-V6
2 1 3 1 2
W002 V6

Figure 9: a) Photograph of the oriented sample of the flanking structure in figure 8. Rectangular boxes denote thinsection locations (see figure 12). The masked arrows point to several of the S_2 shear bands in the sample. b) Photograph of thinsection of the cutting element vein shows three generations of veining labelled 1 to 3. See text for detail. See also figure 10. Thinsection is 2.5 cm wide.

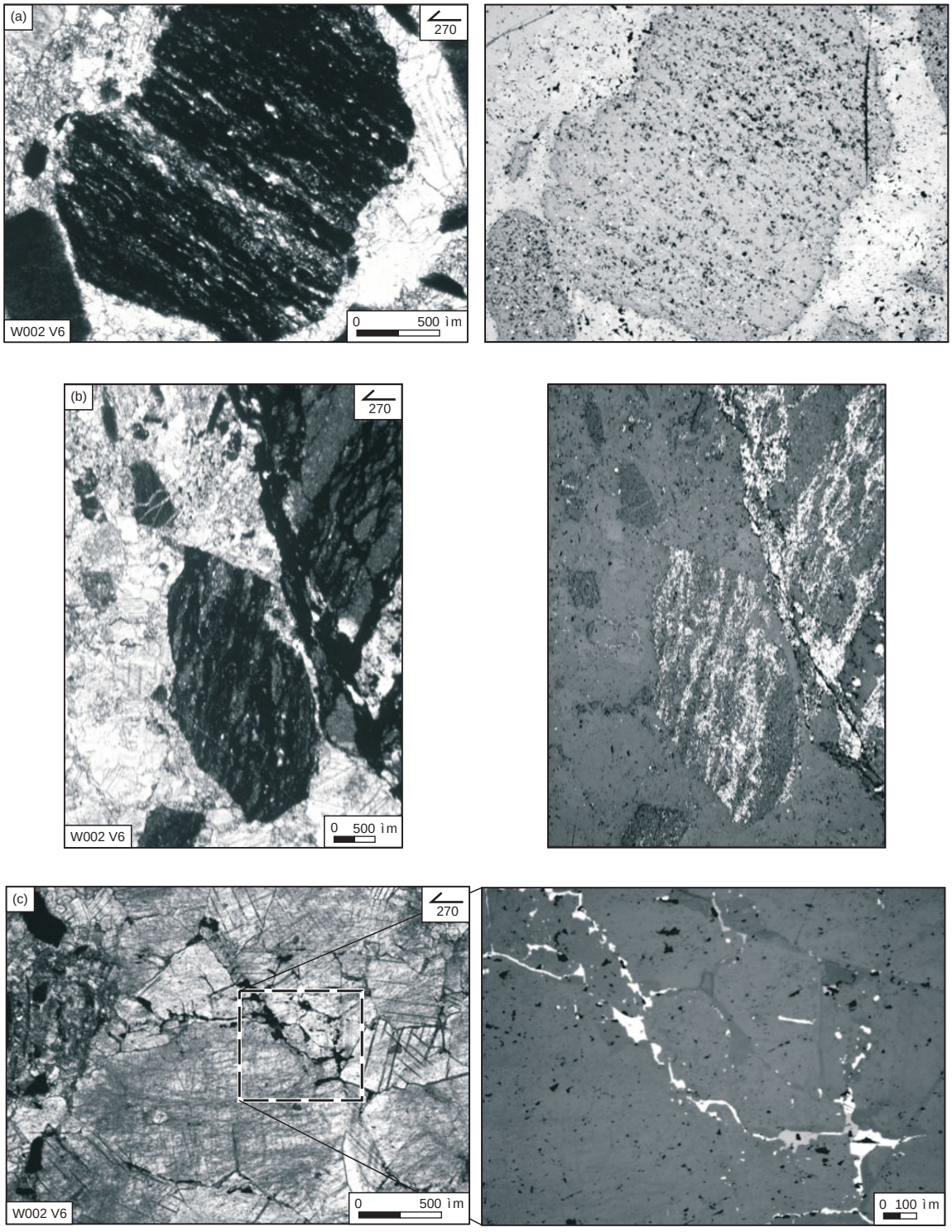
(a)
270
W002 V6
0 500 µm
(b)
270
W002 V6
0 500 µm
(c)
270
W002 V6
0 500 µm
0 100 µm

Figure 10: Photomicrograph of the three generations of veining in the cutting element in figure 9. The left and right columns contain transmitted light (ppl) and reflected light images respectively of vertical E-W sections looking north. a) Second generation breccia clast with opaque anastomosing fabric. The reflected light image demonstrates a lack of fine grained pyrite in the anastomosing opaque seams. b) Shale clast from the second episode of brecciation with fabric the same as the clast in a). The reflected light image shows the opaque seams contain fine grained pyrite. The presence of two generations of breccia clasts with same fabric but only one having pyrite alteration indicates the timing of the alteration. c) The youngest vein generation comprising large clear carbonate (dolomite) crystals with interstitial sphalerite and galena. This generation corresponds to the clear white vein in figure 9, which cuts across the breccia veins.

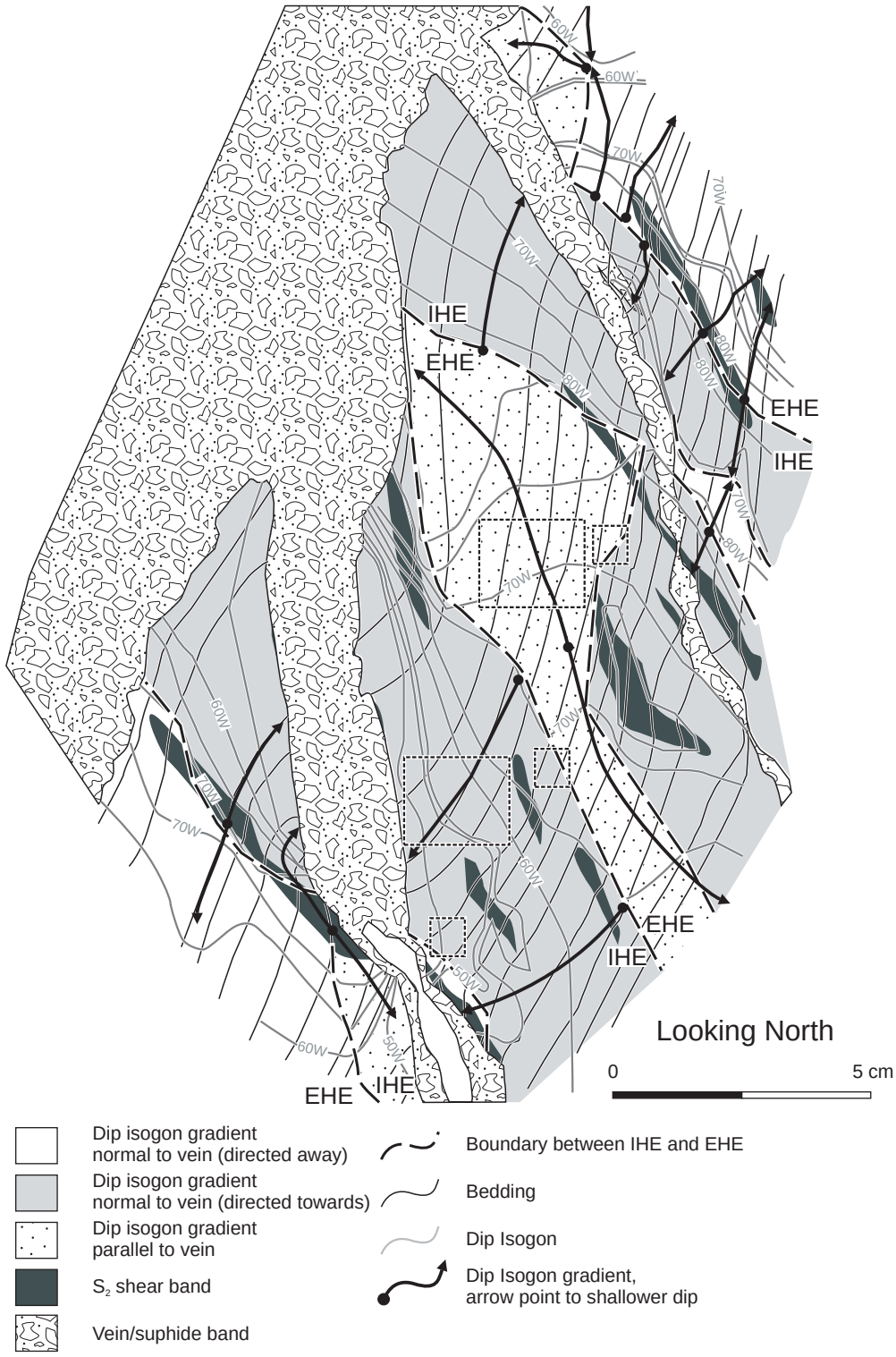
60W
70W
80W
50W
IHE
EHE
Looking North
0
5 cm
Dip isogon gradient
normal to vein (directed away)
Dip isogon gradient
normal to vein (directed towards)
Dip isogon gradient
parallel to vein
S2 shear band
Vein/suphide band
Boundary between IHE and EHE
Bedding
Dip Isogon
Dip Isogon gradient,
arrow point to shallower dip

Figure 11: Bedding dip isogon analysis of the host element of flanking structures. Broken line boxes denote areas in which the density of S_4 is compared (see figure 12). a) Trace of the flanking structure sample. The host element fabric is bedding (narrow solid lines). The thicker grey lines are the bedding dip isogons with the dip labelled at 10° degree intervals. The black filled patches are S_2 shear bands. Dip isogon gradients are illustrated with the heavy solid arrows. The arrows point in the direction of decreasing westwards dip and the solid circles are located at the peak of the gradient, where bedding is steepest. Three domains are recognised based on the direction of the dip isogon gradients with respect to the cutting element veins. See text for details. The boundary between the internal (IHE) and external (EHE) host elements is marked by the broken line.

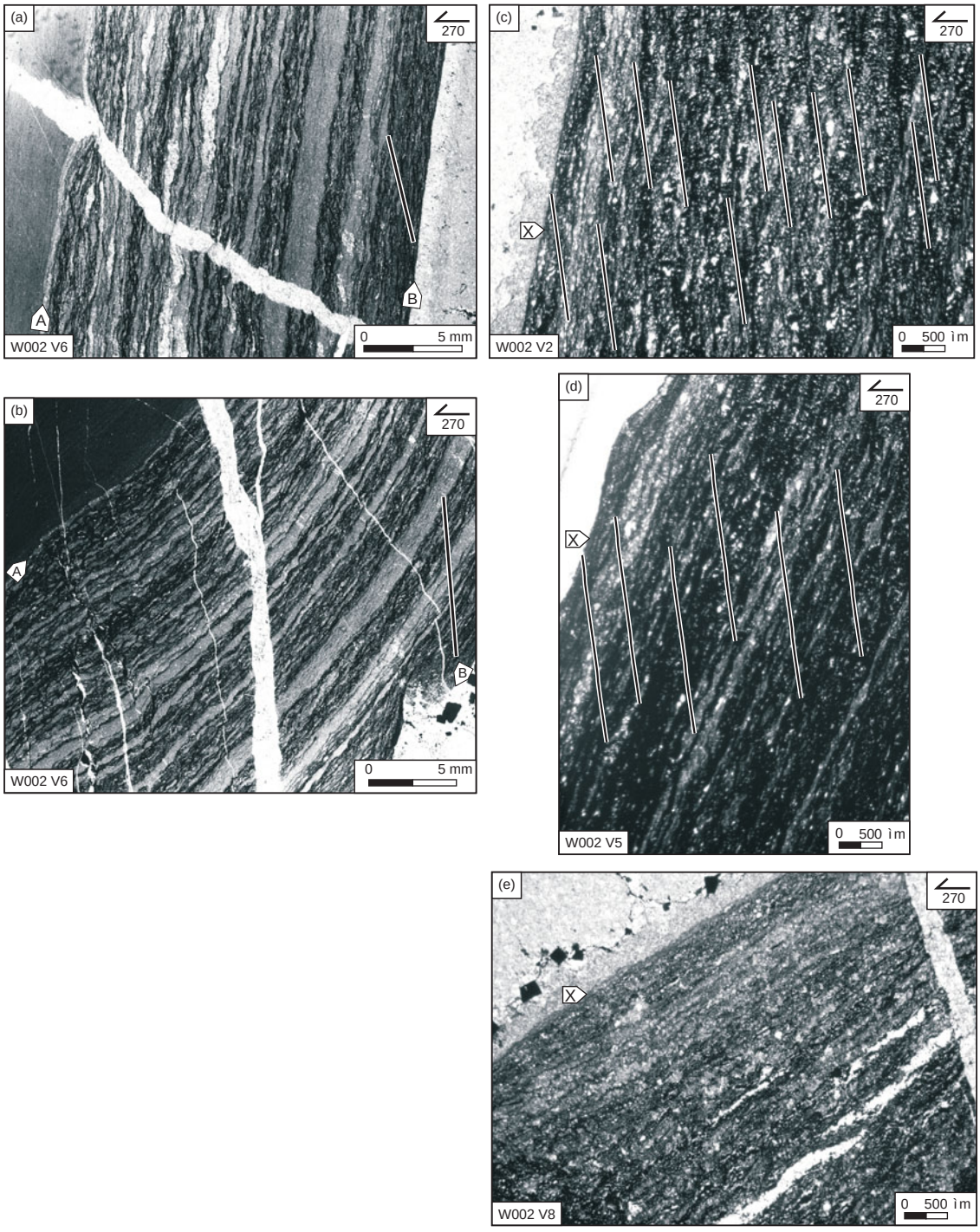

Figure 12: Photomicrographs comparing the density of S_4 between the internal and external host elements. The density of S_4 increases away from the cutting element vein. See figure 9a for locations of photomicrographs. a and b) External and internal host elements respectively. The labels A and B mark corresponding layers in each photomicrograph. c) External host element at higher magnification. An example of S_4 is highlighted with the masked line. d) Boundary between the internal and external host elements. e) Internal host element adjacent to the vein. Note the paucity of S_4 compared to c and d. X marks a corresponding bedding surface in f, g, and h.

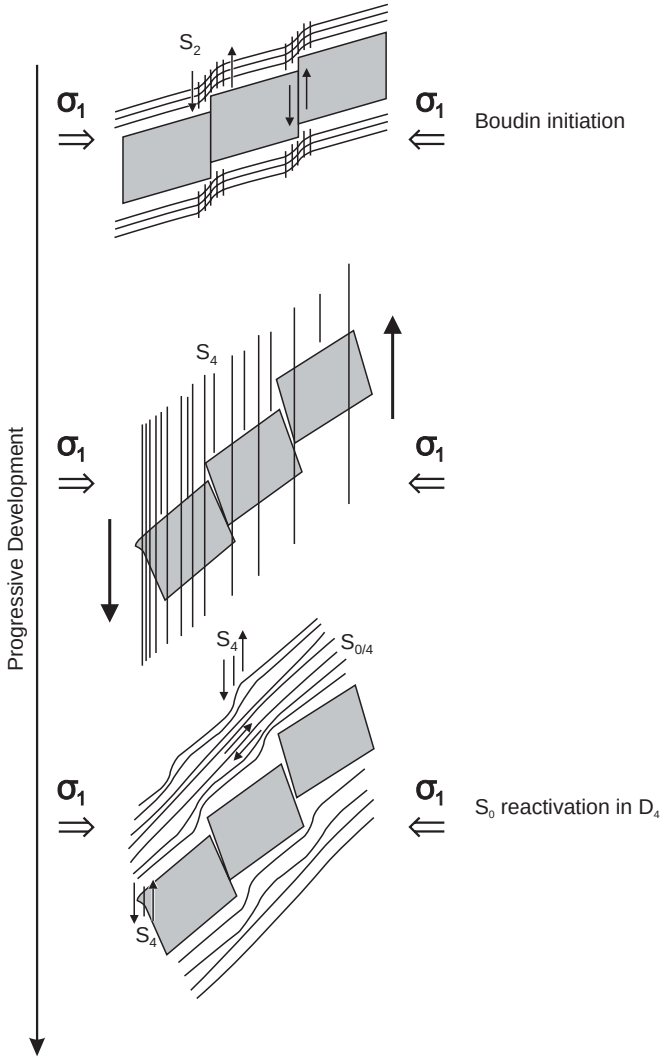

Figure 13: Schematic illustration of asymmetric boudin formation linked to the deformation history. a) The interboudin plane formed during D_2 as a disjunctive S_2 cleavage in massive siltstone and mudstone beds, its equivalent in the shales is a crenulation cleavage. b) Rotation of the boudin train by progressive shearing along S_4. S_4 strain gradients cause relative rotation and separation of boudins. c) Localisation of deformation into the less competent layers causes reactivation of layering next to the boudin train.

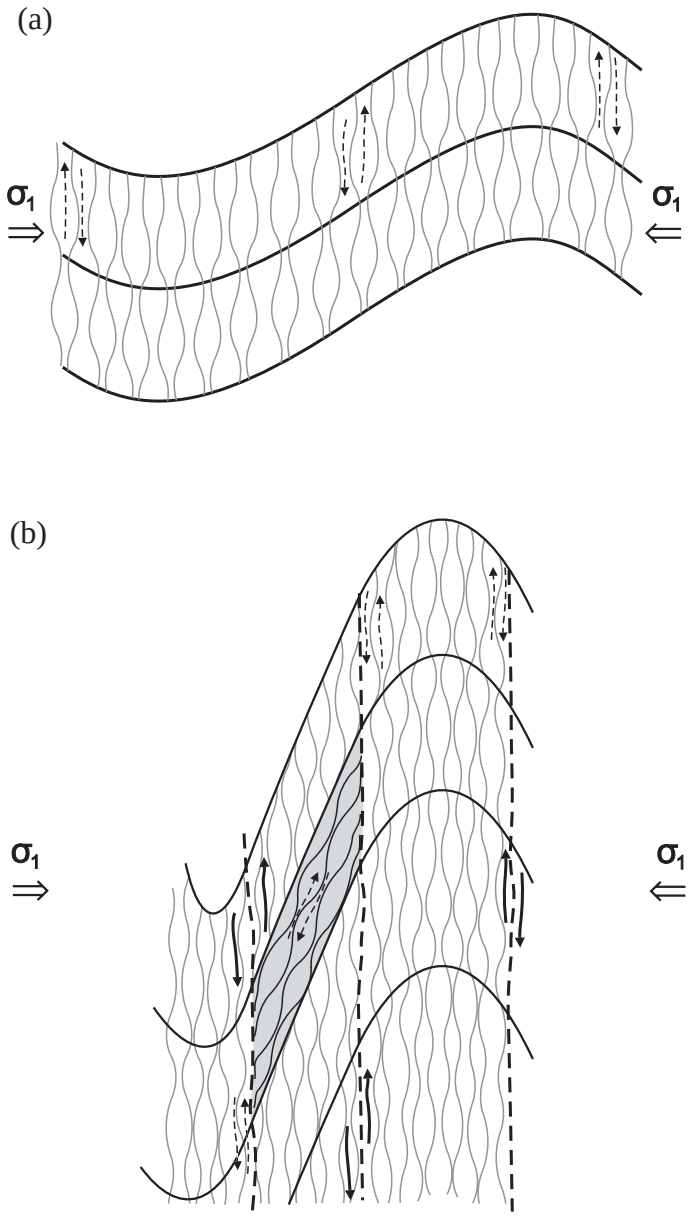

Figure 14: Schematic illustration of reactivation on the limb of a developing fold. a) Early in fold formation with progressive shearing strain occurring around the actively forming axial planar cleavage. b) Later in folding progressive shearing strain in some parts of the rock switches from being around the actively forming axial planar cleavage to around an older foliation as is the case illustrated in the shaded area. The upper and lower processes may occur in the same or different deformations. If the field of observation was limited to the grey area then the interpretation of bulk shearing would be parallel to layering rather than at some angle to it (From Bell, 1991).

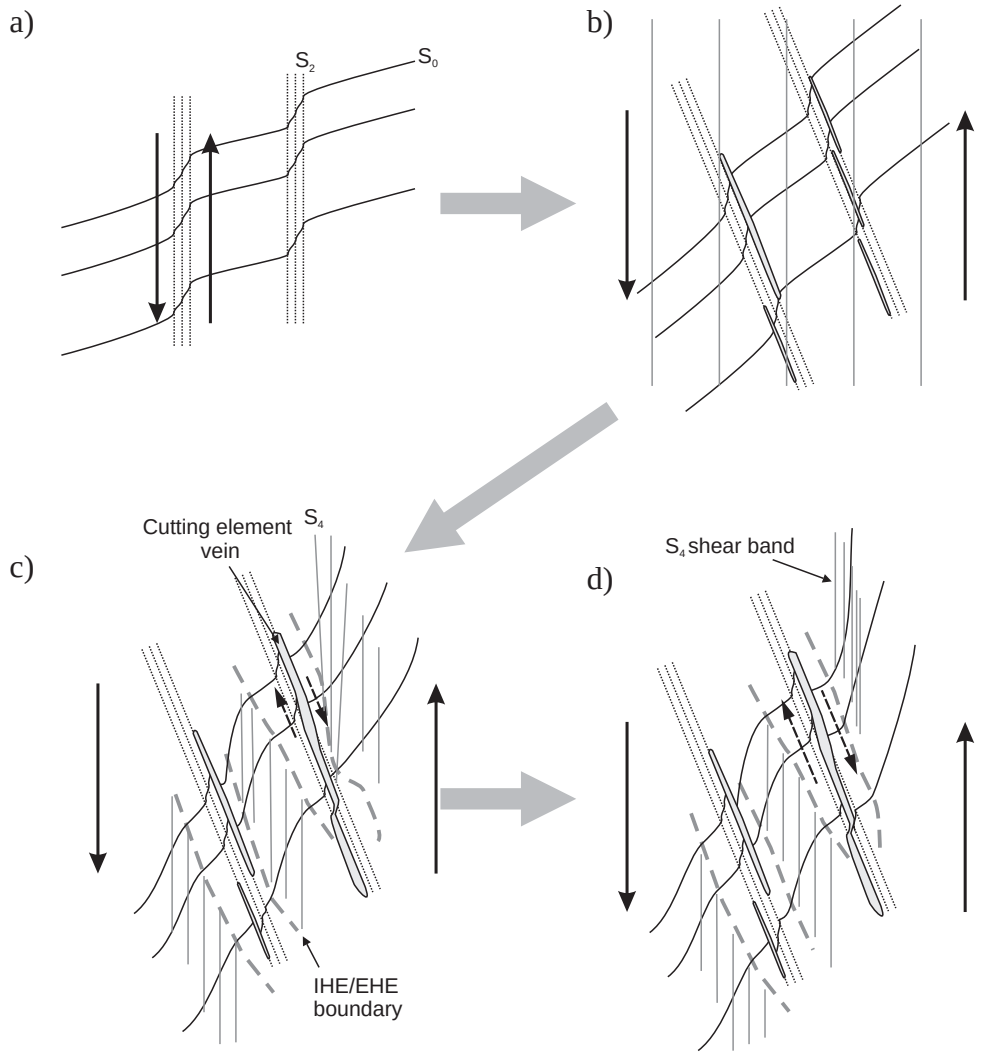

Figure 15: Schematic illustration of the progressive development of the flanking structure studied here. a) S_2 shear bands indicated by the broken lines. b) Rotation of S_2 by reactivation of bedding in D_3. There may also be a component of rotation early in D_4. c) East block down reactivation of the S_2 shear bands, indicated by the dashed arrows by progressive east block up shearing along S_4 (solid vertical arrows). Reactivation of S_2 is accompanied by vein formation and localisation of S_4 which combined with strain shadow influences of the newly formed vein establishes the internal host element (IHE). S_4 shearing is concentrated in to the external host element (EHE) which rotates bedding in the external host element forming the flanking fold. Flanking shear bands are formed where the cutting element vein intersects an S_2 shear band. d) Further localisation of S_4 forming shear bands, tightening the fold and causing additional brecciation along the growing cutting element vein.